

UNIVERSITEIT ANTWERPEN

FACULTEIT WETENSCHAPPEN

DEPARTEMENT FYSICA

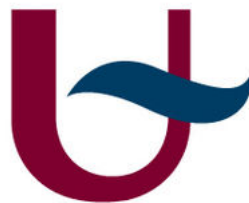
ACADEMIEJAAR 2018-2019

**TRANSVERSE MOMENTUM DEPENDENT PARTON DISTRIBUTION
FUNCTIONS IN QUANTUM CHROMODYNAMICS AND THEIR
APPLICATION TO LHC PHYSICS**

Proefschrift ter verkrijging van de graad van Master in de Fysica

Author:
Aron Mees VAN KAMPEN

Supervisor:
Prof. Dr. Pierre VAN MECHELEN
Co-supervisor:
Prof. Dr. Francesco HAUTMANN



Universiteit
Antwerpen

Samenvatting

De sterke wisselwerking kan nog niet beschreven worden met fysische modellen in de volledige faseruimte. Op korte afstandsschalen (hoge energieën) kan deze goed beschreven worden met kwantumveldentheorie, maar op grote afstandsschalen (lage energieën) is het een moeilijk te bestuderen kracht. Bij hoge energieën gedragen deeltjes die interageren via deze wisselwerking - quarks en gluonen (partonen) - zich als vrije deeltjes, wat *asymptotische vrijheid* wordt genoemd. Maar bij lage energieën zijn ze sterk gekoppeld: ze zijn opgesloten in hadronen (*confinement*). Deze eigenschappen zijn het resultaat van de sterke koppelingsfactor α_s die varieert in functie van de energie, iets wat perfect beschreven is in kwantumchromodynamica (QCD). Vanwege de variërende koppelingsfactor is een perturbatieve aanpak van QCD processen bij lage energieën niet mogelijk. Dit probleem kan worden opgelost met het factorisatie theorema wat dynamica op lage en hoge energieschalen van elkaar scheidt in niet-perturbatieve (zachte) parton distributie functies (PDFs) en een perturbatief (hard) matricelement. PDFs beschrijven de inhoud van hadronen en het matricelement stelt de kwantummechanische overgangswaarschijnlijkheid voor de interactie op hoge energie voor. Deze thesis bespreekt formalismen die de PDFs beschrijven.

Om processen in hoog energetische deeltjesbotsingen die plaatsvinden in deeltjesversnellers te beschrijven moeten PDFs in rekening gebracht worden in de berekeningen. Deze functies beschrijven de dynamica in protonen (of andere hadronen) en zijn universeel: ze hangen niet af van het soort interactie op hoge energie, maar ze zijn wel afhankelijk van de energieschaal. Met fundamentele principes van QCD kan de afhankelijkheid van de PDFs van de schaal uitgedrukt worden door perturbatieve evolutievergelijkingen. De DGLAP evolutievergelijkingen faciliteren de evolutie van collineaire PDFs in een energieschaal μ . Dit is niet de volledige oplossing om het niet-perturbatieve regime te beschrijven; als klein transversaal impuls een rol speelt in de dynamica in het proton worden grote logaritmische factoren van de vorm $\ln(Q^2/q_\perp^2)$ aan de storingsreeks toegevoegd. Fysisch zijn deze factoren te wijten aan de radiatie van gluonen met zeer klein impuls. Men moet daarom de termen met grote logaritmen in de storingsreeks hersommen.

Om hersommatie mogelijk te maken moet de afhankelijkheid van het transversaal impuls aan de PDFs en de evolutievergelijkingen toegevoegd worden. De PDFs zullen dan niet enkel in één dimensie beschreven worden met de fractie van het longitudinaal impuls x , maar ook in het vlak loodrecht op de bewegingsrichting van het proton met het transversaal impuls k_\perp . Transversaal impuls afhankelijke parton distributie functies (TMDs) bevatten meer informatie over de inhoud van hadronen (zoals protonen) en resulteren in meer precieze berekeningen van botsingsprocessen.

In deze thesis zijn formalismen die hersommatie implementeren bestudeerd en met elkaar vergeleken. De methode van Collins, Soper en Sterman (CSS) geeft een uitdrukking voor de differentiële werkzame doorsnede voor het Drell-Yan proces in een kader dat bekend is als TMD factorisatie. De hadronische functies zijn hier gefactoriseerd in drie delen die verschillende groottes van transversaal impuls beschrijven. Een van deze factoren is de Sudakov vorm factor die grote logaritmen (large logarithms) hersommeert. De parton branching (PB) methode is een relatief nieuwe methode en werkt in een ander kader dan CSS. In PB wordt het DGLAP formalisme op een nieuwe manier benaderd; het stelt een iteratieve manier voor om de evolutievergelijkingen op te lossen zodat het geschikt is voor evolutie van TMDs. Dit geeft een intuïtieve en fysische interpretatie: het transversaal impuls van een interagerend parton wordt gegenereerd door meerdere emissies gedurende de evolutie naar een hogere energieschaal. Dit wordt daarom een "step-by-step" procedure genoemd. Kimber, Martin, Ryskin en Watt (KMRW) hebben een methode ontwikkeld die ook gebaseerd is op DGLAP, al genereert deze het transversaal impuls in slechts een stap. Desondanks wordt KMRW veel gebruikt voor experimentele studies omdat het langer bestaat dan de parton branching methode.

Deze drie formalismen zijn in detail geanalyseerd en vergeleken op analytisch vlak en aan de hand van numerieke berekeningen. CSS en PB behandelen verschillende objecten (de werkzame doorsnede en TMDs) maar hebben soortgelijke factoren voor de hersommatie, namelijk de Sudakov vorm factoren. Deze zijn vergeleken en blijken gelijk te zijn tot op orde NNLL (next-to-next-to-leading logarithm). De vergelijking van KMRW met PB is in groot detail uitgevoerd omdat beide methoden evolutievergelijkingen voor TMDs oplossen. De TMDs van deze methoden blijken goed overeen te komen in het midden van het k_{\perp} domein (tussen de onder- en bovenlimiet van de evolutieschaal), maar kleine waarden voor k_{\perp} kunnen niet goed beschreven worden door KMRW. De twee methoden komen ook niet overeen bij grote k_{\perp} .

Abstract

The strong interaction of nature is not yet described by physical models in all kinematic regimes. At short distances (high energies) it is understood to a large extent, while at large distances it is difficult to study. Strongly interacting particles - quarks and gluons (partons) - behave as if they are free particles at high energies: they are asymptotic free. At low energies they are however strongly coupled: they are confined in hadrons. These properties are the result of the coupling strength of the strong interaction α_s which varies with the energy scale. This scale dependence of α_s can be described perfectly by quantum chromodynamics. It implies that a perturbative approach to strong processes at low energies is not possible. However, with the factorization theorem, low and high energy dynamics can be separated into non-perturbative (soft) PDFs and perturbative hard scattering functions. This thesis discusses formalisms that provide descriptions for the non-perturbative part of factorized observables: the PDFs.

To make predictions of processes at high energetic particle collisions that take place in hadron colliders such as the LHC, the PDFs need to be taken into account in the calculations. They describe the dynamics inside the protons. PDFs are universal objects: they do not depend on the hard scattering process, but they are dependent on the energy scale. With fundamental principles of QCD, the dependence on the scale can be expressed by perturbative evolution equations. With the DGLAP evolution equations, one is able to evolve collinear PDFs as function of an energy scale μ . This is not the final method to describe the non-perturbative regime because this approach fails in certain kinematic limits due to soft gluon emission effects. Radiation of such gluons with very small transverse momentum causes logarithmic factors $\ln(Q^2/q_\perp^2)$ at all orders in the perturbation series to be large. The perturbation series therefore needs to be resummed.

In order to include soft gluon resummation, the transverse momentum of the partons has to be included in the evolution equation. The PDFs will then be described not only in one-dimension by the longitudinal momentum fraction x , but also in the plane transverse to the proton's movement by the transverse momentum k_\perp . Transverse momentum dependent parton distributions (TMDs) provide more information on the content of hadrons and result in more accurate calculations of collider processes.

Formalisms that implement soft gluon resummation have been studied and compared. CSS provides an expression for the Drell-Yan cross section in a framework of TMD factorization. The hadronic, soft functions are factorized in three parts that treat different size of transverse momentum. One of these factors is the Sudakov form factor which resums large logarithms. The parton branching method approaches the DGLAP formalism in a new way. The step-by-step solution for the evolution equations of TMDs that is proposed provides an intuitive and physical method: transverse momentum is generated in multiple branchings within the evolution. KMRW is a method that is also based on DGLAP but it has a single-step evolution. Despite that, KMRW is a longer existing method that has already been used for many experimental studies.

These three formalisms have been analyzed in detail by analytical and numerical comparison. CSS and PB treat different objects but have similar resummation factors - the Sudakov form factor - which have been compared. These are equal up to order NNLL. The comparison of KMRW with PB is performed in much detail because they both solve evolution equations for TMDs. These methods appear to be very similar in the middle k_\perp region, but the small k_\perp region is not well described by KMRW and the approaches also differ for large k_\perp .

Contents

I	Quantum Chromodynamics	7
1	QCD as a gauge field theory of the strong interaction	8
1.1	Lie algebras as basis for gauge field theories	8
1.2	The QCD Lagrangian	9
1.3	Renormalization	11
1.3.1	Structure of renormalization	13
1.3.2	Example: gauge boson self energy renormalization	13
1.3.3	Renormalization group	15
1.4	The running coupling α_s and Λ_{QCD}	16
2	Application of QCD to particle collision processes	19
2.1	The theory behind particle physics experiments	19
2.2	Factorization	20
2.2.1	Deep inelastic electron-proton scattering	21
2.2.2	Drell-Yan	23
2.3	DGLAP evolution equations	24
2.3.1	The evolution equations	27
3	Transverse momentum dependent parton distribution functions	28
3.1	Motivation	28
3.1.1	Structure functions from DIS	28
3.1.2	Transverse momentum spectrum from DY	29
3.2	TMDs	31
II	TMD formalisms	32
4	The CSS formalism	33
4.1	Perturbative description	33
4.2	Differential Drell-Yan cross section	34
4.3	Sudakov form factor	36
4.4	Differential cross section with TMD factorization	37
5	The parton branching method	39
5.1	Resolvable and non-resolvable emissions	39

5.1.1	DGLAP splitting functions	40
5.1.2	Evolution equations with real-emission probability	41
5.2	Evolution equations with the Sudakov form factor	43
5.3	Iterative branching procedure	44
5.4	Ordering conditions	45
5.5	TMDs	48
6	KMRW approach	50
6.1	From DGLAP to unintegrated PDFs	50
6.2	Ordering conditions	52
6.2.1	Integral and differential equations KMRW	52
III	Analysis of TMD formalisms	53
7	Comparison of CSS with the parton branching method	54
7.1	Recap of the formalisms	54
7.2	Perturbative coefficients	56
7.2.1	LL coefficients	56
7.2.2	NLL coefficients	56
7.2.3	NNLL coefficients	57
7.3	Renormalization group transformation	58
7.4	Numerical validation	60
7.5	Summary	60
8	Comparison of KMRW with the parton branching method	61
8.1	Parton branching evolution equations in q_{\perp}	61
8.1.1	Evolution equation in the high x regime	62
8.1.2	Evolution equation in the low x regime	63
8.2	Sudakov form factors	64
8.3	Analytical comparison of the evolution equations	65
8.3.1	Equations for collinear PDFs \tilde{f}_a	65
8.3.2	Equations for TMDs	66
8.4	Numerical comparison	67
8.4.1	TMDs versus k_{\perp}	67
8.4.2	TMDs versus x	69
8.4.3	iTMDs	69
8.4.4	Z boson p_{\perp} spectrum	70
8.5	Summary	72
9	Conclusions	74
	References	75

Acknowledgements

I could not have written this thesis as it is in this state without the help of people I admire. I would like to thank my supervisor Professor Francesco Hautmann, Ola Lelek and Lissa Keersmaekers a lot for all their comments on my thesis and for many interesting discussions during this year. By joining this part of the research group, I learned a lot about our research, doing research and scientific writing.

Many thanks to my supervisor Professor Pierre Van Mechelen who gave me the opportunity to join a conference and research visit during this last year of the Master studies and for good advice at any time.

I also want to thank the other members of the particle physics research group in Antwerp for the pleasant interruptions on working days during lunch and coffee breaks. Thanks to my fellow students for reassuring me during hard times, Hannelore for checking the text on language style and my parents for their emotional involvement and support.

List of Abbreviations

AO	Angular ordering	NNLL	Next-to-next-to-leading logarithm
ATLAS	A Toroidal LHC ApparatuS	NLO	Next-to-leading order
BFKL	Balitsky-Fadin-Kuraev-Lipatov	NNLO	Next-to-next-to-leading order
CCFM	Catani-Ciafaloni-Fiorani-Marchesini	ODE	Ordinary differential equation
CERN	Conseil Européen pour la Recherche Nucléaire	PB	Parton branching
CMS	Compact Muon Solenoid	PDF	Parton distribution function
CSS	Collins-Soper-Sterman	PETRA	Proton-Electron Tandem Ring Accelerator
DESY	Deutsches Elektronen Synchrotron	QCD	Quantum Chromodynamics
DGLAP	Dokshitzer-Gribov-Lipatov-Altarelli-Parisi	QED	Quantum Electrodynamics
DIS	Deep inelastic (electron-proton) scattering	QFT	Quantum Field Theory
DY	Drell-Yan	RG	Renormalization group
GeV	Gigaelectronvolt	RGE	Renormalization group equation
HERA	Hadron-Elektron-Ringanlage	SCET	Soft-Collinear Effective Theory
IR	Infrared	SM	Standard Model
KMRW	Kimber-Martin-Ryskin-Watt	SO	Strong ordering
LEP	Large Electron-Positron Collider	SPS	Super Proton Synchrotron
LHC	Large Hadron Collider	TeV	Teraelectronvolt
LL	Leading logarithm	TMD	Transverse momentum dependent parton distribution function
LO	Leading order	uPDF	Unintegrated parton distribution function
MC	Monte Carlo	UV	Ultraviolet
MPI	Multi parton interactions		
NLL	Next-to-leading logarithm		

Introduction

Particle physics studies the smallest objects in the universe. Because of the small distance scales, quantum mechanics applies to the phenomena of interest. Due to the low invariant mass of the particles, high speeds are easily gained so that special relativity is relevant.

In the first half of the twentieth century, the goal was to formulate a single theory that satisfies both quantum mechanics and special relativity which possesses both properties: the particle-wave duality and the Einstein energy-momentum relation. With quantization of the Lagrangian (with functional integrals) or with the Hamiltonian (using creation and annihilation operators) formalism, quantum field theory (QFT) was born. This theory changed the picture of particles (and waves) dramatically: a particle is the excitation of a field in a small region of spacetime. All processes in QFT are described by amplitudes because it is a quantum mechanical theory and particles are superpositions of states.

The standard model (SM) of elementary particle physics contains quantum gauge field theories. These are QFTs with underlying gauge symmetries coming from *Lie groups*. The behavior of three out of four fundamental interactions of nature is described by gauge theories: the strong, weak and electromagnetic interaction. There are associated gauge bosons for all these interactions that couple to the matter particles (fermions) that carry the charge of this specific interaction (electric, weak charge or colour charge). Strong principles of QFT enable us to calculate probabilities for many processes, but it also comes with difficulties like quantization, renormalization and the translation to processes within particle collision experiments. These subtleties are discussed in chapters 1 and 2.

The strong interaction has the highest interaction strength at large distances. But at small distances, it is barely noticeable. This interaction is called "strong" because at reasonable energies in the current state of the universe, the strong interaction causes strongly bounded states of particles while the electromagnetic and weak interactions do not have strongly coupled regions. At increasing energy scales the strong coupling decreases while the coupling strength of electrodynamics increases. Quantum Chromodynamics (QCD) currently provides the best description of the strong interaction. It enables detailed descriptions of a large part of the fundamental processes that take place in collisions of hadrons in hadron collider experiments like those at the Large Hadron Collider (LHC) in Geneva. A full understanding of the behavior of the strong interaction needs both accurate theoretical descriptions of possible processes and very precise measurements of the (final states of the) collisions.

In the end, the SM is not the full story. Gravitation is not included, because we do not know of a renormalizable quantum field theory of gravity. Neutrino masses are experimentally measured via neutrino oscillations, but this does not result from the SM (because here neutrinos are massless particles). Many observations of the outer regions of galaxies hint to the existence of dark matter. The asymmetry between matter and anti-matter in the universe is also a problem that cannot be solved by the SM.

A collective goal of the particle physics community is to establish a good description of the processes in hadron colliders like the LHC at CERN (Conseil Européen pour la Recherche Nucléaire)

and at future colliders that will operate at larger centre-of-mass energies. With a very precise description of what is known, one could observe experimental anomalies that hint to new physics beyond the standard model. In order to test new theories and determine parameters of the SM more precisely with the use of the LHC, a lot of knowledge on particle collisions has been gathered theoretically and experimentally. The collinear factorization theorem is used to calculate cross sections (probabilities for certain processes) using two factorized objects: an hard matrix element and collinear parton distribution functions (PDFs). The latter is of interest in this thesis and describes the parton (gluon or quark) content of an hadron in function of the energy scale μ and the longitudinal momentum fraction x . The collinear factorization framework is however not sufficient. It only contains information in one dimension: that of the proton's beam direction. PDFs that include information on parton dynamics in the transverse plane are needed for a more complete description of proton collisions. This requires the involvement of the parton transverse momentum k_{\perp} . In chapter 3 the need for transverse momentum dependent parton distribution functions (TMDs) is motivated.

Collinear PDFs and TMDs are universal functions; they are process independent quantities, uniquely determined at a certain scale. They can therefore be extracted from experiment. For the dependence of PDFs on the energy scale and on momentum, evolution equations are formulated. The evolution of TMDs and the description of cross sections including transverse momentum dependence (with so-called TMD factorization) is the subject of the main part of this thesis. Three methods that incorporate evolution and the use of TMDs have been studied and compared in detail. Chapter 4 discusses the formalism by Collins-Soper-Sterman (CSS) that formulates the cross section for the Drell-Yan process in the Fourier space of transverse momentum (\mathbf{b} -space). Chapter 5 gives an overview of the recently developed parton branching (PB) method that provides a solution to new TMD evolution equations. A similar approach to PB is that of Kimber-Martin-Ryskin-Watt (KMRW) which is described in chapter 6. The CSS formalism and KMRW approach are compared with parton branching in chapters 7 and 8. This comparison provides more insight in these approaches of TMD evolution and TMD factorization and raises new questions for further research.

The study of literature that resulted in the first six chapters is purely individual work. The results and conclusions presented in the three last chapters are results from research performed by prof. dr. Francesco Hautmann, dr. Aleksandra Lelek, Lissa Keersmaekers and myself. Professor Hautmann and dr. Lelek are authors of the papers on the PB method. We tried to avoid mistakes by calculating everything independently. In the comparison of CSS with PB, I performed all analytical calculations together with Lissa to have two independent results for a cross check. For the comparison of KMRW with PB, I performed the analytical calculations as a cross check and produced all numerical results that are presented here. Many observations and conclusions are made during discussions within the research group.

Part I

Quantum Chromodynamics

1 QCD as a gauge field theory of the strong interaction

This chapter provides a compact description of QCD as the $SU(3)$ gauge field theory describing one of the four forces of nature: the strong force. The fundamental properties that are treated in this chapter are the basic building blocks of the description of high energy proton-proton collisions which will be the subject of Chapter 2.

1.1 Lie algebras as basis for gauge field theories

Mechanisms of the fundamental interactions find their origin in gauge symmetry. Gauge invariance is an important ingredient to construct the gauge field theories which form the main framework of the SM.

Gauge transformations can be interpreted as rotations of internal space; the underlying structure of a field. If θ^a is a phase angle and T^a is a generator of the Lie algebra, a local gauge transformation of a field $\psi(x)$ can be written as:

$$\psi(x) \rightarrow G(x)\psi(x) = e^{i\theta^a(x)T^a}\psi(x). \quad (1.1)$$

The number of generators T^a equals the dimension of the Lie algebra (these are the group elements) and the structure of the group defines their binary operation. The generators can be given in a matrix representation with dimension equal to this of the group. Due to this, generators of groups with dimension larger than one do in general not commute. The commutation relation between two generators writes [1]

$$[T^a, T^b] = if^{abc}T^c, \quad (1.2)$$

where f^{abc} stand for the fully antisymmetric structure constants of the Lie algebra. Groups with dimension one (as $U(1)$) are *abelian*. Lie algebras with higher dimensions have anti-commuting generators and are *non-abelian*. In $SU(2)$, the fully antisymmetric structure constant is the Levi-Cevita symbol ϵ^{abc} and the generators are the Pauli matrices σ^a . In $SU(3)$ the generators are the Gell-Mann matrices T^a , the three dimensional analogs of the Pauli matrices.

Equation (1.1) is a *local* transformation because the phase depends on the spacetime coordinate x . *Global* gauge transformations induce the same phase shift in each spacetime point. In order to construct a general and physical relevant theory, local gauge invariance is a stronger principle and is the symmetry that results in theories that involve gauge bosons (for the gauge field theories within the SM) which represent three out of the four fundamental forces of the universe.

It appears that a classical Lagrangian density of the form $\mathcal{L}(\psi, \partial\psi)$ is not invariant under local gauge transformations, because the transformation of the field ψ is represented as follows:

$$\partial^\mu(G\psi) = (\partial^\mu G)\psi + G(\partial^\mu\psi). \quad (1.3)$$

The term that contains the derivative of the gauge transformation G destroys the invariance of the Lagrangian under these transformations. This is solved by introducing a covariant derivative instead of the partial derivative. The covariant derivative D_μ that leads to a covariant Lagrangian is

$$D_\mu = \partial_\mu - igA_\mu^a T^a, \quad (1.4)$$

where the gauge fields A_μ^a are introduced. These are bosonic fields, for which the associated particles have integer spins and obey Bose-Einstein statistics. The Lagrangian is gauge invariant when the transformation of the fields is of the form:

$$A_\mu \rightarrow GA_\mu G^{-1} - \frac{i}{g}(\partial_\mu G)G^{-1}. \quad (1.5)$$

The Lagrangian can only depend on the covariant derivative of the fields and the fields itself: $\mathcal{L}(\psi, D_\mu\psi)$. As a result, the fields ψ (scalar fermion field) and A^μ (vector boson field) always interact. This is the basis for a gauge field theory.

There are as many vector fields A^μ as there are generators of a group. $U(1)$ is the symmetry group of quantum electrodynamics (QED), which is the abelian gauge field theory of electromagnetism. This Lie algebra has one group element which is associated with the gauge boson field B^μ . $SU(2)$ is the 3-dimensional symmetry group associated to the weak interaction¹ that has three gauge boson fields: W^\pm and Z . $SU(3)$ is the symmetry group of the strong interaction with dimension eight. Charges are related to these three interactions: electromagnetism is ruled by the electric charge, the weak interaction has weak hypercharge and the strong interaction is governed by *colour charge*. The photon is not charged, while the other gauge bosons are. There are eight gauge bosons (gluons) of the strong interaction. Gluons are sometimes associated to two colour carrying particles, while quarks (the strongly interacting fermions) only carry one colour.

As a consequence of the non-commutativity of the $SU(3)$ group elements, the transformation formula (1.5) in the limit for small angles ($\theta^a \ll 1$) differs for abelian and non-abelian groups. In the non-abelian case it is

$$A_\mu^a \rightarrow A_\mu^a + \frac{1}{g}\partial_\mu\theta^a - f^{abc}\theta^b A_\mu^c, \quad (1.6)$$

where the last term is the anti-symmetric part that is only present in non-abelian gauge theories. The second term can easily be recognized as the gauge transformation that is commonly used in electromagnetism (with θ the scalar potential and g the electric charge e).

1.2 The QCD Lagrangian

The field strength of QED, is represented by the field tensor $F_{\mu\nu} = \partial_\mu A_\nu - \partial_\nu A_\mu$, where A_μ stands for the photon field. A non-abelian gauge theory like QCD has a similar field strength tensor, only

¹This is not entirely true: it is a mix of $U(1)$ and $SU(2)$ that describes the weak interaction. Electromagnetism could be described by the $U(1)$ symmetry group only, but a more precise description is that the photon field is also contained in both groups.

there is more than one gauge field. In QCD there are eight gluon fields A_μ^a that are distinguished by their colour charge. Each gluon field has a field strength tensor similar to this from QED. In the non-abelian case, it contains a quadratic term in A_μ^a while in the abelian case it is purely linear in A_μ . The non-abelian field strength tensor equals

$$F_{\mu\nu}^a = \partial_\mu A_\nu^a - \partial_\nu A_\mu^a + gf^{abc}A_\mu^b A_\nu^c. \quad (1.7)$$

From the gauge symmetry group properties, a gauge invariant Lagrangian density which contains the dynamics of the Dirac field ψ (by using the Dirac equation), can be constructed and has the form

$$\mathcal{L}_{\text{YM}}(\psi, D_\mu\psi, \bar{\psi}, D_\mu\bar{\psi}) = \sum_f \bar{\psi}_f (i\not{D} - m_f) \psi_f - \frac{1}{4} F_{\mu\nu}^a F^{\mu\nu a}, \quad (1.8)$$

where $\not{D} = \gamma^\mu D_\mu$. The gamma matrices γ^μ appear in the Dirac equation (see [2]). This Lagrangian density is called the *Yang-Mills* Lagrangian and is a standard part of all non-abelian gauge field theories. In QCD, the Dirac fields describing quarks have three colour components:

$$\psi_f = \begin{pmatrix} \psi_f^{(g)} \\ \psi_f^{(b)} \\ \psi_f^{(r)} \end{pmatrix}, \quad (1.9)$$

where g, b, r are the colour indices. The index f in (1.8) is a flavour index and there is summed over all six quark fields (up, down, strange, charm, bottom and top). The Lagrangian only relies on symmetries and already contains an interaction term of ψ with A^μ and self-interaction terms of the gluon fields. A detailed calculation of the interaction terms can be found in [3].

To formulate a proper quantum field theory, probability amplitudes should be calculated using functional integrals. Moving from functions to functionals, from discrete spaces to fields and from matrix elements to functional integrals is sometimes called the second quantization procedure of a quantum field theory. In the path integral formalism (functional integral formalism) constructed by Feynman, the core idea is to take into account all possible trajectories for a certain process with a weight factor $e^{iS[A]}$, where S is the action: $S[A] = \int d^4x \mathcal{L}$. A propagation amplitude is written as

$$\mathcal{M} = \int \mathcal{D}A \exp \{iS[A]\} = \int \mathcal{D}A \exp \left\{ i \int d^4x \mathcal{L}(\psi, D_\mu\psi, \bar{\psi}, D_\mu\bar{\psi}) \right\}. \quad (1.10)$$

The use of the Yang-Mills Lagrangian of equation (1.8) in this functional integral leads to unphysical behavior, because for longitudinal fields ($A^\mu \sim ck^\mu$) the propagation amplitude diverges. In order to define a physical propagator for the gauge field, the *Faddeev-Popov method* [4] is used to fix the gauge. This means that the parts of the functional integral that are physically interesting and need to be taken into account only once, are isolated. By the insertion of the functional identity [3]

$$1 = \int \mathcal{D}\alpha(x) \delta(G[A^\alpha]) \det \left(\frac{\delta G[A^\alpha]}{\delta \alpha} \right), \quad (1.11)$$

where $A_\mu^\alpha = A_\mu^a + \frac{1}{g} D_\mu \alpha^a$ with D_μ the covariant derivative from (1.4) and α^a is a gauge motion field in the adjoint representation. The function $G[A]$ allows to select only physical configurations of the gauge field. In the Lorentz gauge it is $G[A] = \delta^\mu A_\mu^a(x) - \omega^a(x)$. In the functional integral of (1.10), the $\int \mathcal{D}\alpha$ can be factorized and put in front of the right-hand side. The $\omega^a(x)$ is a

Gaussian distribution and yields a gauge fixing term. The first term of the $G[A]$ function is more delicate to treat because due to this term, the determinant in (1.11) cannot be moved outside of the functional integral $\int \mathcal{D}A$. The argument of the determinant is

$$\frac{\delta G[A^\alpha]}{\delta \alpha} = \frac{1}{g} \partial^\mu D_\mu, \quad (1.12)$$

where D_μ is a function of the field A_μ . To get rid of the determinant in (1.11), it is represented by a functional integral over new anticommuting fields in the adjoint representation:

$$\det \left(\frac{1}{g} \partial^\mu D_\mu \right) = \int \mathcal{D}c \mathcal{D}\bar{c} \exp \left[i \int d^4x \bar{c} (-\partial^\mu D_\mu) c \right], \quad (1.13)$$

where c and \bar{c} are the new ghost fields. The ghost fields are not physical but they cancel the effects of unphysical timelike and longitudinal polarization states of the gluons. This contributes to the full Lagrangian of QCD together with the gauge fixing term:

$$\begin{aligned} \mathcal{L}_{\text{QCD}} &= \mathcal{L}_{\text{YM}} + \mathcal{L}_{\text{gauge fixing}} + \mathcal{L}_{\text{ghost}} \\ &= \sum_f \bar{\psi}_f (i \not{D} - m_f) \psi_f - \frac{1}{4} F_{\mu\nu}^a F^{\mu\nu a} - \frac{1}{2\xi} (\partial_\mu A^\mu)^2 - \bar{c}^a \partial_\mu D_{ac}^\mu c^c, \end{aligned} \quad (1.14)$$

where ξ is the gauge parameter from gauge fixing, c^a and \bar{c}^c are ghost fields and D_{ac}^μ is the covariant derivative in the adjoint representation:

$$D_{ac}^\mu = \partial^\mu \delta_{ac} + g f_{abc} A_b^\mu. \quad (1.15)$$

From the Lagrangian in (1.14), the Feynman rules of QCD can be determined. With these, all possible diagrams that include strong interactions can be drawn and the probability factors that are related to these diagrams (transition probability matrix elements) are calculable. The Feynman rules contain all possible vertices and the propagators of the colour charged fields. These follow directly from the Lagrangian which can be subdivided in $\mathcal{L} = \mathcal{L}_{\text{free}} + \mathcal{L}_{\text{interacting}}$. The vertices are the factors from the interacting part of the Lagrangian where multiple (more than two) fields are present in each term. The propagators are related to the factors from the free Lagrangian that only contains terms that are quadratic in the fields. A more detailed description of the calculation of vertices and propagators can be found in [3].

In table 1.1 all the propagators and vertices of strongly interacting particles are given. With these factors, tree level diagrams² can be calculated straightforwardly. With the calculation of radiative corrections, these rules are not sufficient and lead to divergences in the case of loop diagrams. One needs to renormalize the theory in order to obtain finite results from calculations for parameters and probability factors. The renormalization procedure is discussed in the next section.

1.3 Renormalization

Diagrams that contain loops have probability amplitudes that diverge. This is an ultraviolet (UV) type of divergence. If the number of amplitudes that are UV divergent is finite, the theory is

²Tree level diagrams these do not contain loops.

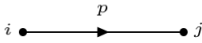
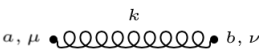
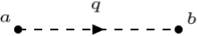
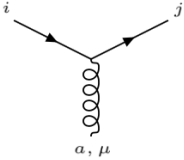
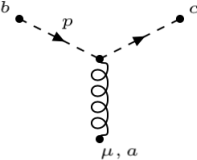
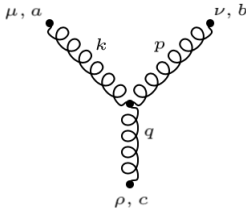
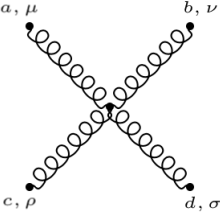
QCD Feynman Rules		
Quark propagator		$= \frac{i\delta^{ij}}{p - m + i\epsilon}$
Gluon propagator		$= \frac{i\delta^{ab}}{\kappa^2 + i\epsilon} \left[g^{\mu\nu} - (1 - \xi) \frac{\kappa^\mu \kappa^\nu}{\kappa^2} \right]$
Ghost propagator		$= \frac{i\delta^{ab}}{q^2 + i\epsilon}$
Quark-gluon vertex		$= -ig\gamma^\mu T_{ij}^a$
Ghost vertex		$= gf^{abc} p^\mu$
Triple gluon vertex		$= gf^{abc} (g^{\mu\nu}(k - p)^\rho + g^{\nu\rho}(p - q)^\mu + g^{\rho\mu}(q - k)^\nu)$
Quartic gluon vertex		$= -ig^2 \left[\begin{aligned} & f^{abe} f^{cde} (g^{\mu\nu} g^{\rho\sigma} - g^{\mu\rho} g^{\nu\sigma}) \\ & + f^{ace} f^{bde} (g^{\mu\rho} g^{\nu\sigma} - g^{\mu\nu} g^{\rho\sigma}) \\ & + f^{ade} f^{bce} (g^{\mu\rho} g^{\sigma\nu} - g^{\mu\sigma} g^{\rho\nu}) \end{aligned} \right]$

Table 1.1: Feynman rules for colour charged particles. Quarks are straight lines, gluons are wavy lines and ghost particles are dashed lines. Flavour indices are denoted by i or j , colour indices by $\{a, b, c, d, e\}$, colour indices are written as Greek letters $\{\mu, \nu, \rho, \sigma\}$. The four-momenta of the particles are written along the lines with Roman letters $\{k, p, q\}$. The Minkowski metric in the vertices and propagators on the right has the diagonal form $diag(1, -1, -1, -1)$.

renormalizable. This applies to QCD since there are seven primitive UV divergent amplitudes. These are diagrams that contain strongly interacting particles (quarks and gluons). The procedure of renormalization consists of three steps: 1) regularization of the divergent amplitudes, 2) renormalization using rescaling of all physical parameters and fields, and 3) removing the regulators and computing all the finite physical quantities.

1.3.1 Structure of renormalization

Dimensional regularization This is the most commonly used regularization method, because it preserves the physical symmetries like gauge- and Lorentz invariance. The key idea of dimensional regularization is to calculate the momentum space integral ($\int d^4k/(2\pi)^4$) of the probability amplitude (1.10) in general for d dimensions. For less than $d = 4$ dimensions, the UV divergence disappears and the integral is calculable analytically. Using $d = 4 - 2\epsilon$ (with $\epsilon \ll 1$, the UV divergence is translated to a pole in $1/\epsilon$ which makes the integral easier to solve with the use of complex analysis. This reduction of dimensions goes along with the introduction of a mass-scale parameter: the renormalization scale μ . The integration over d^4k transforms as

$$\frac{d^4k}{(2\pi)^4} \rightarrow (\mu^2)^\epsilon \frac{d^{4-2\epsilon}k}{(2\pi)^{4-2\epsilon}}. \quad (1.16)$$

Rescaling The fields and parameters we tried to calculate possessed infinities. Therefore, in the rescaling procedure, a bare field G_0 is written as the product of a renormalization constant Z (which contains the infinities) with the renormalized field G :

$$G_0(p_i, \alpha_0) = ZG(p_i, \alpha, \mu), \quad (1.17)$$

with $Z = 1 + \delta$, where δ represents the *counterterms* which contain the divergencies that are implemented in the $1/\epsilon$ pole. α_0 is the bare coupling strength of the corresponding gauge theory and α is the renormalized coupling strength (a further discussion on this can be found in section 1.4). All observable quantities depend on the coupling strength. All fields and parameters of the theory should be rescaled so that relations among the renormalization constants Z_i can be constructed. The Ward identity for QED (derived in [3], section 7.4) is an example of a relation among renormalization constants.

Calculation of physical parameters By calculating all the renormalization constants Z , all renormalized fields and parameters can be extracted from the bare quantities and the probability amplitudes become finite.

1.3.2 Example: gauge boson self energy renormalization

The gauge boson self energy can be formulated perturbatively by drawing all possible loop diagrams of the propagating gauge boson (i.e. photon or gluon). This is represented in figure 1.1 where the blob represents the sum over all possible loops. These loop diagrams can be calculated and renormalized. In the case of QED, the first order contribution to the photon self energy only consists of one diagram represented by a propagating photon containing one fermion loop as

which is the series expansion of:

$$D = D_0 \frac{1}{1 - \Pi(q^2)}. \quad (1.23)$$

By entering the photon propagator as $D = e^2/q^2$, a relation between the bare electric charge e_0 and the renormalized charge e can be found:

$$\begin{aligned} \frac{e_0^2}{q^2} &\rightarrow \frac{e_0^2}{q^2} \frac{1}{1 - \Pi(q^2)} \\ &\simeq \frac{1}{q^2} \frac{e_0^2}{1 - \Pi(0)} \frac{1}{1 - [\Pi(q^2) - \Pi(0)]}, \end{aligned} \quad (1.24)$$

where the rescaling with the structure of equation (1.17) is:

$$\frac{e_0^2}{1 - \Pi(0)} \equiv e^2. \quad (1.25)$$

The dependence of the coupling on q^2 as in equation (1.24) is referred to as the running of the electric coupling α .

The general structure of this is equivalent for the renormalization of the strong coupling α_s although more diagrams have to be calculated and the function $\Pi(q^2)$ becomes more complicated. The running of the strong coupling is discussed in more detail in section 1.4.

1.3.3 Renormalization group

The renormalization procedure implies that all the parameters of the quantum field theory become scale- or distance-dependent. In contrast, the QCD Lagrangian does not contain scale dependencies. It can be argued that physical quantities therefore do not depend on the choice of the scale μ . A technical derivation of this is Wilson's approach and can be found in [3] (chapter 12). This way of describing renormalization results in continuously generated transformations that leave the Lagrangian invariant. Together these are referred to as the renormalization group (RG). It does, however, not have the mathematical structure of a group.

With the condition that a bare physical quantity (denoted by G_0) is independent of the renormalization scale μ , one can describe the μ -dependence of the parameters in the theory. The renormalization group equation (RGE) states that a bare quantity is μ -independent:

$$\frac{dG_0}{d \ln \mu^2} = 0. \quad (1.26)$$

With the relation between the renormalized and bare quantities given in (1.17) this becomes

$$\frac{Z \cdot G}{d \ln \mu^2} = 0. \quad (1.27)$$

Basic differential algebra on (1.27) results in

$$\Rightarrow \frac{\partial G}{\partial \ln \mu^2} + \frac{\partial G}{\partial \alpha} \frac{\partial \alpha}{\partial \ln \mu^2} + G \frac{\partial \ln Z}{\partial \ln \mu^2} = 0. \quad (1.28)$$

With the definitions of the RG β -function:

$$\beta(\alpha) \equiv \frac{\partial \alpha}{\partial \ln \mu^2}, \quad (1.29)$$

and the RG γ -function:

$$\gamma(\alpha) \equiv \frac{\partial \ln Z}{\partial \ln \mu^2}, \quad (1.30)$$

(1.28) becomes:

$$\left[\frac{\partial}{\partial \ln \mu^2} + \beta(\alpha) \frac{\partial}{\partial \alpha} + \gamma(\alpha) \right] G(p_i, \alpha, \mu) = 0. \quad (1.31)$$

G can be measured at a physical scale $\mu = Q$ and the parameters can be rescaled by Q so that $G(p_i, \alpha, \mu) \rightarrow F(x_i, \alpha, t)$ and (1.31) becomes:

$$\left[-\frac{\partial}{\partial t} + \beta(\alpha) \frac{\partial}{\partial \alpha} + \gamma(\alpha) \right] F(x_i, \alpha, t) = 0, \quad (1.32)$$

which is the so-called *Callan Symanzik equation* [3]. The solution to this partial differential equation is of the form:

$$F(t, \alpha) = F(0, \alpha(t)) e^{\int_0^t dt' \gamma(\alpha(t'))}. \quad (1.33)$$

There are two important consequences of this solution. Firstly, it implies that the coupling strength α depends on the scale μ . This leads to the breaking of scale invariance which is a property of the parton model proposed by Björken and Feynman. In chapter 2 this is discussed in more detail. The second implication is that the exponential factor in (1.33) is a modification of the intuitive/engineering dimension because the physical quantity is proportional to:

$$\exp \left\{ \int_0^t dt' \gamma(\alpha(t')) \right\} \sim e^{t\gamma} \sim \left(\frac{Q^2}{\mu^2} \right)^\gamma. \quad (1.34)$$

This factor is a *resummation* factor to all orders, because an exponential function can be expressed as $e^x = \sum_i x^i$, which is a perturbation series to all orders. The factor from (1.34) therefore contains all powers of $\alpha \ln(Q^2/\mu^2)$. Resummation is an important topic in this thesis. First, the coupling factor α (and the analogous factor in QCD α_s) that has been mentioned many times by now is discussed in more detail.

1.4 The running coupling α_s and Λ_{QCD}

In gauge field theories, the coupling strength is scale (μ) dependent. This is referred to as a running coupling: both α (the coupling strength of QED) and α_s (the coupling strength of QCD) are running. At large collider energies nowadays, both parameters are small. The electromagnetic coupling at 90 GeV (roughly the Z boson mass and a common interaction energy of the LEP, Large Electron-Positron collider [6]) is $\alpha \sim 1/128$ and the strong coupling at 90 GeV is $\alpha_s \sim 0.11$. When these parameters are smaller than 1, they are well suited for perturbation theory. Quantities can then be expressed as a power series in the small parameter α or α_s . If these parameters are of order $\mathcal{O}(1)$ or larger, this cannot be done and quantities are not calculable perturbatively using these parameters. This is a crucial point that makes calculations in QCD much more complicated

than in QED: QCD has a decreasing coupling with the energy while the QED coupling increases. In collider processes, interactions at low energy scales are present and are not negligible. In QED this is not causing any problems because α is much smaller than 1, but it is problematic in QCD as α_s is very large. Low order terms in the perturbation series are not sufficient and one has to encounter higher order terms. The perturbation series therefore have to be resummed.

The dependence of the strong coupling on the scale μ originates from the dimensional regularization procedure. The exact dependence can be expressed in terms of the perturbative RG β -function given in (1.29), which can be written as a series expansion:

$$\beta(\alpha_s) = -\alpha_s^2 \sum_{n=0}^{\infty} \beta_n \alpha_s^n \quad (1.35)$$

$$= -\beta_0 \alpha_s^2 - \beta_1 \alpha_s^3 - \beta_2 \alpha_s^4 + \mathcal{O}(\alpha_s^5). \quad (1.36)$$

The determination of the coefficients β_n of the RG β -function requires the calculation of loop diagrams to order $(n+1)$ to obtain the renormalization constants Z_i . The β -function equals the derivative of the renormalized strong coupling which is proportional to a linear combination of the counterterms δ_i . With the calculation of the 1-loop diagrams, one obtains the zeroth order coefficient of the β -function:

$$\beta_0 = \frac{1}{12\pi} (11C_A - 4T_R N_f), \quad (1.37)$$

where C_A is the Casimir invariant that equals the number of colours in the theory, T_R is the trace invariant and N_f is the number of quark flavours. In the SM these parameters are $C_A = 3$, $T_R = 1/2$, $N_f = 6$ [7]. The RG equation can be written (only if α_s is sufficiently small) as

$$\frac{\partial \alpha_s}{\partial \ln \mu^2} = \beta(\alpha_s) \approx -\beta_0 \alpha_s^2. \quad (1.38)$$

Integrating this differential equation yields:

$$\alpha_s(\mu) = \frac{\alpha_s(\mu_0)}{1 + \beta_0 \alpha_s(\mu_0) \ln(\mu^2/\mu_0^2)}. \quad (1.39)$$

In fact, for a good description in the region where α_s becomes larger than 1, the running of the strong coupling cannot be described by only taking into account low order coefficients of the β -function. The renormalization group approach in this non-perturbative regime is not sufficient. Since β_0 for QCD (for $SO(3)$) is negative, for $\mu > \mu_0$

$$\alpha_s(\mu) < \alpha_s(\mu_0), \quad \text{for } \mu > \mu_0. \quad (1.40)$$

This phenomenon is called *asymptotic freedom*, which means that the strength of the strong coupling decreases with increasing energy or decreasing distances. On the other hand, at long distances or low energies, α_s diverges. In those regimes, colour charged particles are strongly coupled. This phenomenon is called *confinement*. The decrease of the coupling strength with the energy can be physically related to virtual emissions of gluons and quarks that respectively screen and anti-screen the colour charge or coupling strength. The first term of the β -function given in (1.37) represents the anti-screening due to gluon loops and the second term represents the screening due to quark/anti-quark pairs. Eventually the anti-screening effect dominates. A detailed description on asymptotic freedom and confinement can be found in [8]. The running

coupling can be measured; measurements from many experiments are combined in one plot which is shown in figure 1.2.

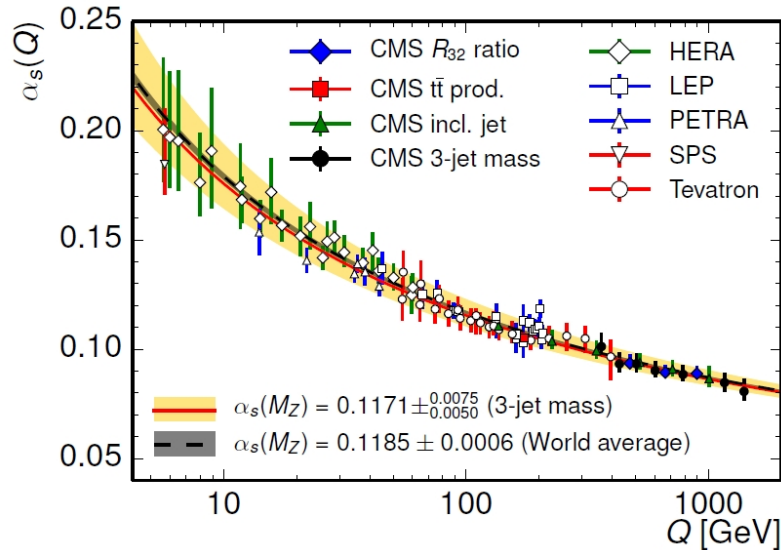


Figure 1.2: Measurements of α_s at different energies from experiments at the HERA collider (Hadron-Elektron-Ringanlage), CMS (Compact Muon Solenoid) experiment at the LHC, LEP, Tevatron, SPS (Super Proton Synchrotron) and PETRA (Proton-Electron Tandem Ring Accelerator). These results confirm the running of the strong coupling [9].

The expression in equation (1.39) blows up when the denominator becomes zero. There is a so-called Landau pole in μ which is defined as Λ_{QCD} and can be derived as follows:

$$0 = 1 + \beta_0 \alpha(\mu_0) \ln \left(\frac{\Lambda_{QCD}^2}{\mu_0^2} \right) \quad (1.41)$$

$$\Rightarrow \Lambda_{QCD}^2 = \mu_0 \exp \left\{ -\frac{1}{\beta_0 \alpha_s(\mu_0^2)} \right\}. \quad (1.42)$$

In fact this parameter is RG invariant, so it does not depend on the choice of μ_0 . Therefore it is a universal energy scale and property of QCD. It takes the value $\Lambda_{QCD} \simeq 200 \text{ MeV} \simeq 1 \text{ fm}^{-1}$. In case of $\mu \gg \Lambda_{QCD}$, the strong coupling $\alpha_s \ll 1$ so that quantities can be expressed as power series in α_s . This is the perturbative regime which can be associated with the region of asymptotic freedom. When $\mu < \Lambda_{QCD}$ the perturbative diagrammatic interpretation of observables is not valid. The coupling strength is much larger than one, and quarks are confined in *hadrons*. Hadrons are (non-elementary) particles that are still not fully understood because the dynamics of the hadronic constituents are non-perturbative. The sequel of this thesis discusses how the structure of hadrons is studied, which formalisms exist and the current developments to improve the description of hadronic dynamics. Especially, the focus lies on the study of the proton (one of many hadrons) because it is the most stable hadron in the universe and is used in scattering experiments.

2 Application of QCD to particle collision processes

Halfway the twentieth century, a "zoo" of hadrons were discovered. Physicists tried to find an elegant and simple structure to describe the hadrons which can be subdivided in *mesons*: hadrons containing two valance quarks (a quark and an anti-quark), and *baryons*: hadrons containing three valance quarks. The theory which was then proposed to classify these hadrons was given the name *Eightfold way* [10]. In this approach, the hadrons were organised in baryon and meson spin-multiplets in which the constituent particles have a different strangeness (number of s-quarks) and electric charge. The multiplets of hadrons are representations of the symmetry group $SU(3)$ (in that time considered as the symmetry of the universe) and these led to the quark model. The three light quark flavours *up*, *down* and *strange* (u, d, s) were predicted by using this model.

One problem remained with the Eightfold way description: the wavefunctions of hadrons that contained a spacial, spin and flavour part were not anti-symmetric. To construct wavefunctions that are anti-symmetric, a *colour* wavefunction with corresponding colour quantum number has to be introduced so that the total anti-symmetric wavefunction would satisfy the Pauli exclusion principle. The number of colours has been measured and equals $N_C = 3$. Hadrons are colour neutral particles; this corresponds to the fact that baryons are built from three different coloured quarks and mesons consist of a colour and anti-colour quark state.

Several years after the construction of the Eightfold way and the quark model, it became clear that quarks are confined and cannot be observed as free particles. With the application of the quantum gauge field theory of $SU(3)$, this confinement effect and asymptotic freedom at high energies can be properly described (as in section 1.4).

2.1 The theory behind particle physics experiments

In order to study the constituents of the proton, one cannot make use of ordinary microscopes that use photons with wavelengths of the order of (~ 400 - 700 nm) because the dimensions of the proton is of the order of a femtometer (10^{-15} m). To probe these short distances, the probing particles are accelerated to large energies. In the HERA collider at DESY (Deutsches Elektronen Synchrotron, Hamburg), electrons were accelerated to probe protons. The process where a high energetic photon is exchanged between the electron and the proton's constituent provides information about the proton's structure. In the LHC, protons are collided with protons and high energetic gauge bosons (i.e. photons, gluons, W/Z bosons) are interchanged. Also more complicated higher order processes with multiple gauge bosons can occur. The probability for higher order processes that

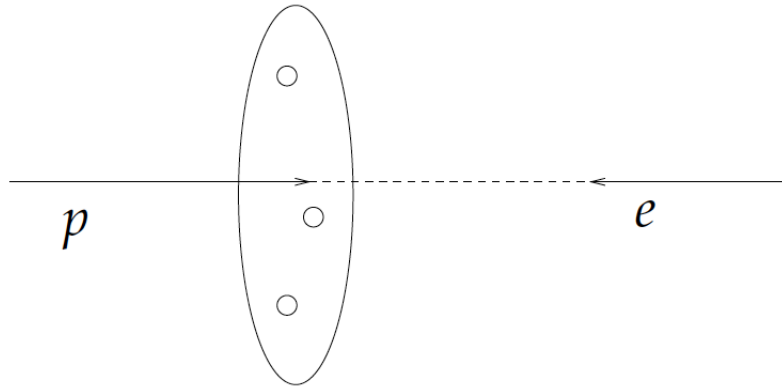


Figure 2.1: The scattering of a proton and electron in the infinite momentum frame.

involve multiple gauge bosons is very small due to the higher powers of coupling factors (these come from the vertex factors) which are smaller than 1. Therefore it is valid to a large extent to only consider the interchange of a single vector boson. The momentum transfer carried by the intermediate boson is indicated with Q . When $Q \gg \Lambda_{QCD}$ ($\alpha_s \ll 1$) the process is referred to as a *hard scattering process*. The remaining partons in the proton are supposed to not take part in the hard scatter process. In this thesis, only single parton interactions are considered. This means that only one parton out of a proton takes part in the hard interaction. In the case of proton-proton collisions, two partons interact: one of each proton. In extensions, multi parton interactions (MPI) can occur. These kind of interactions, where two hard scattering events take place, will become more frequent with the future increasing of the LHC's beam energy (\sqrt{s}) and with a higher rate of collisions per second which is labeled by the luminosity (\mathcal{L}).

Nowadays the large amount of statistics and high precision tracking systems in particle collision experiments provide a picture of the probabilities for all processes that are known or aimed to be found. These probabilities are *cross sections* (denoted by σ), with units of squared meters (m^2)³. Cross sections for certain processes are calculated theoretically and compared with experimental measurements. In high energetic particle collisions, the calculation of the cross section is sophisticated and it is not possible with exact precision using perturbation theory. This is the result of soft (low energetic) dynamics where QCD becomes non-perturbative. Other techniques are necessary to calculate these non-perturbative effects. A light spark in the darkness is a mathematical formalism in which the hard scattering can be separated fully from the low energetic regime and perturbative calculations are still valuable for the high energetic interactions.

2.2 Factorization

The key principle that is used to describe processes of colliding hadrons with leptons and hadrons with hadrons is the separation of long distance (hadronic) and short distance (partonic) dynamics. This principle is called *factorization*. With this, the full partonic factor and the evolution of the hadronic factor(s) can be calculated with perturbation theory. Observables (measurable quantities)

³A more convenient unit is the *barn* ($1b = 10^{-28}m^2$)

can be expressed perturbatively as a power series in α_s :

$$Y(\alpha_s, Q) = \sum_{n=0}^{\infty} \alpha_s^n Y^{(n)}(Q), \quad (2.1)$$

The proton-proton (pp) collision process is of interest in this thesis, but first the proton-electron collision process will be treated. This process has been studied with accelerators before LHC studied pp collision processes. Electron-proton collisions give much cleaner signals which makes them easier to study. In the next subsections, factorization will be described in both ep (DIS) and pp (Drell-Yan) processes.

2.2.1 Deep inelastic electron-proton scattering

Deep inelastic electron-proton scattering (DIS) is a broadly studied process both theoretically (e.g. [8]) and experimentally with HERA. The advantage of colliding protons with electrons is that the signal from a collision is much more clean in comparison to that from pp collisions. A disadvantage is that with electrons, the interaction energies in electron-proton collisions are smaller than in pp collisions because electrons lose much more energy in the form of synchrotron radiation (emission of photons) than protons [11]. The energy loss due to synchrotron radiation is inverse proportional to the mass of the particle. The mass of the electron is much smaller than this of the proton $m_e \sim 10^{-3}m_p$, which causes the stronger radiation. To reach higher energies, two beams of protons are used (as in the LHC), but detection of events and the tracking of the hard scattering is more complicated. With two proton beams, many hard scattering processes are possible. Widely studied examples of processes in pp collisions are neutral vector boson production, which is known as the Drell-Yan (DY) process (discussed in section 2.2.2), and Higgs production.

In the infinite momentum frame for DIS as pictured in figure 2.1, the electron is facing the proton head-on and will interact with only one parton carrying a momentum p being a longitudinal momentum fraction x (between 0 and 1, since it is a fraction) of the proton's momentum P . The transverse momentum of a parton (k_{\perp}) could theoretically take any value since partons can radiate other partons (like electrons radiate photons); momentum conservation should still be guaranteed. The hard scattering interaction is represented as the exchange of a virtual photon with four-momentum q_{μ} with space-like virtuality (the amount that the photon is off its mass shell)

$$Q^2 \equiv -q^{\mu}q_{\mu}. \quad (2.2)$$

The DIS process can be sketched schematically as in figure 2.2. Here the proton and the remnant of the proton after collision with the electron are drawn. This process is inelastic because the remnant of the proton hadronizes.

Due to large velocity ($v \approx c$), the proton is Lorentz-contracted in the longitudinal direction. The interactions among partons are therefore happening time-dilated with respect to the hard scattering interaction. Consequently, the hard scattering and the dynamics in the protons can be separated. The partonic hard scattering event is not sensitive to the long time dynamics in the proton, therefore it is *infrared safe* and calculable perturbatively. The hadronic interactions involve low energy radiation which implies the appearance of non-perturbative effects. Together, these two parts of an event form the cross section. The factorization of the total DIS cross section (σ_{e-p}) can be written as the convolution of a function depending on the hard scale Q and large

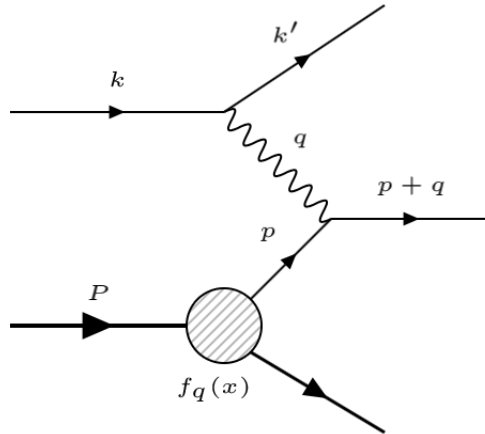


Figure 2.2: Deep inelastic scattering with $p = xP$ the initial longitudinal parton momentum, $Q^2 = -q^2$ the photon virtuality, k the initial and k' the final electron momentum and $f_q(x)$ the probability distribution function of partons in the proton.

parton momenta: $C(Q, \text{parton momenta} > \mu_F)$, and a function depending on a hadronic mass scale (m) and soft momenta: $f(m, \text{parton momenta} < \mu_F)$. The introduced factorization scale μ_F is arbitrary. The factorization scale separates hard and soft momenta and necessarily lies between the hard scale Q and the soft scale m . The cross section of any process could be factorized schematically as:

$$\sigma(Q, m) = C(Q, \text{parton momenta} > \mu_F) \otimes f(m, \text{parton momenta} < \mu_F). \quad (2.3)$$

The DIS cross section can be factorized in a partonic matrix element σ_{e-i} (cf. the $C(Q)$ coefficient) which is related to the hard scattering event and a hadronic soft distribution function f_i that represents low energy dynamics of parton flavour i as follows:

$$\sigma_{e-p}^{(\text{DIS})}(x, Q, m) = \sum_{i=q,g} \int_x^1 dz \sigma_{e-i} \left(\frac{x}{z}, Q, \mu_F \right) f_i(z, \mu_F, m) \left(1 + \mathcal{O} \left(\frac{\Lambda_{QCD}^2}{Q^2} \right) \right). \quad (2.4)$$

This is the collinear factorization of the DIS cross section. Why this is called "collinear" is explained in section 3.2. It agrees with the general form of factorization in equation (2.3) since the integral specifies the convolution of the partonic and hadronic function. Only the corrections of order Λ_{QCD}^2/Q^2 cannot be factorized in hard and soft parts because these result from hadronization effects that occur at long distances. There is interference between the initial state and final state of the process which therefore cannot be described with full factorization. For $Q^2 < \Lambda_{QCD}^2$ the long time dynamics cannot be neglected anymore.

Since there is no interference between different partons i as can be seen in equation (2.4), the so-called *parton distribution functions* (PDFs) f_i are universal functions. This means that they are independent of the process and can be extracted from experiment at certain energy scales.

The DIS differential cross section can be written differently using the observable structure functions that appear in the leptonic and hadronic tensor [12]. It has the form

$$\frac{d\sigma^{(\text{DIS})}}{dx dQ^2} = \frac{4\pi\alpha^2}{xQ^4} \left(\left(1 - y + \frac{y^2}{2}\right) F_2(x, Q^2) - \frac{y^2}{2} F_L(x, Q^2) \right), \quad (2.5)$$

where $y = \frac{q \cdot p}{k \cdot p}$ is the rapidity and $F_L = F_2 - 2xF_1$ (e.g. [8]). These structure functions have similar structures as the total cross section in equation (2.4):

$$F_k(x, Q^2) = \sum_i \int_x^1 dz C_{ki}(x/z, Q^2/\mu^2) f_i(z, \mu^2) + \mathcal{O}\left(\frac{\Lambda_{QCD}^2}{Q^2}\right), \quad (2.6)$$

where the factorization scale is denoted by μ without index F . With a Mellin transformation [13] this simplifies to a normal product instead of a convolution:

$$F_{k,N}(Q^2) = \sum_i C_{ki,N}(Q^2/\mu_F^2) f_{i,N}(\mu_F^2). \quad (2.7)$$

This function is completely factorized, independent on the value of Q^2 . The μ dependence of the factorized functions in both (2.4) and (2.7) implies the breaking of scale invariance as discussed in section 1.3.3. The independence on μ_F of the structure functions F_k and the total cross section σ_{e-p} implies evolution in the factorization scale μ_F of the PDFs f_i . This is discussed further in section 2.3.

2.2.2 Drell-Yan

A Drell-Yan process is the annihilation of two quarks which produces a Z boson or virtual photon (Z/γ). The vector boson decays in a di-lepton pair. The leading order (LO) DY process is purely a QED effect, because there are no gluons involved. This LO hard interaction can be figured simply with a tree diagram as shown in the right part of figure 2.3. On the left side of this diagram, the incoming protons and outgoing remnants are drawn. The parton lines that interact at the hard scattering meet at the Z/γ -vertex.

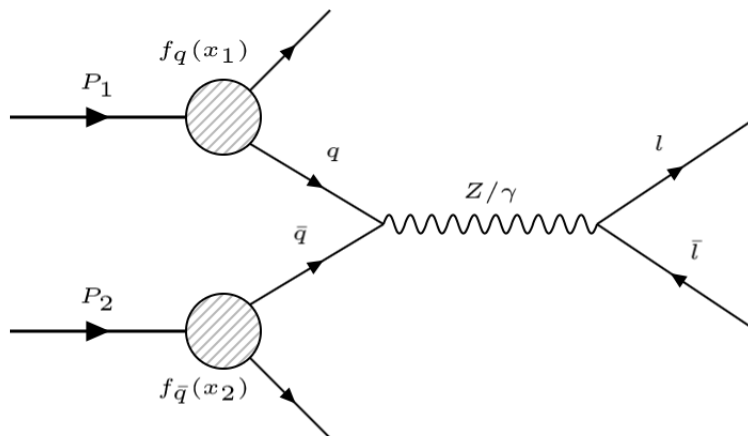


Figure 2.3: Drell-Yan process. The exchanged neutral vector boson has four-momentum q , interacting partons have longitudinal momenta $x_1 P_1$ and $x_2 P_2$ with P_1 and P_2 the momenta of the incoming protons.

The center-of-mass energy is equal to the square root of Mandelstam variable s which is defined as: $\sqrt{s} = \sqrt{(P + P')^2}$. The total DY cross section can be factorized similar to (2.4) with partons

a and b carrying longitudinal momentum fractions ξ_1 and ξ_2 as

$$\sigma^{(DY)}(\sqrt{s}, Q^2) = \sum_{a,b} \int d\xi_1 d\xi_2 H_{ab}(\xi_1 \xi_2 s, Q^2, \mu) f_a(\xi_1, \mu) f_b(\xi_2, \mu) + \mathcal{O}\left(\frac{\Lambda_{QCD}^2}{Q^2}\right). \quad (2.8)$$

For a good description, not only the leading order matrix element $\hat{\sigma}$ (which is purely an electroweak factor) but also higher order diagrams where QCD radiation of quarks and gluons is involved, need to be taken into account. The hard scattering function H_{ab} includes these higher order diagrams, hence it is expansionable in a power series of α_s :

$$H_{ab} = \frac{\sigma^{(0)}(Q^2, \alpha(\mu))}{s} \left(1 + \sum_{n=1}^{\infty} H_{ab}^{(n)} \alpha_s^n(\mu) \right), \quad (2.9)$$

where $\alpha(\mu)$ is the QED coupling strength. The leading order Drell-Yan matrix element giving the probability for the hard process on the right of figure 2.3 is

$$\sigma^{(0)} = \frac{4\pi^2 \alpha^2(\mu)}{9Q^2}. \quad (2.10)$$

The DY cross section contains two non-perturbative parton distribution functions, one for each proton. These have to be extracted from measurements. Though, knowing a PDF at a certain scale μ_0 larger the QCD scale Λ_{QCD} , it should be possible to obtain the PDF at any other scale because of renormalization group invariance. Observable quantities as structure functions and cross sections are independent of the scale μ which thus results in the evolution of the PDFs. The next section discusses how the evolution could be described.

2.3 DGLAP evolution equations

The RGE given in (1.26) applies to observable quantities like structure functions. Together with the factorized form of the structure function as given in (2.7), leaving the parton flavour indices out for the moment, the RGE becomes:

$$\frac{dF}{d \ln \mu^2} = 0 \Rightarrow \frac{d}{d \ln \mu^2} [C(Q, \mu) f(m, \mu)] = 0. \quad (2.11)$$

This yields Callan Symanzik equations for the hard scattering coefficients C and the parton densities f :

$$-\frac{1}{C} \frac{dC}{d \ln \mu^2} = \frac{1}{f} \frac{df}{d \ln \mu^2} = \gamma(\alpha_s(\mu)) \quad (2.12)$$

with γ expansionable in powers of α_s : $\gamma = \sum_{j=1}^{\infty} b_j \alpha_s^j$. This term is the analogue of the separation constant which appears with the separation of variables of an ordinary differential equation (ODE). Equation (2.12) is not an ODE because the terms depend on remaining scales Q and m . Integrating (2.12) over $\ln \mu^2$ gives for the PDF f :

$$f(\mu) = f(\mu_0) \underbrace{\exp \left\{ \int_{\mu_0}^{\mu} \frac{d\mu'}{\mu'} \gamma(\alpha_s(\mu')) \right\}}_{\text{scaling violation factor}}. \quad (2.13)$$

The upper scale of the evolution mostly equals the scale of the hard interaction Q , but here it is generalized with μ . Logarithmic scaling violation of parton distribution functions arises in (2.13) and originates from the anomalous dimension and the strong coupling. This exponential factor resums large logarithms, which can already be seen assuming that the strong coupling is constant:

$$\begin{aligned} \exp \left\{ \int_{\mu_0}^{\mu} \frac{d\mu'}{\mu'} \gamma \right\} &\simeq \exp \left\{ b\alpha_s \ln \frac{\mu}{\mu_0} \right\} \\ &= \sum_{n=1}^{\infty} \frac{1}{n!} b^n \alpha_s^n \ln^n \left(\frac{\mu}{\mu_0} \right). \end{aligned} \quad (2.14)$$

Resummation of this type of logarithms is *Renormalization Group (RG) resummation* for hard scattering scales μ that are much larger than the hadronic scale $\mu_0 \simeq 1$ GeV.

Equation (2.12) can be rewritten in more detail using the flavour indices of the parton distribution function. The anomalous dimension is then represented as matrix kernel where the diagonal elements are kernels for evolution with flavour conservation and non-diagonal elements represent the possibility of flavour changes. It becomes

$$\frac{d}{d \ln \mu^2} f_a(\mu) = \gamma_{ab}(\alpha_s(\mu)) f_b(\mu). \quad (2.15)$$

This is an evolution equation in Mellin space (f and γ have the Mellin index N) which we can transform back to x -space using an anti-Mellin transform (e.g. [13]). The PDF and anomalous dimension transform as follows:

$$f_{N,a}(\mu) = \int_0^1 dx x^{N-1} f_a(x, \mu), \quad (2.16)$$

$$\gamma_{ab}(\alpha_s) = \int_0^1 dx x^{N-1} P_{ab}(x, \alpha_s), \quad (2.17)$$

where $P_{ab}(x, \alpha_s)$ are the Dokshitzer-Gribov-Lipatov-Altarelli-Parisi (DGLAP) splitting functions. These are perturbative functions and commonly depend on the splitting variable z :

$$P_{ab}(\alpha_s, z) = \sum_{n=1}^{\infty} \left(\frac{\alpha_s}{2\pi} \right)^2 P_{ab}^{(n-1)}(z). \quad (2.18)$$

The leading order (LO) splitting function $P_{ab}^{(0)}$ has the interpretation of a probability for parton b with momentum fraction x_b to continue as parton a with momentum fraction x_a and emit a parton with momentum fraction $x_b - x_a = x_b(1 - z)$. This single emission process is shown in figure 2.4.

The four leading order splitting diagrams with corresponding splitting functions are shown in table 2.1. The DGLAP splitting functions are known up to high orders nowadays (in [14] they are given up to N⁴LO) and a high level of precision calculations can be reached with this. The plus prescription inside the splitting functions is defined as

$$\int_0^1 dz \varphi(z) g(z)_+ = \int_0^1 dz [\varphi(z) - \varphi(1)] g(z) \quad (2.19)$$

and obeys the property $\int_0^1 dz [g(z)]_+ = 0$.

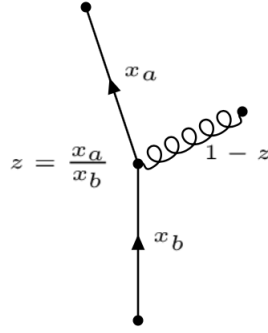


Figure 2.4: Single parton splitting of parton b with momentum fraction x_b in parton a with fraction x_a and parton c with momentum fraction $x_b(1 - z)$.

Splitting functions $P_{ab}^{(0)}$			
$P_{qq}:$ $= C_F \left(\frac{1+z^2}{1-z} \right)_+$	$P_{qg}:$ $= T_R (z^2 + (1-z)^2)$		
$P_{gq}:$ $= C_F \frac{1+(1-z)^2}{z}$	$P_{gg}:$ $= 2C_A \left\{ \left(\frac{1}{1-z} \right)_+ - z + \frac{1-z}{z} \right\} + \left(\frac{11}{6}C_A - \frac{2}{3}T_R N_f \right) \delta(1-z)$		

Table 2.1: Leading order DGLAP splitting functions that represent probabilities for a parton to split in two partons. Colour factors come from $SU(3)$ group properties and take the values: $T_R = \frac{1}{2}$, $C_A = N_C$, $N_f = 6$ and $C_F = \frac{N_C^2 - 1}{2N_C} = \frac{4}{3}$.

QCD momentum sum rule With the physical picture of partons that carry a fraction x of the proton, one can construct a useful identity for splitting functions which is called the *momentum sum rule*. The ansatz to derive this is that all the partons together carry the full momentum of the proton. In other words, the sum of momentum fractions over all partons, weighed with the parton distribution functions, equals one:

$$\int_0^1 dx x \sum_i f_i(x, \mu^2) = 1. \tag{2.20}$$

Here, the momentum sum rule that follows from (2.20) is given (a full derivation can be found in [15]):

$$\sum_a \int_0^1 dz z P_{ab}(z, \mu^2) = 0. \tag{2.21}$$

2.3.1 The evolution equations

The anti-Mellin transform of equation (2.15) to x -space results in the DGLAP evolution equations that incorporate the DGLAP splitting functions and the momentum weighted PDFs $\tilde{f}_a(x, \mu^2) = x f_a(x, \mu^2)$:

$$\frac{\partial \tilde{f}_a(x, \mu^2)}{\partial \ln \mu^2} = \sum_b \int_x^1 dz P_{ab}(\alpha_s(\mu^2), z) \tilde{f}_b\left(\frac{x}{z}, \mu^2\right). \quad (2.22)$$

These integro-differential equations can be solved analytically at fixed order when these splitting functions and a PDF at initial scale μ_0 are known. The PDF is evolved from the initial scale μ_0 to the final scale μ . A fixed order DGLAP calculation in perturbation theory is not sufficient to describe all the components of a collision process. A process known as *soft gluon emission* destroys the ordering of the terms in the perturbation series in powers of α_s . To describe this effect, the PDFs need to get transverse momentum dependence. This will be explored further in chapter 3.

DGLAP incorporates RG resummation to resum large logarithms of the form $\ln(\mu/\mu_0)$. This is sufficient when there is only one hard scale to consider. When multiple scales are involved and are significantly larger than the hadronic scale (~ 1 GeV), additional logarithms arise and other kinds of resummation are needed on top of the RG resummation. In this respect, new formalisms have been developed with the goal to apply them to processes that are studied at particle colliders. Chapter 3 motivates more concretely what new formalisms need to implement and will also describe the effect it has on the description of PDFs. In the chapters 4, 5 and 6, three methods that describe processes with multiple hard scales are discussed in order to compare them in chapters 7 and 8.

3 Transverse momentum dependent parton distribution functions

The DGLAP equations (2.22) are commonly used to construct collinear PDFs $f(x, \mu)$ which only depend on Björken x and the factorization scale μ . With these functions, one has a one-dimensional picture of the proton. There are certain regimes and observables for which the use of collinear PDFs is not sufficient: it is then necessary to include the dynamics of partons in the plane transverse to the proton's direction to have a three-dimensional picture of the proton. The transverse momentum dependence of parton distribution functions should thus be uncovered. There are several approaches to do this. Some of these are discussed in detail in chapters 4, 5 and 6. First it is motivated why this dependency is needed.

3.1 Motivation

Application of collinear factorization as in (2.3) resulted in large progress within particle physics. Because of this, the calculation of observables in large domains is possible and the use in data analysis led to discoveries of new particles, decay channels and information on the structure of the proton. However, there are certain kinematic regions where only finite order perturbative (DGLAP) calculations do not work. Emissions of soft gluons that possess very small transverse momentum lead to large logarithms at all orders in the perturbation series in α_s . This series therefore needs to be resummed. In deep inelastic scattering and Drell-Yan (which were introduced in chapter 2) the kinematic regions of the phase space where resummation is necessary are respectively the asymptotic high energy region (large s) and the low transverse momentum region (small q_\perp).

3.1.1 Structure functions from DIS

In the case of DIS, the use of collinear factorization is not sufficient to obtain structure functions of the proton in the limit of $\sqrt{s} \rightarrow \infty$. For fixed momentum transfer Q they scale like $1/s$. With the current high energies of colliders and the prospects of future collider energies, more events at low x contribute to the measurements. At small longitudinal momenta, the transverse momentum of the partons becomes relatively more important. Without the inclusion of these degrees of freedom, a fixed order perturbative calculation is not precise as can be seen in figure 3.1. The uncertainty envelopes of these collinear gluon distributions at LO, NLO and NNLO are large and do not overlap. Physically the contributions to the low x regime come from soft gluon emissions which

are present at any order in α_s . Terms in the perturbative series expansion of the DIS structure functions are of the form

$$[\alpha_s \ln(\sqrt{s}/Q)]^k, \quad (3.1)$$

where α_s is considered to be small but the logarithms can become very large in the case of a large centre of mass energy \sqrt{s} . These terms have to be resummed to perform correct perturbative calculations. The resummation of these logarithms is not implied in the DGLAP equations. Formalisms that are able to resum these terms are BFKL (Balitsky-Fadin-Kuraev-Lipatov) [16, 17] which is especially well suited for low x calculations, and CCFM (Catani-Ciafaloni-Fiorani-Marchesini) [18] which combines BFKL and DGLAP evolution.

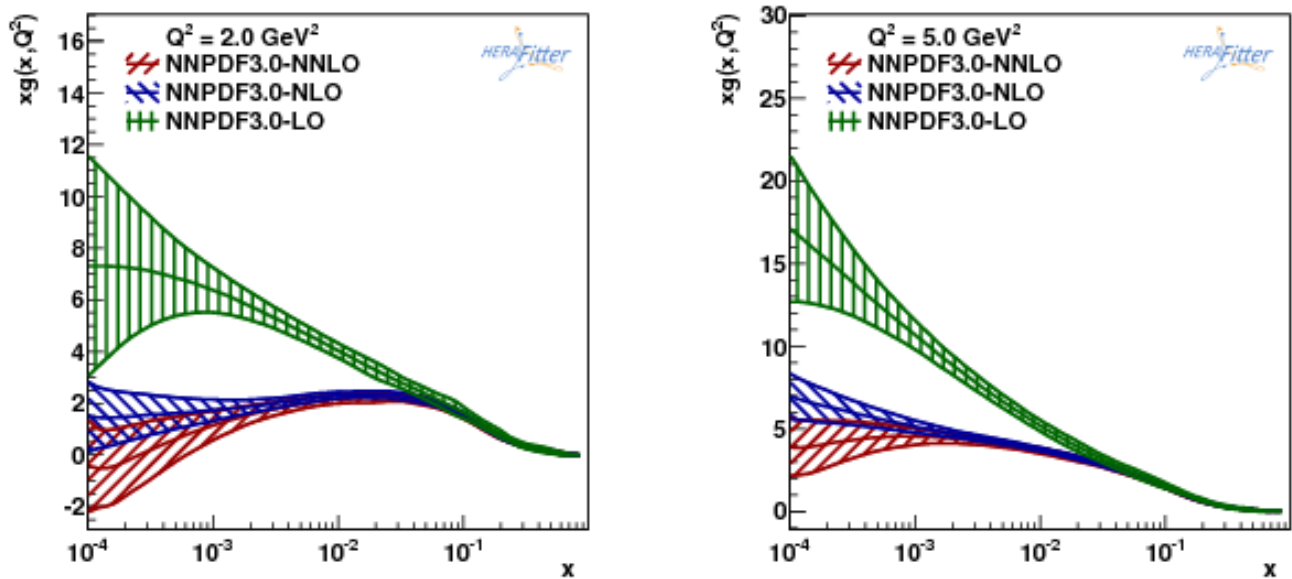


Figure 3.1: The gluon density against longitudinal momentum fraction x for fixed order perturbative calculations at LO, NLO and NNLO. The left plot shows the gluon density at fixed momentum transfer $Q^2 = 2 \text{ GeV}^2$ and the right plot at $Q^2 = 5 \text{ GeV}^2$. [19]

3.1.2 Transverse momentum spectrum from DY

In the case of DY, the transverse momentum (p_\perp) spectrum of the vector boson or final state di-lepton pair is not well described by finite order perturbative calculations of collinear PDFs. This concerns the region of the spectrum where $p_\perp \rightarrow 0$, where QCD effects beyond perturbative fixed order associated with soft multi-gluon radiation become essential. For large p_\perp , above the peak region, the collinear factorization works fine.

In the perturbative series of the transverse momentum spectrum for Drell-Yan large logarithms arise for small parton transverse momentum q_\perp . The terms in the perturbative series are of the form:

$$\alpha_s^k \ln^{2k-1}(Q/q_\perp). \quad (3.2)$$

Terms of the form $\alpha_s^n \ln^{2n-1}(Q/q_\perp)$ are *leading logarithms* (LL). Terms of the form $\alpha_s^n \ln^{2n-2}(Q/q_\perp)$ are *next-to-leading logarithms* (NLL) and so forth.

The q_{\perp} spectrum of the Z boson is measured with high precision at the LHC. In figure 3.2 the measurements are shown together with a theoretical prediction from the Monte Carlo (MC) event generator POWHEG. At low q_{\perp} a DGLAP calculation with parton showering to generate transverse momentum is not sufficient to describe the spectrum at small transverse momentum. With the use of MC techniques for the computation, many perturbative orders can be taken into account and thus the calculation already agrees with the measurement in a large p_{\perp} regime. For $p_{\perp} < 1$ GeV the fit deviates strongly from the measurement because of the lack of soft gluon resummation.

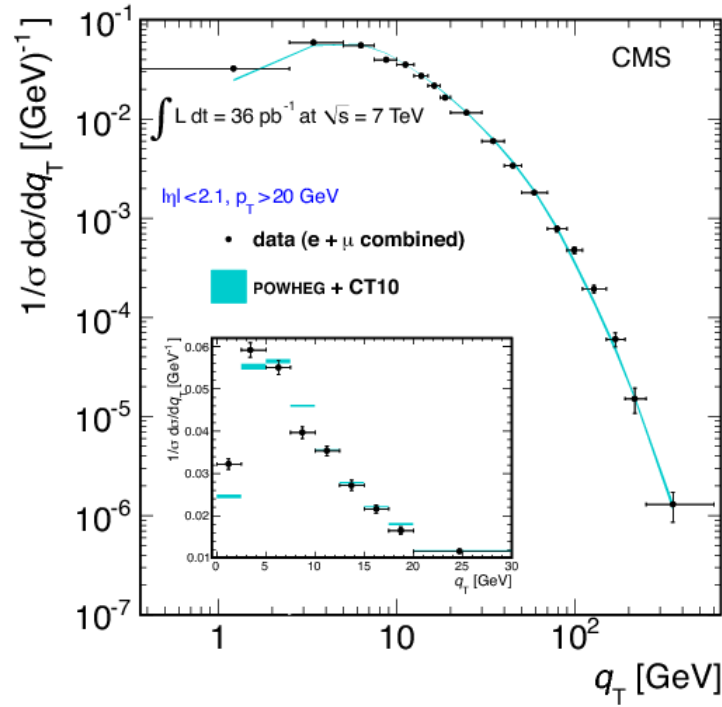


Figure 3.2: Data of the Z boson p_{\perp} spectrum and fit with the POWHEG event generator. In this figure p_{\perp} is denoted by q_{\perp} . [19]

The soft gluon radiation effect can be taken into account by using the TMD theoretical framework. Here a resummation procedure of logarithms of the form in (3.2) should be included. For the Drell Yan cross section, CSS (Collins-Soper-Sterman), variants in Soft-Collinear Effective Theory (SCET) or high- k_{\perp} factorization (as the parton branching method and KMRW, which are exhaustively studied within this thesis) provide frameworks to perform precise calculations in the low transverse momentum region.

3.2 TMDs

Although DGLAP generates transverse momentum during the evolution, namely through splittings of partons, the PDFs do not include this information. More advanced evolution equations that are able to evolve transverse momentum dependent parton distribution functions (TMDs) and that resum the large logarithms are needed. These are PDFs of the form $\mathcal{A}(x, \mathbf{k}_\perp, \mu)$, which are sometimes called *unintegrated parton densities*. Collinear PDFs can be interpreted as TMDs integrated over the transverse momentum:

$$f_i(x, \mu) = \int d^2\mathbf{k}_\perp \mathcal{A}_i(x, \mathbf{k}_\perp, \mu). \quad (3.3)$$

In spite of the many applications of collinear PDFs and the fact that they have been widely used for analysis of high-energy experiments, TMDs are the subject of intensive studies and will increasingly contribute to applications in high-energy physics. As in equation (3.3), the factorized parts of the DIS cross section in (2.4) are integrated over the transverse momentum. This physically means that the transverse momentum stream is limited; there is no connection of the transverse momenta from the PDFs to those in the hard scattering part. In a new description of both the hard scattering matrix element and the PDFs where they are both k_\perp dependent, the transverse momentum flows between these parts. This is often referred to as *TMD factorization*:

$$\sigma(x, Q) \simeq \int dz \int d^2\mathbf{k}_\perp \hat{\sigma}\left(Q, \mu_F, \frac{x}{z}, \mathbf{k}_\perp\right) \mathcal{A}(z, \mu_F, \mathbf{k}_\perp). \quad (3.4)$$

The formalisms that are developed for the high energy and low transverse momentum regions, such as BFKL, CCFM and CSS (cf. sections 3.1.1 and 3.1.2), express the evolution of TMDs with perturbative kernels (like the splitting functions in DGLAP). It is hard to apply the equations of these approaches to general collider kinematics because they only work well for particular observables and in particular kinematic regions. Because of this, other approaches for the evolution of TMDs have been investigated, such as KMRW (Kimber-Martin-Ryskin-Watt) or the parton branching (PB) method.

Part II

TMD formalisms

4 The CSS formalism

The transverse momentum spectrum of Drell-Yan is of large interest because it reflects QCD effects of soft gluon emission and collinear parton emission. The transverse momentum spectrum of the W boson has been measured for the first time in 1991 [20] and calculated perturbatively to next-to-leading-order (NLO) very accurately. Only in the small q_\perp regime, the prediction diverged. With more accurate measurements, this turned out to not be correct. Low transverse momentum is a result of the appearance of soft gluon emissions where radiated gluons have very low momentum and energy. There are two types of soft gluons that can contribute to the parton cascade that propagates to the hard scattering event:

1. The soft gluon continues up to the hard scattering event (and could radiate more partons in the evolution chain). Here, the longitudinal momentum fraction x of the interacting parton is very low. By including higher order splittings, logarithms of the form in (3.1) arise and the evolution of parton distribution functions is described by BFKL (see section 3.1.1).
2. The soft gluon is regarded as the radiated parton (parton c in figure 2.4). The transverse momentum k_\perp of the parton at the hard scattering is very low and logarithms of the form in (3.2) arise.

The second case is of interest in this thesis because these emissions produce large logarithms of the form $\ln(Q^2/q_\perp^2)$. An early treatment of this scenario was done by CSS which started in 1985 [21]. CSS specifically calculates the Drell-Yan differential cross section by taking into account soft gluon emission (the resummation of large logarithms), non-perturbative effects (low energetic processes inside hadrons) and a method to merge the perturbative and non-perturbative regions. The latter will not be discussed here and can be found in [21].

4.1 Perturbative description

The leading contribution to the differential Drell-Yan cross section with soft gluons schematically writes [8]

$$\frac{d\sigma}{dq_\perp^2} \sim \alpha_s \left(A \left(\frac{\ln(Q^2/q_\perp^2)}{q_\perp^2} \right)_+ + B \left(\frac{1}{q_\perp^2} \right)_+ + C(q_\perp^2) \right), \quad (4.1)$$

where Q is the invariant mass of the vector boson (the hard scattering scale), C is an integrable function and A and B are the first order perturbative coefficients from the series expansion in α_s as in (2.1). The plus prescription (see equation (2.19)) is applied to the terms in (4.1) that contain singular contributions from $q_\perp \rightarrow 0$ to include virtual corrections.

For the region $q_\perp \gg Q$, the leading order description of the differential cross section given in (4.1) is sufficient for the description of the large q_\perp tail of the spectrum. But for $q_\perp \ll Q$, higher order splittings (i.e. higher order Feynman diagrams, terms with higher powers in α_s) need to be taken into account. The leading term at small q_\perp is the first term in (4.1). At small q_\perp the higher order terms of the form $\alpha_s^n \ln^{2n-1}(Q^2/q_\perp^2)$ are not negligible anymore. If the differential DY cross section is written with higher order terms in powers of α_s as, it has the form (as in [8])

$$\frac{1}{\sigma} \frac{d\sigma}{dq_\perp^2} \simeq \frac{1}{q_\perp^2} \left[A_1 \frac{\alpha_s}{2\pi} \ln \frac{Q^2}{q_\perp^2} + A_2 \left(\frac{\alpha_s}{2\pi} \right)^2 \ln^3 \frac{Q^2}{q_\perp^2} + \dots + A_n \left(\frac{\alpha_s}{2\pi} \right)^n \ln^{2n-1} \frac{Q^2}{q_\perp^2} + \dots \right]. \quad (4.2)$$

The higher order terms become larger than the lower order terms, which leads to an inaccurate description when fixed order perturbation theory is used. These terms are resummed by the *Sudakov form factor*. The structure of this factor depends on the technique of factorization and separation of small and large transverse momentum that is used. The procedure of calculating the differential DY cross section and resummation proposed by CSS is given here.

4.2 Differential Drell-Yan cross section

The Drell-Yan differential cross section in [21] is divided in a term \tilde{W} that resums large logarithms $\ln Q^2/q_\perp^2$ and a term Y that is finite in q_\perp :

$$\frac{d\sigma}{dQ^2 dy d\mathbf{q}_\perp^2} = \frac{4\pi^2 \alpha^2}{9Q^2 s} \left\{ \frac{1}{(2\pi)^2} \int d^2 \mathbf{b} e^{i\mathbf{q}_\perp \cdot \mathbf{b}} \tilde{W}(\mathbf{b}; Q, x_A, x_B) + Y(\mathbf{q}_\perp; Q, x_A, x_B) \right\}, \quad (4.3)$$

where the first factor before the square brackets equals the leading order hard scattering probability for DY which is proportional to equation (2.10) as $\sigma^{(0)}/s$. Equation (4.3) is differential in transverse momentum q_\perp^2 and also in the hard scale Q^2 and rapidity y . The longitudinal momentum fractions of the interacting partons from proton A and B are respectively x_A and x_B . The hard interaction scale equals $Q^2 = x_A x_B s$ where s is the centre-of-mass energy squared. With the use of \mathbf{b} - the Fourier conjugate of \mathbf{q}_\perp - a proper treatment of transverse momentum conservation is achieved. Transverse momentum conservation can namely be written as [8]

$$\delta^2 \left(\mathbf{q}_\perp - \sum_{i=1}^n \mathbf{k}_{\perp,i} \right) = \frac{1}{(2\pi)^2} \int d^2 \mathbf{b} e^{i\mathbf{b} \cdot \mathbf{q}_\perp} \prod_{i=1}^n e^{-i\mathbf{b} \cdot \mathbf{k}_{\perp,i}} \quad (4.4)$$

in the case of n soft gluon emissions. The two-fold integral over \mathbf{b} in (4.3) and (4.4) is the anti-Fourier transform to ordinary phase space.

The term $Y(\mathbf{q}_\perp)$ in (4.3) contains the contribution from $q_\perp > \Lambda_{QCD}$. This contribution is contained in the leading order terms in powers of α_s (as in equation (4.1)) because for large transverse momentum these contain the main contributions to the differential cross section. The factorized form of this function in CSS is [21]

$$Y(\mathbf{q}_\perp; Q, x_A, x_B) = \sum_{a,b} \int_{x_A}^1 \frac{d\xi_A}{\xi_A} \int_{x_B}^1 \frac{d\xi_B}{\xi_B} \sum_{N=1}^{\infty} \left(\frac{\alpha_s(\mu)}{\pi} \right)^N R_{ab}^{(N)} \left(\mathbf{q}_\perp, Q, \frac{x_A}{\xi_A}, \frac{x_B}{\xi_B}; \mu \right) \times f_{a/A}(\xi_A, \mu) f_{b/B}(\xi_B, \mu), \quad (4.5)$$

where $R_{ab}^{(N)}$ are the regular perturbative coefficients coming from the hard scattering contribution. The singular part only contributes when $q_{\perp} \rightarrow 0$, which is not the regime that is represented by this term. The soft contribution is contained in the non-perturbative parton distribution functions f_a and f_b . The splitting variable is noted with ξ . Notice the agreement with the Drell-Yan factorization in (2.8). The Y term is not of much interest because it is negligible compared to the W term when the transverse momentum is small.

The term $\tilde{W}(\mathbf{b})$ in (4.3) contains the contribution from $q_{\perp} \ll Q$ and is written with the tilde because it is a Fourier transformed function of \mathbf{q}_{\perp} . In this regime the large logarithms in (4.2) have to be resummed to all orders.

For the determination of an expression for \tilde{W} , the regime of small transverse momentum is divided in three parts characterized by the transverse momentum k_{\perp} of the partons in the chain where partons are radiated up to the hard interaction: i) $k_{\perp} \ll 1/b$ described by a factor f , ii) $k_{\perp} \sim 1/b$ described by a factor C , iii) $1/b < k_{\perp} < Q$ described by a factor \sqrt{s} . This first term in the square brackets of (4.3) can be expressed in the following form:

$$\begin{aligned} \tilde{W}(\mathbf{b}; Q, x_A, x_B) = & \sum_{a,b} \int_{x_A}^1 \frac{d\xi_A}{\xi_A} \int_{x_B}^1 \frac{d\xi_B}{\xi_B} \int d^2\mathbf{k}_{\perp,a} e^{-i\mathbf{b}\cdot\mathbf{k}_{\perp,a}} \tilde{\mathcal{F}}_{a/A}(\mathbf{k}_{\perp,a}; Q, \xi_a, \mu) \\ & \times \int d^2\mathbf{k}_{\perp,b} e^{-i\mathbf{b}\cdot\mathbf{k}_{\perp,b}} \tilde{\mathcal{F}}_{b/B}(\mathbf{k}_{\perp,b}; Q, \xi_b, \mu) \end{aligned} \quad (4.6)$$

where the $\tilde{\mathcal{F}}_i = \int d^2\mathbf{b} e^{i\mathbf{b}\cdot\mathbf{k}_{\perp,i}} \mathcal{F}_i$. One could interpret the function \mathcal{F} as a TMD because it depends on the parton transverse momentum k_{\perp} . These TMDs can be factorized according to the above mentioned subdivision of transverse momentum k_{\perp} regimes:

$$\mathcal{F}_{q/i} \sim f_{q/i} \otimes C_{jq} \otimes \sqrt{S}. \quad (4.7)$$

This is a form of TMD factorization. Schematically the hadronic processes up to the Drell-Yan event can be drawn in a diagram as in figure 4.1 that represents something similar to parton evolution.

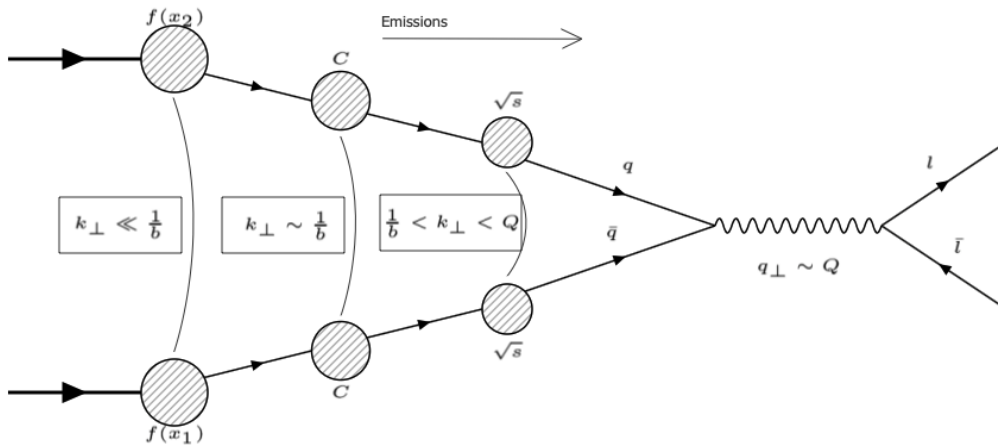


Figure 4.1: The soft radiative part (left part) from the DY differential cross section sketched as a chain up to the hard scattering event (right part) and factorized in three regimes depending on the transverse momentum.

The functions C and \sqrt{S} could be interpreted as corrections to the parton distribution functions $f_{a/A}$ and $f_{b/B}$. The PDFs are non-perturbative functions and can be evolved with for example DGLAP. However, the objects C and \sqrt{S} contain large enough momenta to be calculable perturbatively. The C coefficients contain the singular parts of the hard scattering function and have index j to label the flavour of the annihilating quark or antiquark in the hard interaction. This coefficient will not be discussed in much detail (more on this can be found in chapter 13 of [22]). The third factor is the Sudakov form factor that resums large logarithms of the form $\ln(Q^2 b^2)$. The derivation of the Sudakov form factor according to [21, 23] is discussed in the next section.

4.3 Sudakov form factor

Renormalization group invariance implies evolution equations for the TMDs:

$$\frac{\partial \mathcal{F}(\mathbf{b}; Q)}{\partial \ln Q^2} = \left[K(\mathbf{b}\mu; \alpha_s(\mu)) + G(Q/\mu; \alpha_s(\mu)) \right] \mathcal{F}(\mathbf{b}; Q), \quad (4.8)$$

where K and G have perturbation series expansions in α_s and the dependence on the momentum fraction has not been written. The b and Q dependences are separated on the right hand side of (4.8). Just as in deriving DGLAP, the two terms equal a separation constant (an anomalous dimension) with opposite sign. This is expressed in the RGEs:

$$-\mu \frac{d}{d\mu} K(\mathbf{b}\mu; \alpha_s(\mu)) = \gamma_K(\alpha_s(\mu)) = \mu \frac{d}{d\mu} G(Q/\mu; \alpha_s(\mu)). \quad (4.9)$$

This factor γ_K controls the large logarithms because by integration of these equations, one obtains the logarithms $\ln(b\mu)$ and $\ln(Q^2/\mu^2)$. This is similar to RG resummation from (2.14), but in this case it resums not only terms due to large μ but also large b (or small k_\perp). With this in mind, it is a matter of implementing the RGE's in (4.8) (see [21] for details). With boundaries in μ of c_1/b (lower) and $c_2 Q$ (upper) this becomes

$$\frac{\partial \mathcal{F}(\mathbf{b}; Q)}{\partial \ln Q^2} = -\frac{1}{2} \left[\left(\int_{c_1^2/b^2}^{c_2^2 Q^2} \frac{d\mu^2}{\mu^2} A(\alpha_s(\mu); c_1) \right) + B(\alpha_s(c_2 Q); c_1, c_2) \right] \mathcal{F}(\mathbf{b}; Q), \quad (4.10)$$

where A and B can be expressed as perturbation series expansions in α_s . The integration of this over $\ln \mu^2$ results in an expression for \mathcal{F} in which logarithms of the form $\ln(Q^2/\mu^2)$ are resummed to all orders:

$$\begin{aligned} \mathcal{F}(\mathbf{b}; Q) &= \exp \left(-\frac{1}{2} \int_{c_1^2/b^2}^{c_2^2 Q^2} \frac{d\mu^2}{\mu^2} \left[\ln \left(\frac{c_2^2 Q^2}{\mu^2} \right) A(\alpha_s(\mu); c_1) + B(\alpha_s(c_2 Q); c_1, c_2) \right] \right) \\ &\quad \times \mathcal{F}(\mathbf{b}; c_1/(c_2 b)), \end{aligned} \quad (4.11)$$

$$\Rightarrow \mathcal{F}(\mathbf{b}; Q) = \sqrt{S}(b, Q) \times \mathcal{F}(\mathbf{b}; c_1/(c_2 b)). \quad (4.12)$$

The Sudakov form factor is proportional to the exponential factor from (4.11) (\sqrt{S} in (4.12)). The soft function \mathcal{F} appears twice in the differential cross section and therefore the Sudakov equals the exponential factor squared:

$$S = \sqrt{S} \cdot \sqrt{S} = \exp \left(- \int_{c_1^2/b^2}^{c_2^2 Q^2} \frac{d\mu^2}{\mu^2} \left[\ln \left(\frac{c_2^2 Q^2}{\mu^2} \right) A(\alpha_s(\mu); c_1) + B(\alpha_s(c_2 Q); c_1, c_2) \right] \right) \quad (4.13)$$

This is a resummation factor similar to that from RG resummation (equation (2.14)), only this resums other logarithms which become large for low transverse momentum. The coefficients A and B are expansionable in power series⁴ in α_s :

$$A_a(\alpha_s) = \sum_{n=1}^{\infty} \left(\frac{\alpha_s}{2\pi}\right)^n A_a^{(n)}, \quad B_a(\alpha_s) = \sum_{n=1}^{\infty} \left(\frac{\alpha_s}{2\pi}\right)^n B_a^{(n)}. \quad (4.14)$$

The resummed series expansion of (4.13) is ordered in logarithmic powers and in the strong coupling with terms of the form $\alpha_s^n \ln^{2n-j} Q/\mu$. The leading logarithmic (LL) contribution is contained only in $A^{(1)}$, the next-to-leading logarithmic (NLL) terms are contained in $A^{(2)}$ and $B^{(1)}$ and so forth. These coefficients can be found in the literature [24, 25]. At LO they are given by

$$A_q^{(1)} = 2C_F, \quad A_g^{(1)} = 2C_A, \quad (4.15)$$

$$B_q^{(1)} = -3C_F, \quad B_g^{(1)} = -\frac{1}{3}(11C_A - 2N_f) \quad (4.16)$$

and NLO coefficients that will be used later on are

$$A_q^{(2)} = 2C_F C_A \left(\frac{67}{18} - \frac{\pi^2}{6}\right) - \frac{20}{9} C_F N_f T_R, \quad (4.17)$$

$$A_g^{(2)} = 2C_A^2 \left(\frac{67}{18} - \frac{\pi^2}{6}\right) - \frac{20}{9} C_A N_f T_R, \quad (4.18)$$

$$B_q^{(2)} = C_F^2 \left(\pi^2 - \frac{3}{4} - 12\zeta(3)\right) + C_F C_A \left(\frac{11}{9}\pi^2 - \frac{193}{12} + 6\zeta(3)\right) + C_F T_R N_f \left(\frac{17}{3} - \frac{4}{9}\pi^2\right). \quad (4.19)$$

4.4 Differential cross section with TMD factorization

There is no Q dependence in the leftover part $\mathcal{F}(\mathbf{b}, c_1/(c_2 b))$ in (4.12). This factor contains the contributions from the PDFs f and additional factors C_{ij} . The latter are perturbative coefficients in the TMD factorization which do not enter the Sudakov form factor because they take into account emissions with smaller transverse momentum than the Sudakov form factor does. However, k_{\perp} is still large enough to calculate the coefficients perturbatively. These coefficient functions can be written as [26]

$$C_{ij}(\alpha_s, z) = \delta_{ij} \delta(1-z) + \sum_{n=1}^{\infty} \left(\frac{\alpha_s}{2\pi}\right)^n C_{ij}^{(n)}(z). \quad (4.20)$$

\tilde{W} can be expressed using (4.6) and the previous results as [21]:

$$\begin{aligned} \tilde{W}(\mathbf{b}; Q, x_A, x_B) &= \sum_{a,b} \int_{x_A}^1 \frac{d\xi_A}{\xi_A} \int_{x_B}^1 \frac{d\xi_B}{\xi_B} f_{a/A}(\xi_A, \mu) f_{b/B}(\xi_B, \mu) \\ &\times \sum_j e_j^2 C_{ja} \left(\frac{x_A}{\xi_A}, \mathbf{b}; \alpha_s(\mu), \mu\right) C_{jb} \left(\frac{x_B}{\xi_B}, \mathbf{b}; \alpha_s(\mu), \mu\right) \\ &\times \exp \left(- \int_{c_1^2/b^2}^{c_2^2 Q^2} \frac{d\mu^2}{\mu^2} \left[\ln \left(\frac{c_2^2 Q^2}{\mu^2} \right) A_j(\alpha_s(\mu); c_1) + B_j(\alpha_s(c_2 Q); c_1, c_2) \right] \right) \end{aligned} \quad (4.21)$$

⁴Here, a different convention than that used in many CSS papers is used. For later convenience the factor $(\alpha_s/(2\pi))^n$ is used while most CSS papers that have been studied for this thesis use $(\alpha_s/\pi)^n$.

The summation over j takes into account the different quark flavour annihilations at the hard scattering event. Since the c_1 and c_2 coefficients are integration constants, they can be set to 1 for clarity. Equation (4.3) can then be written as [21]:

$$\begin{aligned} \frac{d\sigma}{dQ^2 dy d\mathbf{q}_\perp^2} &= \frac{1}{(2\pi)^2} \int d^2\mathbf{b} e^{i\mathbf{b}\cdot\mathbf{q}_\perp} \frac{\sigma^{(0)}(Q^2)}{s} \sum_{a,b} \int_{x_A}^1 \frac{d\xi_A}{\xi_A} \int_{x_B}^1 \frac{d\xi_B}{\xi_B} f_{a/A}(\xi_A, \mu) f_{b/B}(\xi_B, \mu) \\ &\times \sum_j e_j^2 C_{ja} \left(\frac{x_A}{\xi_A}, \mathbf{b}; \alpha_s(\mu), \mu \right) C_{jb} \left(\frac{x_B}{\xi_B}, \mathbf{b}; \alpha_s(\mu), \mu \right) \\ &\times \exp \left(- \int_{1/b^2}^{Q^2} \frac{d\mu^2}{\mu^2} \left[\ln \left(\frac{Q^2}{\mu^2} \right) A_j(\alpha_s(\mu)) + B_j(\alpha_s(\mu)) \right] \right) \\ &+ \frac{4\pi^2 \alpha^2}{9Q^2 s} Y(\mathbf{q}_\perp; Q, x_A, x_B). \end{aligned} \quad (4.22)$$

In [26] the structure of (4.22) was revised to include the process dependence of this formula. When *inclusive* processes are considered, all possible final states have to be taken into account. The final state consists of colour neutral particles (vector bosons, hadrons, jets, leptons, etcetera). Dependence on the final state is denoted by the index F . In the final formulation of the first CSS paper [21], only the LO partonic cross section ($\sigma^{(0)}/s$) is used. The radiation of partons before the hard scattering is treated by the W and Y . The LO partonic cross section could be extended to include higher order Feynman diagrams in α_s . Process dependence (denoted by an upper index F) and higher order QCD corrections (radiation of partons) are encountered by the substitution

$$\sigma^{(0)}(Q^2) \rightarrow \sigma_{j\bar{j}}^F(Q^2, \alpha_s(Q^2)). \quad (4.23)$$

This hard scattering factor is non-trivial and can be divided in the leading order, process dependent matrix element and a factor with higher order corrections as [26]

$$\sigma_{j\bar{j}}^F(Q^2, \alpha_s(Q^2)) = \sigma_{j\bar{j}}^{(0)F}(Q^2) H_j^F(\alpha_s(Q^2)), \quad (4.24)$$

where the perturbative function H_j^F has a power series expansion in α_s :

$$H_j^F(\alpha_s) = 1 + \sum_{n=1}^{\infty} \left(\frac{\alpha_s}{2\pi} \right)^n H_j^{F(n)}. \quad (4.25)$$

The cross section is then written as

$$\begin{aligned} \frac{d\sigma}{dQ^2 dy d\mathbf{q}_\perp^2} &= \frac{1}{(2\pi)^2} \int d^2\mathbf{b} e^{i\mathbf{b}\cdot\mathbf{q}_\perp} \sum_{j\bar{j}} \frac{\sigma_{j\bar{j}}^{(0)F}(Q^2)}{s} H_j^F(\alpha_s(Q^2)) \sum_{a,b} \int_{x_A}^1 \frac{d\xi_A}{\xi_A} \int_{x_B}^1 \frac{d\xi_B}{\xi_B} \\ &\times f_{a/A}(\xi_A, \mu) f_{b/B}(\xi_B, \mu) e_j^2 C_{ja}^F \left(\frac{x_A}{\xi_A}, \mathbf{b}; \alpha_s(\mu), \mu \right) C_{jb}^F \left(\frac{x_B}{\xi_B}, \mathbf{b}; \alpha_s(\mu), \mu \right) \\ &\times \exp \left(- \int_{1/b^2}^{Q^2} \frac{d\mu^2}{\mu^2} \left[\ln \left(\frac{Q^2}{\mu^2} \right) A_j^F(\alpha_s(\mu)) + B_j^F(\alpha_s(\mu)) \right] \right) \\ &+ \frac{4\pi^2 \alpha^2}{9Q^2 s} Y(\mathbf{q}_\perp; Q, x_A, x_B). \end{aligned} \quad (4.26)$$

The connection between the coefficients results from RG properties. This has many consequences and becomes important in the analysis of CSS in comparison with the parton branching method. In the next chapter a description of the the parton branching method is given.

5 The parton branching method

The parton branching (PB) method is a recently developed method to obtain TMDs that is described in [27] and [28]. PB has a different framework than CSS - which causes major difficulties in comparing these approaches - because it does not focus on the differential DY cross section. Instead, the PB method is concerned with QCD evolution equations for collinear PDFs and TMDs. It is constructed for general purposes (not only for the Drell-Yan process) and finds its basis at the DGLAP evolution equations - one could see the PB method as an extension of this formalism. The *unitarity approach* in the DGLAP formalism is a treatment in which soft gluons are resummed. All sorts of branchings in the evolution cascade, like the ones that do not give any problems in the perturbation series and the ones that do because of small momentum, are then taken into account appropriately. This soft gluon resummation is done by introducing the Sudakov form factor, other emissions are taken into account by real-emission probabilities. A profound derivation of the evolution equations that are used in the PB method can be found in [28].

5.1 Resolvable and non-resolvable emissions

Soft radiated partons have very low momentum, so the splitting variable z is close to 1. The region of splittings that involve these soft gluons can be defined by the region where $z > z_M$. The infrared (IR) cut-off z_M - the soft-gluon resolution parameter - is arbitrary but a physical choice relies on $1 - z_M \sim \mathcal{O}(\Lambda_{\text{QCD}}/\mu)$. Physically, the partons that are radiated with $z_M < z < 1$ are not distinguishable from their origin particle, that is why they are called *non-resolvable*. The integral over the splitting variable in equation (2.22) can be divided in a resolvable and non-resolvable part:

$$\frac{\partial \tilde{f}_a(x, \mu^2)}{\partial \ln \mu^2} = \sum_b \int_x^{z_M} P_{ab}(\alpha_s(\mu^2), z) \tilde{f}_b\left(\frac{x}{z}, \mu^2\right) + \sum_b \int_{z_M}^1 P_{ab}(\alpha_s(\mu^2), z) \tilde{f}_b\left(\frac{x}{z}, \mu^2\right). \quad (5.1)$$

The second integral in (5.1) contains divergences. To eliminate these divergences and merge the two terms, properties of the structure of the DGLAP splitting functions are used. One cannot neglect the second term completely, because virtual contributions have to be taken into account. In the next subsection, the DGLAP splitting functions and coefficients are given since they will come in handy in the comparison with CSS later on.

5.1.1 DGLAP splitting functions

Any splitting function (for all flavour combinations a and b and any order in α_s) can be decomposed as

$$P_{ab}(\alpha_s, z) = D_{ab}(\alpha_s)\delta(1-z) + \left(\frac{K_{ab}(\alpha_s)}{1-z}\right)_+ + R_{ab}(\alpha_s, z). \quad (5.2)$$

K_{ab} contains the infrared singularities of the splitting functions for $z \rightarrow 1$ (non-resolvable) and D_{ab} reflects virtual corrections that come from loop diagrams. The splitting variable for a loop diagram is $z = 1$, yielding the Dirac delta function in this term. D and K are both diagonal in flavour: $D_{ab} = \delta_{ab}d_a$ and $K_{ab} = \delta_{ab}k_a$ (where the δ is the Kronecker delta). All coefficients can be written as series expansions in α_s :

$$k_a(\alpha_s) = \sum_{n=1}^{\infty} \left(\frac{\alpha_s}{2\pi}\right)^n k_a^{(n-1)}, \quad (5.3)$$

$$d_a(\alpha_s) = \sum_{n=1}^{\infty} \left(\frac{\alpha_s}{2\pi}\right)^n d_a^{(n-1)}, \quad (5.4)$$

$$R_{ab}(\alpha_s, z) = \sum_{n=1}^{\infty} \left(\frac{\alpha_s}{2\pi}\right)^n R_{ab}^{(n-1)}(z). \quad (5.5)$$

The lowest order (LO and NLO) coefficients will be of use in the analytical comparison in the next chapter. They are taken from literature [28]. At leading order in α_s for quark (q) and gluon (g), the splitting function coefficients are:

$$k_q^{(0)} = 2C_F, \quad k_g^{(0)} = 2C_A, \quad (5.6)$$

$$d_q^{(0)} = \frac{3}{2}C_F, \quad d_g^{(0)} = \frac{11}{6}C_A - \frac{2}{3}T_R N_f, \quad (5.7)$$

$$\begin{aligned} R_{gg}^{(0)}(z) &= 2C_A \left(\frac{1-z}{z} + z(1-z) - 1 \right), \\ R_{gq}^{(0)}(z) &= R_{q\bar{q}}^{(0)}(z) = C_F \frac{1+(1-z)^2}{z}, \\ R_{qq}^{(0)}(z) &= R_{q\bar{q}}^{(0)}(z) = T_R(z^2 + (1-z)^2), \\ R_{q\bar{q}}^{(0)}(z) &= R_{\bar{q}q}^{(0)}(z) = -C_F(1+z)\delta_{ij}, \quad R_{\bar{q}\bar{q}}^{(0)} = R_{q\bar{q}}^{(0)} = 0, \end{aligned} \quad (5.8)$$

where $C_F = \frac{N_c^2-1}{2N_c} = 3/2$ is the quark colour factor and $C_A = 3$ is the gluon colour factor. The LO (one-loop) k coefficient indicates a part of the probability for partons to split. Gluons are radiating more strongly than quarks which is reflected in the fact that the LO k gluon coefficient is larger than this coefficient for quarks.

At next-to-leading order (NLO), the k and d coefficients are:

$$k_q^{(1)} = 2C_F C_A \left(\frac{67}{18} - \frac{\pi^2}{6} \right) - C_F T_R N_f \frac{20}{9}, \quad (5.9)$$

$$k_g^{(1)} = 2C_A^2 \left(\frac{67}{18} - \frac{\pi^2}{6} \right) - C_A T_R N_f \frac{20}{9}, \quad (5.10)$$

$$d_q^{(1)} = C_F^2 \left(\frac{3}{8} - \frac{\pi^2}{2} + 6\zeta(3) \right) + C_F C_A \left(\frac{17}{24} + \frac{11}{18}\pi^2 - 3\zeta(3) \right) - C_F T_R N_f \left(\frac{1}{6} + \frac{2}{9}\pi^2 \right), \quad (5.11)$$

$$d_g^{(1)} = C_A^2 \left(\frac{8}{3} + 3\zeta(3) \right) - \frac{4}{3} C_A T_R N_f - C_F T_R N_f. \quad (5.12)$$

The $R_{ab}^{(1)}$ coefficients are much lengthier and can be found in literature [28]. NLO coefficients are calculated from two-loop splittings, so both quark and gluon radiation is involved in these coefficients.

5.1.2 Evolution equations with real-emission probability

The DGLAP evolution equations (2.22) can be written using the decomposition of the splitting functions (5.2):

$$\frac{\partial \tilde{f}_a(x, \mu^2)}{\partial \ln \mu^2} = \sum_b \int_x^1 dz \left(D_{ab}(\alpha_s(\mu^2)) \delta(1-z) + \left(\frac{K_{ab}(\alpha_s(\mu^2))}{1-z} \right)_+ + R_{ab}(\alpha_s(\mu^2), z) \right) \tilde{f}_b \left(\frac{x}{z}, \mu^2 \right). \quad (5.13)$$

The goal in this subsection is to obtain evolution equations that include all kinds of emissions; resolvable and non-resolvable, but without having a divergent term as the second term on the right-hand side of (5.1). In short, this is done by first treating the non-resolvable contributions from the plus prescription term. By introducing a cut-off z_M close to one, it is a good approximation to only consider contributions up to $\mathcal{O}(1-z_M)$ of the parton distributions in the non-resolvable region. With this $f_b(x/z, \mu^2) \rightarrow f_b(x, \mu^2)$ and the integral over $K_{ab}(\alpha_s)$ is not divergent anymore. The finite part is then defined as the *real emission branching probability* $P_{ab}^{(R)}$. By using the momentum sum rule, the remaining integrals with virtual contributions can also be written in terms of $P_{ab}^{(R)}$.

Lets perform these steps to construct the iteratively solvable evolution equations. First consider the second term of the right-hand side of (5.13), use (2.19) to obtain

$$\int_x^1 dz \left(\frac{K_{ab}(\alpha_s)}{1-z} \right)_+ \tilde{f}_b \left(\frac{x}{z}, \mu^2 \right) = \int_x^1 dz \frac{K_{ab}(\alpha_s)}{1-z} \tilde{f}_b \left(\frac{x}{z}, \mu^2 \right) - \int_0^1 dz \frac{K_{ab}(\alpha_s)}{1-z} \tilde{f}_b(x, \mu^2) \quad (5.14)$$

and split the integrals on the right-hand side in a resolvable part and a non-resolvable part using the cut-off z_M :

$$\begin{aligned} \int_x^1 dz \left(\frac{K_{ab}(\alpha_s)}{1-z} \right)_+ \tilde{f}_b \left(\frac{x}{z}, \mu^2 \right) &= \underbrace{\int_x^{z_M} dz \frac{K_{ab}(\alpha_s)}{1-z} \tilde{f}_b \left(\frac{x}{z}, \mu^2 \right) - \int_0^{z_M} dz \frac{K_{ab}(\alpha_s)}{1-z} \tilde{f}_b(x, \mu^2)}_{\text{resolvable}} \\ &+ \underbrace{\int_{z_M}^1 dz \frac{K_{ab}(\alpha_s)}{1-z} \tilde{f}_b \left(\frac{x}{z}, \mu^2 \right) - \int_{z_M}^1 dz \frac{K_{ab}(\alpha_s)}{1-z} \tilde{f}_b(x, \mu^2)}_{\text{non-resolvable}}. \end{aligned} \quad (5.15)$$

Since z_M is close to one, the parton distribution in the non-resolvable region can be expanded as function of $1 - z$:

$$\tilde{f}_b(x/z, \mu^2) = \tilde{f}_b(x, \mu^2) + (1 - z) \frac{\partial \tilde{f}_b}{\partial \ln x}(x, \mu^2) + \mathcal{O}(1 - z)^2 \quad (5.16)$$

and only terms up to $\mathcal{O}(1 - z_M)$ are taken into account such that the second and fourth term of (5.15) cancel each other. Then, the full evolution equations can be written as follows:

$$\begin{aligned} \frac{\partial \tilde{f}_a(x, \mu^2)}{\partial \ln \mu^2} = & \sum_b \int_x^{z_M} dz \left(\frac{K_{ab}(\alpha_s(\mu^2))}{1 - z} + R_{ab}(\alpha_s(\mu^2), z) \right) \tilde{f}_b(x/z, \mu^2) \\ & + \sum_b \left(\int_x^1 D_{ab}(\alpha_s(\mu^2)) \delta(1 - z) dz - \int_0^{z_M} K_{ab}(\alpha_s(\mu^2)) \frac{1}{1 - z} dz \right) \tilde{f}_b(x, \mu^2), \end{aligned} \quad (5.17)$$

where R_{ab} is only integrated up to z_M because there is a very small contribution from the non-resolvable region to this. The D_{ab} term contains the Dirac delta function $\delta(1 - z)$ so that this term is proportional to $\tilde{f}_b(x, \mu^2)$. Together with the second term of (5.15), it forms the virtual and non-resolvable part. The first term in (5.17) contains the real emission parts. The integrand in the brackets of the first integral is therefore defined as the real-emission branching probability (in [8] it is named the unregularized splitting function and denoted by \hat{P}):

$$P_{ab}^{(R)}(\alpha_s, z) = \frac{K_{ab}(\alpha_s)}{1 - z} + R_{ab}(\alpha_s, z). \quad (5.18)$$

The virtual and non-resolvable part of (5.17) can also be expressed in terms of $P_{ab}^{(R)}$. This is done by subtracting the momentum sum rule (equation (2.21)). This is valid because the momentum sum rule equals zero. Furthermore, indices of D_{ab} and K_{ab} are switched, which is valid because these diagonal matrices. Equation (5.17) then becomes

$$\begin{aligned} \frac{\partial \tilde{f}_a(x, \mu^2)}{\partial \ln \mu^2} = & \sum_b \int_x^{z_M} dz P_{ab}^{(R)}(\alpha_s(\mu^2), z) \tilde{f}_b(x/z, \mu^2) \\ & + \sum_b \left(\int_x^1 D_{ba}(\alpha_s(\mu^2)) \delta(1 - z) dz - \int_0^{z_M} K_{ba}(\alpha_s(\mu^2)) \frac{1}{1 - z} dz \right. \\ & \left. - \int_0^1 z P_{ba}(\alpha_s(\mu^2), z) dz \right) \tilde{f}_a(x, \mu^2). \end{aligned} \quad (5.19)$$

By using the decomposition of the splitting function as in (5.2), the D terms are cancelled and the K terms merge together (when the integral from z_M to 1 is neglected). Because of this, the evolution equations can be written only in terms of the real-emission branching probability

$$\frac{\partial \tilde{f}_a(x, \mu^2)}{\partial \ln \mu^2} = \sum_b \left(\int_x^{z_M} dz P_{ab}^{(R)}(\alpha_s(\mu^2), z) \tilde{f}_b(x/z, \mu^2) - \int_0^{z_M} dz z P_{ba}^{(R)}(\alpha_s(\mu^2), z) \tilde{f}_a(x, \mu^2) \right). \quad (5.20)$$

5.2 Evolution equations with the Sudakov form factor

Even though the non-resolvable soft gluon emissions have been dealt with, the form of (5.20) is not preferred, as it is not solvable analytically neither does it have the right structure to be solved with the Monte Carlo (MC) techniques [29]. To be suitable for the MC approach, the Sudakov form factor is introduced into the evolution equations. With this, an interpretation in terms of probabilities arises, which allows for an iterative solution with a very intuitive interpretation. In the parton branching method, each iteration is interpreted as an additional parton emission in the branching cascade up to the hard scale. A large number of possible parton emissions in the evolution can be taken into account in the numerical approach.

The Sudakov form factor is defined as:

$$\Delta_a(z_M, \mu^2, \mu_0^2) = \exp \left\{ - \sum_b \int_{\mu_0^2}^{\mu^2} \frac{d\mu'^2}{\mu'^2} \int_0^{z_M} dz z P_{ba}^{(R)}(\alpha_s(\mu'^2), z) \right\}. \quad (5.21)$$

With the insertion of the real emission splitting functions from (5.18) this becomes

$$\Delta_a(z_M, \mu^2, \mu_0^2) = \exp \left\{ - \sum_b \int_{\mu_0^2}^{\mu^2} \frac{d\mu'^2}{\mu'^2} \int_0^{z_M} dz \left[\frac{z}{1-z} K_{ab}(\alpha_s) + z R_{ab}(\alpha_s, z) \right] \right\}. \quad (5.22)$$

This factor has the interpretation of a probability for a parton a to *not* split into a parton b . For readability, the dependence of the Sudakov on z_M will not be written in the sequel. Also the dependence on the lower scale μ_0 is usually not written: $\Delta(z_M, \mu, \mu_0) = \Delta(\mu)$.

For future discussion (chapter 7) it is convenient to rewrite the Sudakov form factor. The full splitting function can be split up in a real and virtual contribution: $P_{ab} = P_{ab}^{(R)} + P_{ab}^{(V)}$. With the application of the momentum sum rule (2.21), the real-emission probability can be transformed into the virtual part $P_{ab}^{(V)}$. The Sudakov then transforms to

$$\Delta_a(\mu^2, \mu_0^2) = \exp \left\{ - \sum_b \int_{\mu_0^2}^{\mu^2} \frac{d\mu'^2}{\mu'^2} \int_0^{z_M} dz \left[\frac{K_{ab}(\alpha_s)}{1-z} - D_{ab}(\alpha_s) \delta(1-z) \right] \right\}, \quad (5.23)$$

where the summation can easily be performed yielding

$$\Delta_a(\mu^2, \mu_0^2) = \exp \left\{ - \int_{\mu_0^2}^{\mu^2} \frac{d\mu'^2}{\mu'^2} \int_0^{z_M} dz \left[\frac{k_a(\alpha_s)}{1-z} - d_a(\alpha_s) \delta(1-z) \right] \right\}. \quad (5.24)$$

With this quantity, the evolution equations so far (5.20) can be written in a form which only involves the real-emission probability $P_{ab}^{(R)}$ and the Sudakov form factor Δ_a :

$$\frac{\partial}{\partial \ln \mu^2} \left(\frac{\tilde{f}_a(x, \mu^2)}{\Delta_a(\mu^2)} \right) = \sum_b \int_x^{z_M} dz P_{ab}^{(R)}(\alpha_s(\mu^2), z) \frac{\tilde{f}_b(x/z, \mu^2)}{\Delta_a(\mu^2)}. \quad (5.25)$$

Integration of this integro-differential equation over μ^2 results in an integral equation of the Fredholm type (see equation (2.32) in [28]) which can be solved iteratively:

$$\tilde{f}_a(x, \mu^2) = \Delta_a(\mu^2) \tilde{f}_a(x, \mu_0^2) + \sum_b \int_{\mu_0^2}^{\mu^2} \frac{d\mu'^2}{\mu'^2} \frac{\Delta_a(\mu'^2)}{\Delta_a(\mu'^2)} \int_x^{z_M} dz P_{ab}^{(R)}(\alpha_s(\mu'^2), z) \tilde{f}_b(x/z, \mu'^2). \quad (5.26)$$

In section 5.5, the extension of this equation will be discussed to include also transverse momentum dependence. In the next section, the iterative procedure of solving the evolution equations in this form will be described.

5.3 Iterative branching procedure

Equation (5.26) provides an intuitive interpretation of the evolution process in the PB method. The first term on the right-hand side is the PDF at scale μ_0 multiplied with the Sudakov (no-branching probability) at scale μ . This term can be interpreted as evolution of parton flavour a from μ_0 to μ without any emission. The second term takes into account all possibilities for the parton to split and change flavour by the summation over flavour b such that parton a is produced at the end. Here emissions are generated, which can be seen from the presence of the real-emission probability. The \tilde{f}_b at the end of (5.26) gets replaced by the previous result in each iteration. The PB method thus performs a so-called *step-by-step evolution* procedure.

Figure 5.1 shows three diagrams of the first three iterations (or steps) from solving the evolution equations. The left diagram represents the case of **no branching** between scale μ_0 and upper scale μ . If only this is taken into account, the solution of (5.26) is

$$\tilde{f}_a^{(0)}(x, \mu^2) = \Delta_a(\mu^2) \tilde{f}_a(x, \mu_0^2). \quad (5.27)$$

The middle diagram represents the scenario of **one branching** at intermediate scale μ' . Taking this diagram into account is done by substitution of the previous result into the right-hand side of the main equation (5.26). The new term additional to that in (5.27) becomes

$$\tilde{f}_a^{(1)}(x, \mu^2) = \sum_b \int_{\mu_0^2}^{\mu^2} \frac{d\mu'^2}{\mu'^2} \frac{\Delta_a(\mu^2)}{\Delta_a(\mu'^2)} \int_x^{z_M} dz P_{ab}^{(R)}(\alpha_s(\mu'^2), z) \Delta_b(\mu') \tilde{f}_b\left(\frac{x}{z}, \mu_0^2\right). \quad (5.28)$$

The right diagram has **two branchings**: a branching at scale μ' and one at μ'' . This is obtained by substitution of $\tilde{f}_b^{(0)} + \tilde{f}_b^{(1)}$ in the right-hand side of (5.26). The new term in the solution compared to those in (5.27) and (5.28) becomes

$$\begin{aligned} \tilde{f}_a^{(2)}(x, \mu^2) = & \sum_b \int_{\mu_0^2}^{\mu^2} \frac{d\mu''^2}{\mu''^2} \frac{\Delta_a(\mu^2)}{\Delta_a(\mu''^2)} \int_x^{z_M} dz_2 P_{ab}^{(R)}(\alpha_s(\mu''^2), z_2) \times \\ & \times \sum_c \int_{\mu_0^2}^{\mu''^2} \frac{d\mu'^2}{\mu'^2} \frac{\Delta_b(\mu''^2)}{\Delta_b(\mu'^2)} \int_{x/z_2}^{z_M} dz_1 P_{bc}^{(R)}(\alpha_s(\mu'^2), z_1) \Delta_c(\mu') \tilde{f}_c\left(\frac{x}{z_1 z_2}, \mu_0^2\right). \end{aligned} \quad (5.29)$$

The full solution for the PDF is the sum of all these contributions:

$$\tilde{f}_a(x, \mu^2) = \sum_i \tilde{f}_a^{(i)}(x, \mu^2). \quad (5.30)$$

The integrals can be continuously solved and iterations can be performed easily with the numerical Monte Carlo method. The parton branching method does this and generates transverse momentum $k_{\perp, i}$ in each splitting. Additional conditions are needed in order to include this k_{\perp} dependence of the parton distributions and thus to construct TMDs. The general equation (5.26) therefore needs to be adapted and an interpretation of the generation and ordering of transverse momentum in each splitting has to be set up. In the next section, the kinematics of a branching cascade including transverse momentum are discussed.

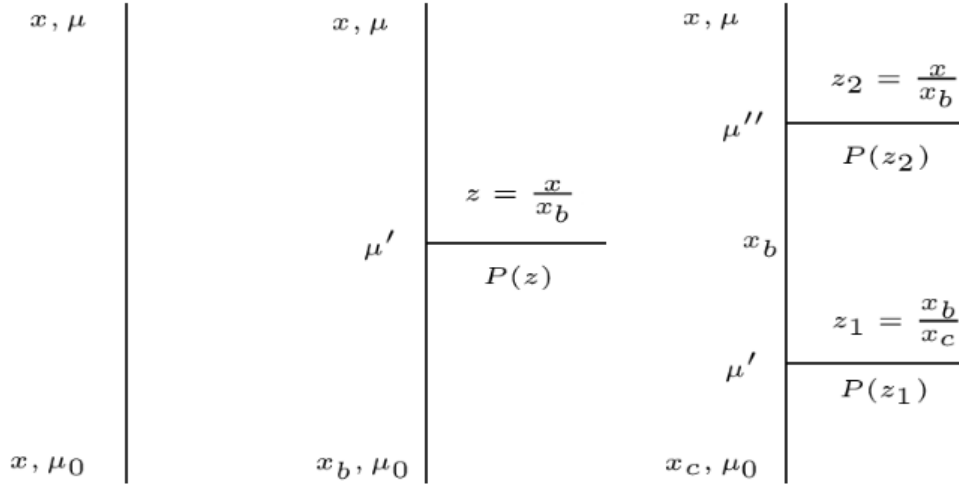


Figure 5.1: A schematic representation of the first three steps in the step-by-step evolution. Respectively no branching, one branching and two branchings are drawn.

5.4 Ordering conditions

The evolution scale variable μ' in the evolution equations has a mass dimension, but it can be associated with kinematic variables. The association of the evolution variable with the virtuality (proportional to the four-momentum squared) of the partons in the evolution cascade leads to an ordering of branchings that is related to a kinematic variable such as the transverse momentum.

The four-momentum of a parton can be noted as $k = (k^0, k^1, k^2, k^3) = (E_k, k_\perp, k^3)$. In light-cone variables the vector is written as $k = (k^+, k^-, k_\perp)$ where $k^\pm = \frac{1}{\sqrt{2}}(k^0 \pm k^3)$. An identity that comes in handy is:

$$k^2 = 2k^+k^- - k_\perp^2, \quad (5.31)$$

which can be easily proven by rewriting the norm of k . The minus component of the momentum can be written using this as:

$$k^- = \frac{k^2 + k_\perp^2}{2k^+} \quad (5.32)$$

For the fundamental splitting process shown in figure 5.2, minus component conservation can be expressed (using (5.32)) as:

$$\frac{k_b^2 + k_{\perp,b}^2}{2k_b^+} = \frac{k_a^2 + k_{\perp,a}^2}{2k_a^+} + \frac{q_c^2 + q_{\perp,c}^2}{2q_c^+}. \quad (5.33)$$

For longitudinal momentum fractions it holds that $x_a = zx_b$ and $x_c = (1-z)x_b$. It can be assumed that similar relations hold for the plus component momenta: $k_a^+ = zk_b^+$, $q_c^+ = (1-z)k_b^+$. With this the kinematic relation (5.33) becomes:

$$k_b^2 + k_{\perp,b}^2 = \frac{k_a^2 + k_{\perp,a}^2}{z} + \frac{q_c^2 + q_{\perp,c}^2}{1-z}. \quad (5.34)$$

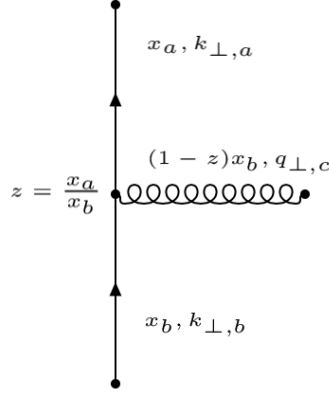


Figure 5.2: Basic splitting process with longitudinal momentum fractions x_b , $x_a = zx_b$, $x_c = (1-z)x_b$ and transverse momenta $k_{\perp,a}$, $k_{\perp,b}$, $q_{\perp,c}$.

Logical assumptions that can be made are the on-shellness of particle b and c : $k_b^2 = q_c^2 = 0$, and that $k_{\perp,b}^2 \ll k_{\perp,a}^2$. Together with the association of the evolution scale with the virtuality of parton a ($\mu'^2 = -k_a^2$), one obtains the **virtual ordering** condition [15]:

$$q_{\perp,c}^2 = -(1-z)k_a^2, \implies q_{\perp,c}^2 = (1-z)\mu'^2. \quad (5.35)$$

Since the splitting variable and the evolution scale become related, the IR cut-off z_M becomes dependent on μ' and becomes a dynamical variable. Virtual ordering thus implies a dynamical cut-off given by:

$$z_M = 1 - \left(\frac{q_0}{\mu'} \right)^2, \quad (5.36)$$

where $q_0 \equiv q_{\perp,0}$ is the minimum transverse momentum of parton c , with which it can be resolved.

With the additional assumption $z \rightarrow 0$, one obtains **transverse momentum ordering** (or p_{\perp} ordering). In p_{\perp} ordering the cut-off z_M is fixed and the scale equals transverse momentum of parton c :

$$q_{\perp,c}^2 = \mu'^2. \quad (5.37)$$

By taking into account the *colour coherence* QCD phenomenon from soft gluon emission [30,31], the sequential branchings can be ordered according to their angles with respect to the initial direction so that $\theta_{i+1} > \theta_i$. This is visualized in figure 5.3 where the vertical line represents the evolution of a parton from the proton up to the hard scattering (upper grey zone). Lets define the *rescaled transverse momentum* which has already been used in the early paper by G. Marchesini [32]:

$$\bar{q}_{\perp,c} = \frac{|q_{\perp,c}|}{1-z}. \quad (5.38)$$

In the PB method, the evolution is ordered in rescaled transverse momentum: $\bar{q}_{i+1} > \bar{q}_i$ ⁵. The **angular ordering** condition follows from the association of the evolution scale with the rescaled transverse momentum:

$$q_{\perp,c}^2 = (1-z)^2 \mu'^2. \quad (5.39)$$

⁵The CCFM formalism also has an ordering of the evolution but there it is $\bar{q}_{i+1} > z\bar{q}_i$

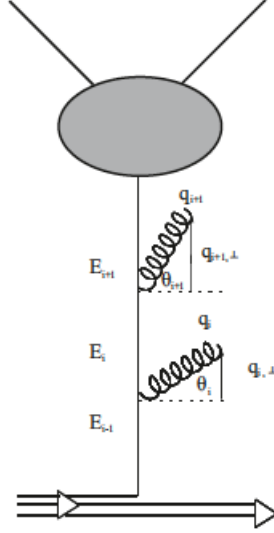


Figure 5.3: Cascade of soft gluons radiated by a parton that evolves up to the hard scattering process. The soft gluons are ordered in their angles so that $\theta_{i+1} > \theta_i$. [15]

Together with (5.39), a full angular ordering condition has a dynamical cut-off for equal reason as for virtuality ordering; it is given by:

$$z_M = 1 - \frac{q_0}{\mu'}. \quad (5.40)$$

All three ordering conditions are summarized in table 5.1.

	Evolution scale	IR cut-off	Scale of α_s
p_\perp ordering	$q_{\perp,c}^2 = \mu'^2$	$z_M = \text{fixed}$	$\alpha_s(\mu'^2)$
Virtuality ordering	$q_{\perp,c}^2 = (1-z)\mu'^2$	$z_M = 1 - \left(\frac{q_0}{\mu'}\right)^2$	$\alpha_s((1-z)\mu'^2)$
Angular ordering	$q_{\perp,c}^2 = (1-z)^2\mu'^2$	$z_M = 1 - \left(\frac{q_0}{\mu'}\right)$	$\alpha_s((1-z)^2\mu'^2)$

Table 5.1: Ordering conditions of the PB method with their properties.

5.5 TMDs

With the interpretation of the evolution scale and with an ordering condition, one can keep track of each emission process in the evolution cascade. The transverse momentum of the parton that enters the hard scattering process is simply the sum of all transverse momenta that were emitted in the cascade:

$$\mathbf{k}_\perp = - \sum_c \mathbf{q}_{\perp,c}. \quad (5.41)$$

To define evolution for TMDs consistently, the full implementation of an ordering condition is necessary to take care of the IR sensitivity of these functions. The implementation of an ordering condition - including a relation of transverse momentum $q_{\perp,c}$ and the cut-off z_M with the scale - into (5.26) results in evolution equations for TMDs:

$$\begin{aligned} \tilde{\mathcal{A}}_a(x, k_\perp, \mu^2) &= \Delta_a(\mu^2) \tilde{\mathcal{A}}_a(x, k_\perp, \mu_0^2) + \sum_b \int \frac{d^2 \mu'_\perp}{\pi \mu'^2} \frac{\Delta_a(\mu^2)}{\Delta_a(\mu'^2)} \Theta(\mu^2 - \mu'^2) \Theta(\mu'^2 - \mu_0^2) \\ &\times \int_x^{z_M} dz P_{ab}^{(R)}(\alpha_s(a^2(z)q'_\perp), z) \tilde{\mathcal{A}}_b(x/z, k_\perp + a(z)\mu_\perp, \mu'^2), \end{aligned} \quad (5.42)$$

where the second argument of the initial TMD $\tilde{\mathcal{A}}_b$ specifies the method in which transverse momentum is gathered in each branching. The function $a(z)$ depends on the ordering condition that is used:

$$a(z) = \begin{cases} 1 & \text{for } p_\perp \text{ ordering,} \\ \sqrt{1-z} & \text{for virtuality ordering,} \\ 1-z & \text{for angular ordering.} \end{cases} \quad (5.43)$$

The three parts that are influenced by an ordering condition are all present in (5.42). With the integration over k_\perp , this becomes an evolution equation for collinear parton densities (see eq. (3.3)). Then, if the scale of α_s is taken to be μ' and $z_M = 1$, the DGLAP evolution equation is restored.

Similar to the expression for collinear PDFs, (5.42) can be solved numerically as well. Such numerical calculations have been performed using the three cases of $a(z)$, but with fixed values of the cut-off z_M . Results of these calculations for gluon TMDs using transverse momentum ordering and angular ordering with different fixed values of z_M are shown in figure 5.4. From the comparison of the left plots (p_\perp ordering) with the right plots (angular ordering), the conclusion has been made in [28] that with the implementation of angular ordering in the formalism, one obtains stable, z_M independent TMDs.

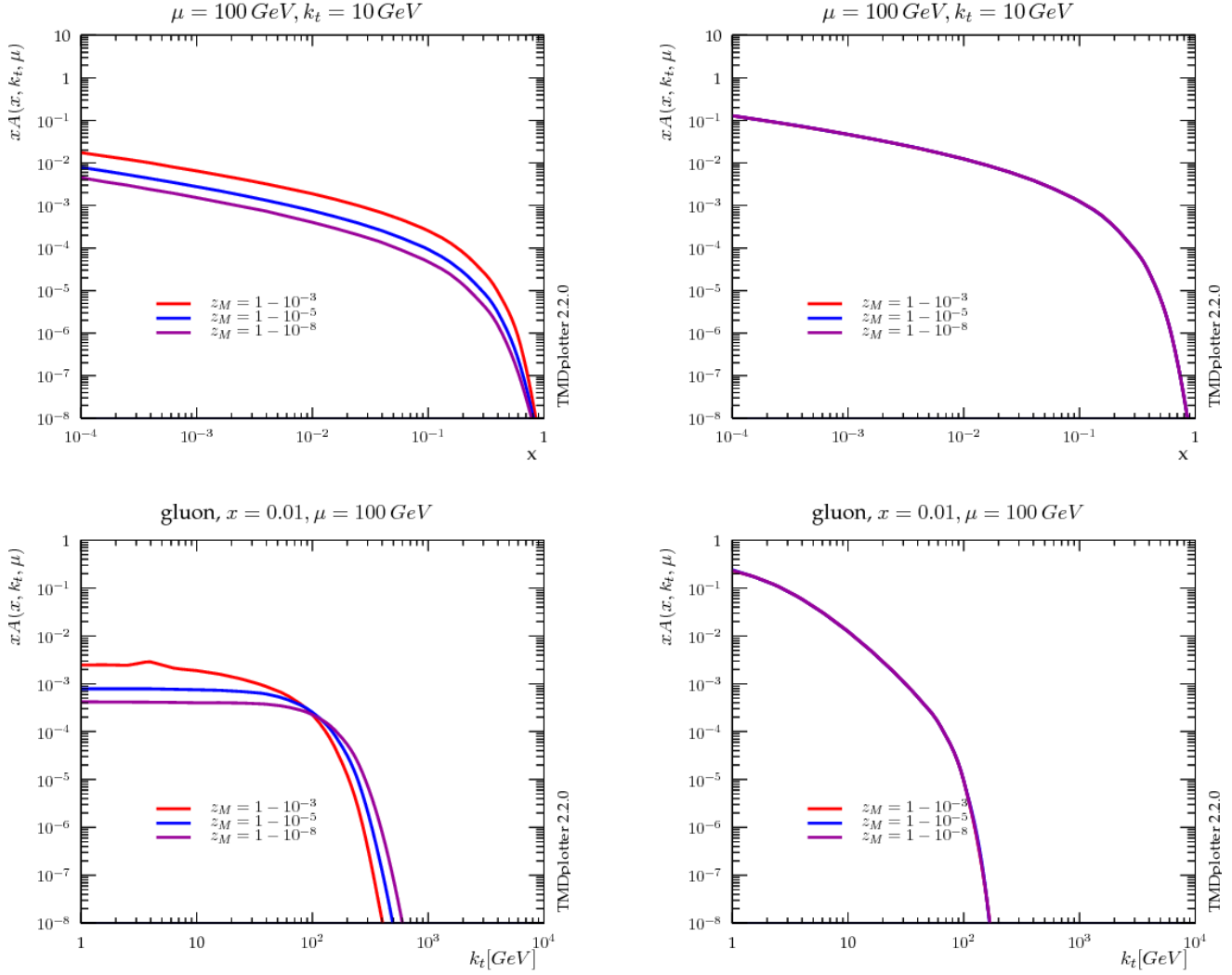


Figure 5.4: TMDs constructed by the parton branching method using transverse momentum ordering (left plots) and angular ordering (right plots). These are calculated with (5.42) and the ordering conditions from table 5.1 and equation (5.43). The upper plots are functions of x with a fixed value of $k_\perp = 10$ GeV, the lower plots are functions of k_\perp with fixed $x = 0.01$. Three curves on each plot have the same conditions, except for different fixed values for $z_M = 1 - 10^{-3}$, $1 - 10^{-5}$ and $1 - 10^{-8}$ which are respectively represented by the red, blue and purple curves. [28]

6 KMRW approach

In the early 2000's, M.A. Kimber, A.D. Martin, M.G. Ryskin and G. Watt (KMRW) published papers [33–35] in which a method to obtain unintegrated parton distributions was proposed and justified by computations, and where also fits to deep inelastic structure functions F_2 were made. A recent application and test of KMRW in experimental analysis is done by authors of [36].

The motivation that led to the construction of KMRW is similar to the motivation for parton branching. TMDs, or unintegrated distributions (uPDFs) as they are called in the papers of KMRW, are necessary for multi-scale processes but the evolution can be constructed with only one evolution scale by consideration of a kinematic ordering condition. The second scale (transverse momentum) enters the uPDF at the last step of the evolution. In fact, KMRW does not provide a step-by-step solution, but a single-step procedure. A single-scale evolution is derived from the DGLAP equations. With the notion that the essential evolution quantity is the emission angle, a form of angular ordering is imposed with the introduction of the IR cut-off Δ . The analogy with the IR cut-off z_M from PB is: $z_M = 1 - \Delta$.

6.1 From DGLAP to unintegrated PDFs

To construct uPDFs $f_a(x, k_\perp, \mu^2)$ starting from the DGLAP evolution equations, the DGLAP evolution scale is associated with the parton transverse momentum $\mu = |\mathbf{k}_\perp| = k_\perp$ and virtual contributions are included by the Sudakov form factor $T_a(\mu, \mu_0)$. The unintegrated distributions represent similar hadronic objects as TMDs.

By leaving out non-resolvable contributions that come from soft gluon emission, unintegrated parton densities can be defined in terms of integrated (collinear) parton densities $D_a(x, \mu^2)$ as:

$$f_a(x, k_\perp) = \left. \frac{\partial D_a(x, \mu^2)}{\partial \ln \mu^2} \right|_{\mu^2=k_\perp}. \quad (6.1)$$

The collinear PDFs evolve according to the DGLAP equations (2.22). For this, the region of splitting variables is limited to $[x, 1 - \Delta]$ and the solution to DGLAP for integrated PDFs writes

$$\frac{\partial D_a(x, \mu^2)}{\partial \ln \mu^2} = \sum_b \int_x^{1-\Delta} \frac{dz}{z} P_{ab}(z, \mu^2) D_b\left(\frac{x}{z}, \mu^2\right), \quad (6.2)$$

where the parton distributions are not momentum weighted. This equation only describes a part of the full evolution, because it is the resolvable part. The virtual emissions are then included with

an additional term and the association of the evolution scale with parton transverse momentum in the DGLAP equations [37]:

$$\frac{\partial D_a(x, k_\perp)}{\partial \ln k_\perp^2} = \sum_b \int_x^{1-\Delta} \frac{dz}{z} P_{ab}(z, k_\perp) D_b\left(\frac{x}{z}, k_\perp\right) - D_a(x, k_\perp) \sum_b \int_0^{1-\Delta} dz z P_{ba}(z, k_\perp). \quad (6.3)$$

The soft gluon emission terms that are present in these evolution equations are resummed with a Sudakov form factor. It is defined by KMRW as

$$T_a(\mu, k_\perp) = \exp\left(-\int_{k_\perp^2}^{\mu^2} \frac{dk_\perp'^2}{k_\perp'^2} \sum_b \int_0^{1-\Delta} dz z P_{ba}(z, k_\perp')\right) \quad (6.4)$$

and has the same interpretation as the Sudakov in CSS and PB. KMRW notes this with the name "survival probability" for a parton between the scales k_\perp and μ . The resummed unintegrated parton distributions (or TMDs) are then constructed by the multiplication of (6.3) with the Sudakov form factor. After some rearrangement this can be written in the compact form:

$$\frac{\partial [T_a(\mu, k_\perp) D_a(x, k_\perp)]}{\partial \ln k_\perp^2} = T_a(\mu, k_\perp) \sum_b \int_x^{1-\Delta} \frac{dz}{z} P_{ab}(z, k_\perp) D_b\left(\frac{x}{z}, k_\perp\right). \quad (6.5)$$

This ordinary differential equation can be solved by integration over the transverse momentum scale variable from μ_0 to μ , which yields a solution for integrated PDFs:

$$D_a(x, \mu) = T_a(\mu, \mu_0) D_a(x, \mu_0) + \underbrace{\int_{\mu_0^2}^{\mu^2} \frac{dk_\perp^2}{k_\perp^2} T_a(\mu, k_\perp) \sum_b \int_x^{1-\Delta} \frac{dz}{z} P_{ab}(z, k_\perp) D_b\left(\frac{x}{z}, k_\perp\right)}_{f_a(x, k_\perp, \mu)}. \quad (6.6)$$

Equation (6.5) is similar to (6.1), but now the virtual contribution is included by the Sudakov form factor. The integrand is interpreted by KMRW as the uPDF. This is the foundation of KMRW, namely that transverse momentum dependent uPDFs can be obtained from collinear PDFs with an integral equation that is:

$$f_a(x, k_\perp, \mu) = T_a(\mu, k_\perp) \sum_b \int_x^{1-\Delta} \frac{dz}{z} P_{ab}(z, k_\perp) D_b\left(\frac{x}{z}, k_\perp\right). \quad (6.7)$$

Moreover, by using (6.5) a differential formula for uPDFs can be defined:

$$f_a(x, k_\perp, \mu) = \frac{\partial [T_a(\mu, k_\perp) D_a(x, k_\perp)]}{\partial \ln k_\perp^2}. \quad (6.8)$$

The solution of the integral equation can be interpreted as the last step of the evolution in which the full transverse momentum of the parton that interacts at the hard scale is generated.

6.2 Ordering conditions

This section discusses the IR cut-off parameter Δ , which is variable in the KMRW approach. One choice of parameterization of this cut-off, called strong ordering (SO), is

$$\Delta = \frac{k_{\perp}}{\mu}. \quad (6.9)$$

Another ordering choice is *angular ordering* (AO), which is constructed to enlarge the k_{\perp} region for which the parton densities could be defined. In AO, the cut-off is taken to be

$$\Delta = \frac{k_{\perp}}{k_{\perp} + \mu}. \quad (6.10)$$

With this parameterization, the parton transverse momentum is not limited by the hard scale μ but it can become larger. The region in k_{\perp} in which the uPDFs are defined, differs for these ordering conditions: for SO $k_{\perp} \leq \mu(1-x)$ and for AO $k_{\perp} \leq \mu(1/x-1)$. The region of transverse momentum in AO is much larger than in SO. However, this results to complications in the Sudakov form factor (6.4). In case of angular ordering, when $k_{\perp} > \mu$, the argument of the exponent is positive and the Sudakov becomes larger than one. Since the Sudakov has the interpretation of a survival probability, this is not physical. KMRW solves this by fixing the Sudakov factor to 1 in this region of large k_{\perp} :

$$T_a(\mu, k_{\perp}) = 1 \text{ for } k_{\perp} > \mu. \quad (6.11)$$

6.2.1 Integral and differential equations KMRW

Equations (6.7) and (6.8) are mathematically equivalent when $\Delta = 0$. Despite this, initial PDFs $D_a(x, k_{\perp})$ are taken from other models or libraries and are not necessarily consistent with the cut-off used by KMRW with strong or angular ordering. Then, the integration up to $1 - \Delta$ is not equivalent to solving the differential equation. In [37], (6.7) and (6.8) are compared numerically. It is concluded there that the integral definition of KMRW is the preferred model because TMDs obtained by the differential definition with SO have discontinuities and negative parts in the region where $k_{\perp} > \mu$. For AO, the differential formulation results in discontinuities at large k_{\perp} . This is due to the unphysical behaviour of the KMRW Sudakov as described above.

Note that the structure of (6.6) is very similar to the integrated evolution equations from parton branching (5.26). This encourages a comparison of the two methods. Furthermore, the KMRW approach is commonly used for the construction of PDFs in general. If the relatively new PB approach has advantages compared to KMRW, then these should be argued and clarified. This comparison is performed and described in chapter 8.

Part III

Analysis of TMD formalisms

7 Comparison of CSS with the parton branching method

The approaches from the previous chapters provide descriptions of the hadronic processes in larger regimes of the phase space than this of the standard DGLAP approach. PB and CSS are set up independently and include transverse momentum dependencies. They both rely on the basic principles of QCD which were treated in chapters 1 and 2.

The CSS formalism exists for a long time already and is a widely accepted and used method which provides a detailed description of the Drell-Yan process. This process has extensively been studied by many researchers, both theoretically and experimentally. Basically, this formalism improved the collinear factorization formula for DY (2.8) with TMD factorization. The main formula for the differential DY cross section of CSS (4.22) involves the resummation of large logarithms from small q_\perp contributions as does the PB method.

Since CSS is widely used, it is very valuable to compare the relatively new parton branching method with it. The formalism of the PB method is very promising for future application which has been argued in recent papers [?, 15, 27, 28, 38]. A difficulty in the comparison with CSS lies in the different frameworks in which these methods are formulated. CSS provides an expression for the differential Drell-Yan cross section, while PB gives evolution equations for TMDs. However, the factorized forms of the formulas contain similar objects. In this thesis the Sudakov form factors of the formalisms are compared in detail.

7.1 Recap of the formalisms

Lets first formulate important properties of the formalisms that are useful for the comparison. The PB method provides a solution of evolution equations for PDFs. For collinear PDFs these equations are

$$\tilde{f}_a(x, \mu^2) = \Delta_a(\mu^2) \tilde{f}_a(x, \mu_0^2) + \sum_b \int_{\mu_0^2}^{\mu^2} \frac{d\mu'^2}{\mu'^2} \frac{\Delta_a(\mu^2)}{\Delta_a(\mu'^2)} \int_x^{z_M} dz P_{ab}^{(R)}(\alpha_s(\mu'^2), z) \tilde{f}_b(x/z, \mu'^2). \quad (7.1)$$

For TMDs this is very similar and can be found in equation (5.42). The Sudakov form factor from parton branching given in equation (5.24) can be rewritten in terms of transverse momentum q_\perp

with the use of the angular ordering condition (5.39). This gives⁶

$$\Delta_a(\mu, q_0) = \exp \left\{ - \int_{q_0^2}^{\mu^2} \frac{dq_{\perp}^2}{q_{\perp}^2} \int_0^{1-\frac{q_{\perp}}{\mu}} dz \left[\frac{k_a(\alpha_s(q_{\perp}))}{1-z} - d_a(\alpha_s(q_{\perp}))\delta(1-z) \right] \right\}. \quad (7.2)$$

By performing the integration over z , the first term in the exponential becomes

$$\int_0^{1-\frac{q_{\perp}}{\mu}} \frac{dz}{1-z} = \frac{1}{2} \ln \left(\frac{\mu^2}{q_{\perp}^2} \right) \quad (7.3)$$

and the second term of (7.2) integrated over z is trivial due to the Dirac delta function. The PB Sudakov can then be written in a similar way as the Sudakov from CSS:

$$\Delta_a(\mu, q_0) = \exp \left\{ - \int_{q_0^2}^{\mu^2} \frac{dq_{\perp}^2}{q_{\perp}^2} \left[\frac{1}{2} \ln \left(\frac{\mu^2}{q_{\perp}^2} \right) k_a(\alpha_s(q_{\perp})) - d_a(\alpha_s(q_{\perp})) \right] \right\}. \quad (7.4)$$

In CSS, the formulas are given in impact parameter space (\mathbf{b} -space), which is obtained by the two-dimensional Fourier transformation from transverse momentum \mathbf{q}_{\perp} to the impact parameter \mathbf{b} . Doing this for the Sudakov form factor in (7.4) would result in a very similar expression where the perturbative functions k and d are preserved. Because of this, the current form of the PB Sudakov is well-suited for a comparison with the Sudakov form factor from CSS.

In CSS, the main result is the expression for the differential cross section (4.26), which can be written in a simplified version as

$$\frac{d\sigma}{dq_{\perp}^2} \simeq \sum_{a,b} H_{ab}^F(Q^2/\mu^2, \alpha_s(\mu)) \int d^2\mathbf{b} e^{i\mathbf{b}\cdot\mathbf{q}_{\perp}} \mathcal{F}_{a/A}(\mathbf{b}, Q, \mu, x_A) \mathcal{F}_{b/B}(\mathbf{b}, Q, \mu, x_B). \quad (7.5)$$

This clearly has the structure of a factorized formula where the hard part H_{ab}^F is separated from the soft parts represented by the TMDs \mathcal{F} . CSS then factorizes a TMD in three factors: f_a , C_{ab} and resummation factor \sqrt{S} as illustrated in equation (4.7). Although the Sudakov form factors defined by these two methods look different at first sight, it is valuable to investigate whether these are actually the same factors. The CSS Sudakov form factor equals

$$S(Q, b) = \exp \left\{ - \int_{1/b^2}^{Q^2} \frac{d\mu^2}{\mu^2} \left[\ln \left(\frac{Q^2}{\mu^2} \right) A_a(\alpha_s(\mu)) + B_a(\alpha_s(\mu)) \right] \right\}, \quad (7.6)$$

where the integration constants c_1 and c_2 have been set to 1 and the perturbative coefficients $A_a(\alpha_s)$ and $B_a(\alpha_s)$ are expansionable in powers of α_s as in (4.14).

It is important for the comparison to note that the Sudakov form factor of CSS comes from two soft factors: $\tilde{\mathcal{F}}_{a/A}$ and $\tilde{\mathcal{F}}_{b/B}$ which both contain a factor \sqrt{S} (see (4.12)). In PB, the Sudakov is defined within one TMD. Therefore, the square root of the Sudakov from CSS would be analogous to the Sudakov from PB:

$$\sqrt{S(Q, b)} = \exp \left\{ - \frac{1}{2} \int_{1/b^2}^{Q^2} \frac{d\mu^2}{\mu^2} \left[\ln \left(\frac{Q^2}{\mu^2} \right) A_a(\alpha_s(\mu)) + B_a(\alpha_s(\mu)) \right] \right\}. \quad (7.7)$$

The goal of this chapter is to relate the perturbative coefficients from the functions A and B to these of the functions k and d .

⁶This is approximately valid. In the next chapter, a formal way of applying change of integration variables is described for the PB evolution equations and the Sudakov form factor.

7.2 Perturbative coefficients

The Sudakov form factors in (7.4) and in (7.7) have similar structures. The splitting kernel $k_a(\alpha_s)$ and the coefficient $A(\alpha_s)$ are both multiplied with the logarithm that has the evolution variable in the denominator and the upper scale in the nominator. The $d_a(\alpha_s)$ takes the same place in the form factor as $B_a(\alpha_s)$. By considering the series expansions of these perturbative functions in both formalisms (given in (4.14), (5.3) and (5.4)), $\Delta_a(\mu, q_0)$ and $\sqrt{S(Q, b)}$ correspond if and only if:

$$k_a^{(i)} = A_a^{(i+1)}, \quad (7.8)$$

$$\text{and } d_a^{(i)} = -\frac{1}{2}B_a^{(i+1)}. \quad (7.9)$$

These coefficients are compared order by order. First, the leading logarithmic (LL) terms are considered, then next-to-leading logarithmic (NLL) and finally the next-to-next-to-leading logarithmic (NNLL) terms. The LL and NLL coefficients do correspond, but from NNLL on, they do not with a first observation. The difference should be compensated in other parts of the evolution equations⁷.

7.2.1 LL coefficients

The leading logarithmic contributions in PB appear in $k_a^{(0)}$ and in CSS these are represented by $A_a^{(1)}$. The quark contribution ($a = q$) to the LO splitting coefficient is related to this from CSS as

$$k_q^{(0)} = 2C_F = A_q^{(1)} \quad (7.10)$$

and the gluon contribution ($a = g$) to the LO splitting coefficient is

$$k_g^{(0)} = 2C_A = A_g^{(1)}. \quad (7.11)$$

These coefficients agree one to one, as is needed for equal Sudakov factors given in the condition in (7.8). Thus at LL, where the resummed terms are of the form $\alpha_s^n \ln^{2n-1}(\mu^2/q_\perp^2)$, PB and CSS are equal. [39]

7.2.2 NLL coefficients

The next-to-leading logarithmic contributions in the PB Sudakov are contained in the coefficients $k^{(1)}$ (5.9) and $d^{(0)}$ (5.7). In CSS, these arise in the $A^{(2)}$ and $B^{(1)}$ coefficients given in (4.17) and (4.16).

The $k_q^{(1)}$ and $A_q^{(2)}$ coefficients correspond exactly:

$$k_q^{(1)} = 2C_F C_A \left(\frac{67}{18} - \frac{\pi^2}{6} \right) - \frac{20}{9} C_A T_R N_f = A_q^{(2)}, \quad (7.12)$$

⁷Actually, the CSS formula is not an evolution equation. It is a formula for the DY cross section, but it uses (TMD) factorization of hard and soft parts and resummation of soft gluon emissions which is also one of the fundamentals of the PB evolution equations.

as do the gluon coefficients $k_g^{(1)}$ and $A_g^{(2)}$ given in (5.10) and (4.18):

$$k_g^{(1)} = 2C_A^2 \left(\frac{67}{18} - \frac{\pi^2}{6} \right) - C_A T_R N_f \frac{20}{9} = A_g^{(2)}. \quad (7.13)$$

The coefficients $d_q^{(0)}$ and $B_q^{(1)}$ differ by a sign and factor 1/2:

$$d_q^{(0)} = \frac{3}{2}C_F = -\frac{1}{2}B_q^{(1)}, \quad (7.14)$$

as does the gluon contribution to the NLL coefficients:

$$d_g^{(0)} = \frac{11}{6}C_A - \frac{2}{3}T_R N_f = -\frac{1}{2}B_g^{(1)}, \quad (7.15)$$

which corresponds to the condition for equal Sudakov factors given in (7.9). Up to NLL ($\alpha_s^n \ln^{2n-2}(\mu^2/q_\perp^2)$) PB and CSS correspond. [39]

7.2.3 NNLL coefficients

For the next-to-next-to-leading logarithmic contributions, the $d_q^{(1)}$ and $B_q^{(2)}$ coefficients are investigated. They are given respectively in equations (5.11) and (4.19). The $k^{(2)}$ and $A^{(3)}$ coefficients are much lengthier because these are higher order coefficients in the strong coupling expansion (they go along with a factor of α_s^3).

The difference between the NNLL coefficients is calculated to further investigate the origin later. An overall factor in the outcome is avoided by the multiplication of $d_q^{(1)}$ with -2 so that

$$B_q^{(2)} - (-2 \cdot d_q^{(1)}) = C_F C_A \left(\frac{22}{9}\pi^2 - \frac{176}{12} \right) + C_F T_R N_f \left(\frac{16}{3} - \frac{8}{9}\pi^2 \right). \quad (7.16)$$

Collecting the terms with π^2 yields

$$B_q^{(2)} - (-2 \cdot d_q^{(1)}) = \frac{\pi^2}{6}C_F \left(\frac{44}{3}C_A - \frac{16}{3}T_R N_f \right) - \frac{1}{3}C_F(44C_A - 16T_R N_f). \quad (7.17)$$

Here the zeroth order coefficient of the β -function $\beta_0 = \frac{1}{12\pi}(11C_A - 4T_R N_f)$ is recognized:

$$B_q^{(2)} - (-2 \cdot d_q^{(1)}) = \zeta(2)C_F(16\pi\beta_0) - \frac{1}{3}C_F(48\pi\beta_0), \quad (7.18)$$

where $\zeta(2) = \pi^2/6$. This can be written compactly as

$$B_q^{(2)} - (-2) \cdot d_q^{(1)} = 16C_F\pi\beta_0(\zeta(2) - 1). \quad (7.19)$$

Since the difference is fully proportional to β_0 , we can predict that the origin of this difference comes from properties of the renormalization group (see section 1.3.3). The key idea of the dependence of the perturbative coefficients of CSS on the renormalization procedure is the *process dependence* of the formalism. Here only the Drell-Yan process has been discussed and therefore all the coefficients that are given are those for DY. It is possible to construct a relation between process dependent functions and process independent ones. The PB formalism is process independent because it makes use of the DGLAP splitting functions which are not process dependent. The relation with process independent coefficients can be made by using a renormalization group transformation. The principles of an RG transformation are discussed qualitatively in the next section.

7.3 Renormalization group transformation

The TMD factorized form of the cross section by CSS (4.26) consists of several perturbative functions: A_a and B_a which are contained in the Sudakov form factor \sqrt{S} , C_{qj} coefficients and a hard scattering function H_{ab}^F . These functions are not unambiguously determined; parts of these functions can be transformed to others by performing a renormalization group transformation. The non-zero difference of the NNLL coefficients from the Sudakov form factor can be declared by the fact that an RG transformation of the (process dependent) hard scattering function yields factors that can be absorbed by the Sudakov form factor.

To make this more qualitative, consider the CSS expression for the DY cross section. The process dependent hard scattering factor is composed of the leading order matrix element and a factor H^F containing higher order corrections:

$$\begin{aligned}
\frac{d\sigma}{dQ^2 dy d\mathbf{q}_\perp^2} &\simeq \sum_{q,\bar{q}} \frac{\sigma^{(0)F}}{s} H^F(\alpha_s(\mu)) \int d^2\mathbf{b} e^{i\mathbf{b}\cdot\mathbf{q}_\perp} \sum_{j_1, j_2} \int_{x_1}^1 \frac{d\xi_1}{\xi_1} \int_{x_2}^1 \frac{d\xi_2}{\xi_2} \\
&\times \exp\left(-\int_{c_0/b^2}^{M^2} \frac{d\mu'^2}{\mu'^2} \left[A_i(\alpha_s(\mu')) \ln\left(\frac{M^2}{\mu'^2}\right) - B_i(\alpha_s(\mu')) \right]\right) \\
&\times C_{qj_1}\left(\frac{x_1}{\xi_1}, \mathbf{b}; \alpha_s\left(\frac{c_0}{b^2}\right), \mu\right) C_{qj_2}\left(\frac{x_2}{\xi_2}, \mathbf{b}; \alpha_s\left(\frac{c_0}{b^2}\right), \mu\right) \\
&\times f_{j_1}(\xi_1, \mu) f_{j_2}(\xi_2, \mu) + \{q_\perp\text{-finite terms}\}. \tag{7.20}
\end{aligned}$$

The integration limits of the integral over the evolution variable μ in the second line of (7.20) are written with an arbitrary integration constant c_0 and hard interaction energy scale M (where M is used because at the hard scattering massive bosons are produced).

The hard scattering function H^F causes the dependence of the other perturbative functions A , B and C on the process and on the *resummation scheme* [40, 41]. That is, they are connected by a renormalization group transformation of the partonic matrix element $H(\alpha_s(\mu))$ from a low scale c_0/b^2 to a high scale M^2 . Such a transformation is performed by the integration of the RGE which writes

$$\frac{\partial \ln H^F}{\partial \ln \mu^2} = \gamma_H(\alpha_s(\mu^2)), \tag{7.21}$$

where γ_H is the anomalous dimension related to the hard scattering matrix element. Integration over $\ln \mu^2$ gives

$$H^F(\alpha_s(M^2)) = \exp\left\{\int_{c_0/b^2}^{M^2} \frac{d\mu'^2}{\mu'^2} \gamma_H(\alpha_s(\mu'^2))\right\} H^F(\alpha_s(c_0/b^2)). \tag{7.22}$$

The exponential that arises is a resummation factor as shown in section 1.3.3 equation (1.34). This factor can merge with the Sudakov form factor which then takes the following form:

$$S(\mu, b) = \exp\left\{-\int_{c_0/b^2}^{M^2} \frac{d\mu'^2}{\mu'^2} \left[A_i(\alpha_s(\mu'^2)) \ln\left(\frac{M^2}{\mu'^2}\right) + B_i(\alpha_s(\mu'^2)) - \gamma_H(\alpha_s(\mu'^2)) \right]\right\}. \tag{7.23}$$

The RG transformation results in an extra term in the Sudakov form factor and a different scale of the factor H in (7.20). It can therefore affect the coefficients of the functions A_a and B_a , but

also the C_{qj} coefficients. They become process dependent due to mixing with the hard scattering function. Concerning the B function, with an RG transformation it can transform to a process independent function (without the upper index F) as

$$B_i^F(\alpha_s(\mu'^2)) = B_i(\alpha_s(\mu'^2)) - \gamma_H(\alpha_s(\mu'^2)), \quad (7.24)$$

in which (7.21) can be substituted to get

$$B_i^F(\alpha_s) = B_i(\alpha_s) - \frac{\partial \ln H^F(\alpha_s)}{\partial \ln \mu^2}, \quad (7.25)$$

and with use of the perturbation series expansions (1.29) and (1.38) this becomes

$$B_i^F(\alpha_s) = B_i(\alpha_s) - \beta(\alpha_s) \frac{\partial \ln H^F(\alpha_s)}{\partial \alpha_s}. \quad (7.26)$$

This connects the process independent function $B(\alpha_s)$ to the process dependent one $B^F(\alpha_s)$ with a term depending on the RG β -function and the hard scattering function H^F (which is clearly process dependent). These functions have perturbation series expansions that were given in (1.36) and (4.25). Substitution of these in (7.26) gives

$$B^F(\alpha_s(\mu'^2)) = B(\alpha_s(\mu'^2)) - \left(-\beta_0 \alpha_s^2 - \beta_1 \alpha_s^3 + \mathcal{O}(\alpha_s^4) \right) \left(\frac{H^{F(1)}}{\pi} + \frac{2\alpha_s}{\pi^2} H^{F(2)} + \mathcal{O}(\alpha_s^2) \right). \quad (7.27)$$

From this it can be seen that the $B^{(0)}$ and $B^{(1)}$ coefficients do not change with an RG transformation. The H function does not influence the LL and NLL coefficients because the lowest order term of the β -function is of second order in α_s . The calculation for the second order coefficient of B is as follows: first, the series expansions are substituted in (7.26). Then, to obtain the second order coefficient, only the term in α_s^2 remains. Here one has to be careful as the B function series expansion is defined with factors $(\alpha_s/\pi)^n$. When considering the second order coefficient, the last term in (7.27) gets an additional factor of π^2 . The transformation from a process dependent NNLL B coefficient to a process independent one is as follows:

$$B^{F(2)} = B^{(2)} + \pi \beta_0 H^{F(1)}. \quad (7.28)$$

The hard matrix element H , the coefficient functions C_{qj} and the perturbative functions of the Sudakov form factor A_i and B_i are thus related by a renormalization group transformation [26, 41]. Since H is process dependent and resummation scheme dependent, these other perturbative functions are too. At the time CSS was constructed, the Sudakov form factor $S(\mu, b)$ was supposed to be a process independent (universal) resummation factor. Due to RG properties and the mixing of perturbative functions, it is not.

In the evolution equations of PB there is no similar hard function like $\frac{\sigma_s^{(0)}}{s} H^F$ in the DY differential cross section. This could not have been the case since the PB formalism does not specify the process of consideration; it only determines evolution of the soft parts of the factorization.

7.4 Numerical validation

At this point, the difference between the NNLL coefficients from CSS and PB - $B^{(2)}$ and $d^{(1)}$ - given in (7.19) can be subjected to the relation in (7.28).

In [25] the result of the calculation for the hard scattering function is given. The notation in this paper is different: here the process dependent hard function \mathcal{A} represents the part that is not IR divergent. Equation 22 in [25] represents the same relation as in (7.28). Using the conventions from part I of this thesis, an additional factor 2π needs to be added to the zeroth order β -function coefficient. This relation with our conventions is

$$B_q^{DY(2)} = -2d_q^{(1)} + 2\pi\beta_0 \left(\frac{2}{3}C_F\pi^2 + \mathcal{A}_q^{DY}(\phi) \right). \quad (7.29)$$

With the expression for \mathcal{A}_q^{DY} given in eq. 15 in [25] this becomes

$$B_q^{DY(2)} = -2d_q^{(1)} + 2\pi\beta_0 \left(\frac{2}{3}C_F\pi^2 + C_F \left(-8 + \frac{2}{3}\pi^2 \right) \right). \quad (7.30)$$

By rearrangement of these terms and the use of the Riemann zeta function, this results in

$$B_q^{DY(2)} = -2d_q^{(1)} + 16\pi\beta_0 C_F (\zeta(2) - 1), \quad (7.31)$$

which agrees with the difference that has been found between the NNLL PB and CSS coefficients in (7.19). After applying an RG transformation, these NNLL coefficients thus correspond.

7.5 Summary

This chapter has provided a detailed comparison of the perturbative functions that appear in the soft gluon resummation factors of CSS and PB. The coefficients of these perturbative functions are classified according to the logarithmic powers to compare the functions order by order. In sections 7.2.1 and 7.2.2 it is shown that both the quark and gluon contributions to the leading logarithmic and next-to-leading logarithmic coefficients are equal (leaving out some overall factors) in the formalisms of consideration. The next-to-next-to-leading logarithmic coefficients however do not correspond (section 7.2.3). The reason for the inconsistency is the process dependence of all the perturbative coefficients inside the CSS formula. They can be connected with a renormalization group transformation. Specifically the B function in CSS and d function used by PB at NNLL are compared. With a transformation to a process independent B function as given in equation (7.28), the two coefficients do agree.

8 Comparison of KMRW with the parton branching method

KMRW has been a commonly and successfully used approach to obtain TMDs (or uPDFs) for about 20 years. The PB method also provides a new method to obtain TMDs using similar principles as those used by KMRW. For this reason, it is interesting to compare PB with KMRW both analytically and numerically. In this chapter the differences that have been found and investigated will be presented and described.

In KMRW evolution, the dependence of the uPDFs on k_\perp enters at the last step of the evolution. This is already one of the crucial differences with the approach of the evolution cascade by parton branching, where an iterative way of solving the evolution equations implies the generation of transverse momentum in all steps. By comparing the collinear evolution equations of KMRW and PB, it seems that these are very similar at first sight. However, with a detailed comparison of all the parts of the equations and interpretation of all the factors and limits, crucial differences emerged. To be able to make this comparison, the two equations (5.26) and (6.6) have to be written in the same form. This means that both should be integral equations with equal evolution variables. The parton branching equation is therefore rewritten with the transverse momentum q_\perp as evolution variable by the implementation of the angular ordering condition.

8.1 Parton branching evolution equations in q_\perp

The angular ordering condition is reflected in three parts of the evolution equations which has been summarized in table 5.1: i) the cut-off parameterization of the splitting variable z_M , ii) the scale at which α_s is evaluated and iii) the calculation of transverse momentum q_\perp . The last part cannot be seen in the equation for collinear PDFs \tilde{f} (5.26), but it can in these for TMDs $\tilde{\mathcal{A}}$ (5.42).

The angular ordering condition is applied to the scale of α_s and the cut-off for z so that the second term of the evolution equation (5.26) becomes:

$$\sum_b \int_{\mu_0^2}^{\mu^2} \frac{d\mu'^2}{\mu'^2} \frac{\Delta_a(\mu^2)}{\Delta_a(\mu'^2)} \int_x^{1-\frac{q_0}{\mu'}} dz P_{ab}^{(R)}(\alpha_s((1-z)^2\mu'^2), z) \tilde{f}_b\left(\frac{x}{z}, \mu'^2\right). \quad (8.1)$$

According to the angular ordering condition, the transverse momentum q_\perp depends on the evolution scale μ' and the splitting variable z . In order to make the substitution of integration variable μ' to q_\perp , the order of integration should be interchanged from $\int d\mu' \int dz$ to $\int dz \int d\mu'$. The integrand does not change with the shuffling of integrals, but the integration boundaries do. In figure 8.1 a plot of the integration region is shown from which the integration limits can be read. The

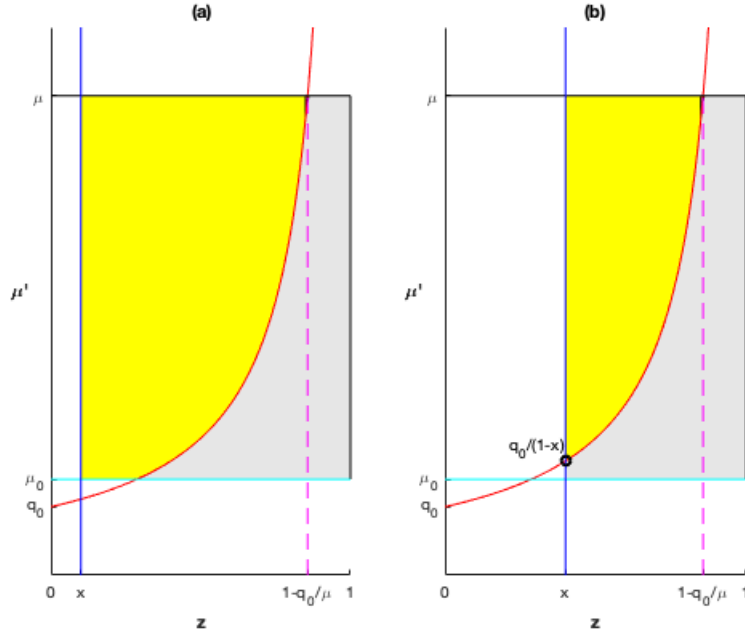


Figure 8.1: Regions of integration in two scenarios characterized by the value of x . a) low x regime: $x < 1 - q_0/\mu_0$ b) high x regime: $x > 1 - q_0/\mu_0$.

curve that is drawn represents the variable $z_M = 1 - q_0/\mu'$ (for the angular ordering condition). The region where z is smaller than this curve (yellow area) is the resolvable region over which is integrated. On the right side of this curve (grey area), splittings are non-resolvable. Two possible scenarios are drawn: one where $q_0 > (1 - x)\mu_0$ and one where $q_0 < (1 - x)\mu_0$.

A priori there is no physical relation between the lower transverse momentum limit q_0 and lower energy scale μ_0 . Though, in the right plot the effective lower scale is not μ_0 but $q_0/(1 - x)$. From another point of view, one could fix q_0 and μ_0 and consider the two regions to have different values of x . The left plot then figures the region $x < 1 - q_0/\mu_0$ (low x) and the right plot the large x region where $x > 1 - q_0/\mu_0$. With this approach, the interchange of the integrals in (8.1) is performed separately for the low and the high x regimes.

8.1.1 Evolution equation in the high x regime

This concerns the scenario in figure 8.1 (b). When $x > 1 - q_0/\mu_0$, the integration in (8.1) is first performed over z in the region $x < z < 1 - q_0/\mu'$ followed by the integration over μ' in the region $q_0/(1 - x) < \mu' < \mu$. After interchanging the order of integration, the integral over μ' will be performed first within $q_0/(1 - z) < \mu' < \mu$ followed by the integral over z within $x < z < 1 - q_0/\mu$:

$$\int_x^{1 - \frac{q_0}{\mu}} dz \int_{\left(\frac{q_0}{1-z}\right)^2}^{\mu^2} \frac{d\mu'^2}{\mu'^2}. \quad (8.2)$$

At this point, the transformation to rescaled transverse momentum $\mu' = q_\perp/(1-z)$ can be performed. This yields

$$\sum_b \int_x^{1-\frac{q_0}{\mu}} dz \int_{q_0^2}^{(1-z)^2 \mu^2} \frac{dq_\perp^2}{q_\perp^2} \frac{\Delta_a(\mu^2)}{\Delta_a\left(\frac{q_\perp^2}{(1-z)^2}\right)} P_{ab}^{(R)}(\alpha_s(q_\perp^2), z) \tilde{f}_b\left(\frac{x}{z}, \frac{q_\perp^2}{(1-z)^2}\right). \quad (8.3)$$

The integrals can be interchanged again in a similar way. Only the upper limit for the integral in q_\perp changes to $(1-x)\mu$. The full evolution equations then become

$$\begin{aligned} \tilde{f}(x, \mu^2) &= \Delta_a(\mu^2) \tilde{f}_a(x, \mu_0^2) \\ &+ \sum_b \int_{q_0^2}^{(1-x)^2 \mu^2} \frac{dq_\perp^2}{q_\perp^2} \int_x^{1-\frac{q_\perp}{\mu}} dz \frac{\Delta_a(\mu^2)}{\Delta_a\left(\frac{q_\perp^2}{(1-z)^2}\right)} P_{ab}^{(R)}(\alpha_s(q_\perp^2), z) \tilde{f}_b\left(\frac{x}{z}, \frac{q_\perp^2}{(1-z)^2}\right). \end{aligned} \quad (8.4)$$

8.1.2 Evolution equation in the low x regime

In the scenario of figure 8.1(a), the integration area (yellow) can be obtained by the calculation of the same integral as in the high x region with an additional subtraction of the region where $\mu' < \mu_0$. Similar as in (8.2), the interchanged integrals have boundaries that are changed:

$$\int_x^{1-\frac{q_0}{\mu}} dz \int_{\left(\frac{q_0}{1-z}\right)^2}^{\mu^2} \frac{d\mu'^2}{\mu'^2} - \int_x^{1-\frac{q_0}{\mu_0}} dz \int_{\left(\frac{q_0}{1-z}\right)^2}^{\mu_0^2} \frac{d\mu'^2}{\mu'^2}. \quad (8.5)$$

Similar to the procedure for the high x regime, the substitution of rescaled transverse momentum is performed to yield the evolution equations:

$$\begin{aligned} \tilde{f}_a(x, \mu^2) &= \Delta_a(\mu^2) \tilde{f}_a(x, \mu_0^2) + \\ &+ \int_{q_0^2}^{(1-x)^2 \mu^2} \frac{dq_\perp^2}{q_\perp^2} \int_x^{1-\frac{q_\perp}{\mu}} dz \Delta_a\left(\mu^2, \frac{q_\perp^2}{(1-z)^2}\right) P_{ab}^{(R)}(\alpha_s(q_\perp^2), z) \tilde{f}_b\left(\frac{x}{z}, \frac{q_\perp^2}{(1-z)^2}\right) \\ &- \int_{q_0^2}^{(1-x)^2 \mu_0^2} \frac{dq_\perp^2}{q_\perp^2} \int_x^{1-\frac{q_\perp}{\mu_0}} dz \Delta_a\left(\mu^2, \frac{q_\perp^2}{(1-z)^2}\right) P_{ab}^{(R)}(\alpha_s(q_\perp^2), z) \tilde{f}_b\left(\frac{x}{z}, \frac{q_\perp^2}{(1-z)^2}\right). \end{aligned} \quad (8.6)$$

A property of the PB Sudakov has been used here which is proved in the next section. The upper scale μ^2 comes from the nominator and the lower scale $\frac{q_\perp^2}{(1-z)^2}$ from the denominator. The second line equals that of (8.4). This formula can be rearranged to separate the low q_\perp integration. This region is characterized by the limits $q_0 < q_\perp < (1-x)\mu_0$. Equation (8.6) then becomes:

$$\begin{aligned} \tilde{f}_a(x, \mu^2) &= \Delta_a(\mu^2) \tilde{f}_a(x, \mu_0^2) + \\ &+ \int_{(1-x)^2 \mu_0^2}^{(1-x)^2 \mu^2} \frac{dq_\perp^2}{q_\perp^2} \int_x^{1-\frac{q_\perp}{\mu}} dz \Delta_a\left(\mu^2, \frac{q_\perp^2}{(1-z)^2}\right) P_{ab}^{(R)}(\alpha_s(q_\perp^2), z) \tilde{f}_b\left(\frac{x}{z}, \frac{q_\perp^2}{(1-z)^2}\right) \\ &+ \int_{q_0^2}^{(1-x)^2 \mu_0^2} \frac{dq_\perp^2}{q_\perp^2} \int_{1-\frac{q_\perp}{\mu_0}}^{1-\frac{q_\perp}{\mu}} dz \Delta_a\left(\mu^2, \frac{q_\perp^2}{(1-z)^2}\right) P_{ab}^{(R)}(\alpha_s(q_\perp^2), z) \tilde{f}_b\left(\frac{x}{z}, \frac{q_\perp^2}{(1-z)^2}\right). \end{aligned} \quad (8.7)$$

8.2 Sudakov form factors

First, as a side remark to the previous section; the parton branching Sudakov form factor can also be rewritten in terms of transverse momentum q_\perp . In the high x regime, no additional term arises in the exponent. In the low x regime there is an additional term, the Sudakov then becomes

$$\Delta_a(\mu, \mu_0) = \exp \left(- \sum_b \int_{\mu_0^2}^{\mu^2} \frac{dq_\perp^2}{q_\perp^2} \int_0^{1-\frac{q_\perp}{\mu}} dz P_{ba}^{(R)}(\alpha_s(q_\perp^2), z) + \right. \\ \left. - \sum_b \int_{q_0^2}^{\mu_0^2} \frac{dq_\perp^2}{q_\perp^2} \int_{1-\frac{q_\perp}{\mu_0}}^{1-\frac{q_\perp}{\mu}} dz z P_{ba}^{(R)}(\alpha_s(q_\perp^2), z) \right). \quad (8.8)$$

Before comparing the evolution equations of PB with theses of KMRW, properties of the Sudakov form factors of both methods are discussed. The lower scale is not written generally: $\Delta_a(\mu, \mu_0) = \Delta_a(\mu)$. With the angular ordering cut-off, the fraction of two Sudakov form factors

$$\frac{\Delta_a(\mu^2)}{\Delta_a(\tilde{\mu}^2)} = \frac{\exp \left(- \sum_b \int_{\mu_0^2}^{\mu^2} \frac{d\mu'^2}{\mu'^2} \int_0^{1-q_0/\mu'} dz z P_{ba}^{(R)}(\alpha_s((1-z)\mu')) \right)}{\exp \left(- \sum_b \int_{\mu_0^2}^{\tilde{\mu}^2} \frac{d\mu'^2}{\mu'^2} \int_0^{1-q_0/\mu'} dz z P_{ba}^{(R)}(\alpha_s((1-z)\mu')) \right)}, \quad (8.9)$$

can be written as

$$\frac{\Delta_a(\mu^2)}{\Delta_a(\tilde{\mu}^2)} = \exp \left(- \sum_b \int_{\tilde{\mu}^2}^{\mu^2} \frac{d\mu'^2}{\mu'^2} \int_0^{1-q_0/\mu'} dz z P_{ba}^{(R)}(\alpha_s((1-z)\mu')) \right) \\ = \Delta_a(\mu^2, \tilde{\mu}^2). \quad (8.10)$$

This quotient thus equals one Sudakov with lower scale $\tilde{\mu}$ and upper scale μ .

In part II (TMD formalisms), it has been stated that the Sudakov form factor can be interpreted as a probability for parton a to not radiate a parton b . This is approximately valid as long as one integrates the splitting variable over a constant interval with a fixed cut-off z_M close to one. A property of a probability factor is that multiplication of two factors gives the probability for both processes. This property has been checked for both the PB and KMRW Sudakov form factors. Since these have different definitions, the interpretation and outcome of Sudakov multiplications also differs.

The product of two form factors in the PB method is

$$\Delta_a(\mu_2, \mu_1) \Delta_a(\mu_1, \mu_0) = \Delta_a(\mu_2, \mu_0), \quad (8.11)$$

which follows from (8.10). This is a property of probability factors, but it does not prove that the Sudakov form factor is one. When z_M is fixed, (8.11) works for both KMRW as PB. When ordering conditions are applied and z_M becomes variable, this still holds for PB with angular ordering in the low x regime (8.8) or PB written with a general scale μ' (5.21), but it does not for KMRW. The Sudakov form factor in KMRW reads

$$T_a(\mu, k_\perp) = \exp \left(- \int_{k_\perp^2}^{\mu^2} \frac{dq_\perp^2}{q_\perp^2} \sum_b \int_0^{1-\Delta(q_\perp, \mu)} dz z P_{ba}(z, q_\perp) \right). \quad (8.12)$$

The crucial difference with the PB Sudakov from (5.21) is that the cut-off in KMRW depends on the upper scale of the evolution k_\perp . When angular ordering is applied to PB, the IR cut-off becomes this from (5.40), which is independent on the upper and lower scales of the evolution variable μ' . Due to the μ -dependence of Δ in (8.12) on μ , (8.11) does not hold for KMRW with strong or angular ordering where the product of two Sudakov factors is

$$\begin{aligned} T_a(\mu, k_\perp)T_a(k_\perp, \mu_0) &= \\ &= \exp \left(- \sum_b \left\{ \int_{k_\perp^2}^{\mu^2} \frac{dq_\perp^2}{q_\perp^2} \int_0^{1-\Delta(q_\perp, \mu)} dz - \int_{\mu_0^2}^{k_\perp^2} \frac{dq_\perp^2}{q_\perp^2} \int_0^{1-\Delta(q_\perp, k_\perp)} dz \right\} z P_{ba}^{(R)}(z, q_\perp) \right) \end{aligned} \quad (8.13)$$

and these integrals can not be merged to one term in the exponent because the upper limits for z differ, concluding that

$$T_a(\mu, k_\perp)T_a(k_\perp, \mu_0) \neq T_a(\mu, \mu_0). \quad (8.14)$$

The probabilistic feature of the Sudakov is not required for a justified evolution. Previous results only indicate differences between PB and KMRW properties.

8.3 Analytical comparison of the evolution equations

The PB equations are now at a stage in which they can be compared to the KMRW equations. To make this comparison more clear, the notation conventions used by KMRW that were used in chapter 6 are changed to these used by PB. The integral definition of the KMRW evolution equations for collinear (integrated) PDFs (6.6) is then written as

$$\begin{aligned} \tilde{f}(x, \mu) &= T_a(\mu, \mu_0) \tilde{f}_a(x, \mu_0) \\ &+ \int_{\mu_0^2}^{q_{\perp, max}} \frac{dq_\perp^2}{q_\perp^2} T_a(\mu, q_\perp) \sum_b \int_x^{1-\Delta} dz P_{ab}^{(R)}(\alpha_s(q_\perp^2), z) \tilde{f}_b\left(\frac{x}{z}, q_\perp^2\right). \end{aligned} \quad (8.15)$$

From here onwards this equation will be compared with the PB equation for collinear PDFs with angular ordering in the low x region given in (8.4). The notation T for the KMRW Sudakov remains because the Sudakov form factors do not correspond exactly as argued in the previous section. An additional factor z in the second line of (8.15) comes from the use of momentum-weighted collinear PDFs (contrary to the non-momentum weighted PDFs D_a). The cut-off Δ is regulated by the choice of ordering, this can either be strong ordering: $\Delta^{SO} = \frac{q_\perp}{\mu}$, or angular ordering: $\Delta^{AO} = \frac{q_\perp}{q_\perp + \mu}$. Consequently, the upper limit of the transverse momentum (denoted by $q_{\perp, max}$) also depends on the ordering. Originally, the upper limit of the evolution variable was μ , but with SO the transverse momentum is limited by $q_{\perp, max}^{(SO)} = \mu(1-x)$ and for AO by $q_{\perp, max}^{(AO)} = \mu(1-x)/x$. With AO, the domain of transverse momentum can therefore be enlarged much beyond the hard scale μ .

8.3.1 Equations for collinear PDFs \tilde{f}_a

Already within the evolution equations for collinear PDFs, differences between KMRW and PB are present. Comparing (8.15) with (8.4) leads to the following observations (similarities and differences) [42]:

- Both equations have the strong coupling evaluated in the same scale: $\alpha_s(q_\perp)$.
- The lower limit of the transverse momentum inside the PB Sudakov form factor is $\mu' = q_\perp/(1-z)$ while this of KMRW is just q_\perp .
- The scale of the initial PDF differs. Parton branching has $\tilde{f}_b(x/z, q_\perp^2/(1-z)^2)$ while KMRW has $\tilde{f}_b(x/z, q_\perp^2)$.
- The upper integration limits for $\int dq_\perp$ and $\int dz$ differ.

The second and third observations are due to the association of μ' with the rescaled transverse momentum $\bar{q}_\perp = q_\perp/(1-z)$ in PB. In KMRW, only the integration variable is associated to the transverse momentum.

Equation (8.4) is given in the form where angular ordering according to the PB method is applied. The transverse momentum then has a maximum value that equals $(1-x)\mu$, with μ the hard scattering scale. KMRW has two types of ordering: strong and angular ordering. These conditions specify the cut-off (Δ) dependence on k_\perp and with that the k_\perp domain of the PDFs. These expressions are given in 6.2. SO and AO only influence the upper limits of the integrals of (8.15). The maximum values of transverse momentum are given above. With the use of SO in KMRW, both upper integration limits correspond with the upper limits in PB with angular ordering. With AO in KMRW, both upper limits differ from these in PB.

8.3.2 Equations for TMDs

A fundamental difference between the two methods lies in the evaluation of TMDs. KMRW defines a TMD (or uPDF) as the unintegrated part of the second term from (8.15)

$$\tilde{f}_{\text{TMD}}(x, \mu, k_\perp) = T_a(\mu, q_\perp) \sum_b \int_x^{1-\Delta} dz P_{ab}^{(R)}(\alpha_s(q_\perp^2), z) \tilde{f}_b\left(\frac{x}{z}, q_\perp^2\right). \quad (8.16)$$

Equation (8.15) could thus be written as

$$\tilde{f}(x, \mu) = T_a(\mu, \mu_0) \tilde{f}_a(x, \mu_0) + \int_{\mu_0^2}^{(1-x)^2 \mu^2} \frac{dq_\perp^2}{q_\perp^2} \tilde{f}_{\text{TMD}}(x, \mu, k_\perp). \quad (8.17)$$

In PB, the TMDs are evolved using equation (5.42) with the iterative branching procedure (as are collinear PDFs) and includes a specific prescription for the calculation of the transverse momentum according to an ordering condition as given in (5.43). Such a prescription on the construction of transverse momentum is not given in KMRW because it generates all the transverse momentum in one step. UPDFs constructed by KMRW do not gather transverse momentum through a cascade of branchings as in PB. The second scale (transverse momentum) enters the uPDF only in the last step.

A crucial observation in the general procedure to obtain TMDs is that KMRW does not evolve TMDs or uPDFs. Instead, these are calculated from a collinear PDF as in equation (8.16) (equal to (6.7)).

8.4 Numerical comparison

With a numerical comparison of the methods, analytical differences could be illustrated by differences in plots of TMDs or even collinear PDFs obtained from TMDs (by integration over the transverse momentum). A TMD from KMRW has been taken from `TMDlib` [43, 44]. This is a recently developed library that includes many TMDs from different formalisms. This library is still growing since interest in TMDs is growing in many regions of the high energy physics community. Unfortunately, there is only one available TMD from KMRW which is named MRW-CT10nlo [45]. MRW is an alternative name for KMRW. CT10nlo [46] is the starting collinear PDF from which the uPDF is constructed using the integral formulation of KMRW (6.7) with the AO condition from (6.10). With this ordering, the cut-off $(1 - \frac{q_\perp}{q_\perp + \mu})$ does not correspond to this of PB in angular ordering $(1 - \frac{q_0}{\mu'})$.

A code to evolve PDFs according to the parton branching method has been used. This is the `updfevolv-2.4.00-beta04` evolution code [47]. An early version of this was constructed for the evolution with the CCFM equation, but the version that has been used (version 2.4.04) evolves PDFs according to the PB method. Monte Carlo techniques are used to solve the evolution equations numerically.

The generation of TMDs with both methods should be performed with equal initial conditions. One starts from an initial collinear distribution. Since the available KMRW uPDF is constructed with CT10nlo as initial PDF, this is also taken as the starting distribution for the evolution with the PB method. The `updfevolv`-code adds an intrinsic (starting) transverse momentum distribution to this collinear PDFs so that the initial distribution has k_\perp dependence. Then, within the branching cascade procedure, transverse momentum is generated in each step.

Several kinematic regimes are considered in the numerical calculations of TMDs or uPDFs. In the following sections, plots are shown of TMDs at fixed values of x in section 8.4.1, of TMDs at fixed values of k_\perp in section 8.4.2 and TMDs that are integrated over the transverse momentum (iTMDs) in section 8.4.3.

8.4.1 TMDs versus k_\perp

In figure 8.2 four plots are shown of gluon TMDs that are evolved to equal scales and plotted for fixed values of x . The red curves are results from KMRW with angular ordering (AO) and the use of the differential definition (6.5), which is the only available TMD from this method in the `TMDlib` library (where it is called MRW instead of KMRW). The blue curves are results from the PB method using angular ordering. The x -axis represents the transverse momentum of the evolved parton at the hard scale which is k_t (k_\perp in (5.41)).

Several observations from these plots can be made. [42]

First, at k_\perp below the lowest evolution scale (1 GeV) the TMDs from KMRW show a constant behaviour and suddenly raise from the low scale to higher k_\perp while the PB TMDs are continuously decreasing towards larger transverse momentum. The origin of this difference lies in the step-by-step evolution of PB and the last step evolution of KMRW. In one step, emitted partons cannot obtain smaller transverse momentum than the lowest scale. However, with the multiple-step approach of PB, the vectorial sum of transverse momentum in different directions can be smaller than the lowest evolution scale. Moreover, due to the association of the scale with the rescaled

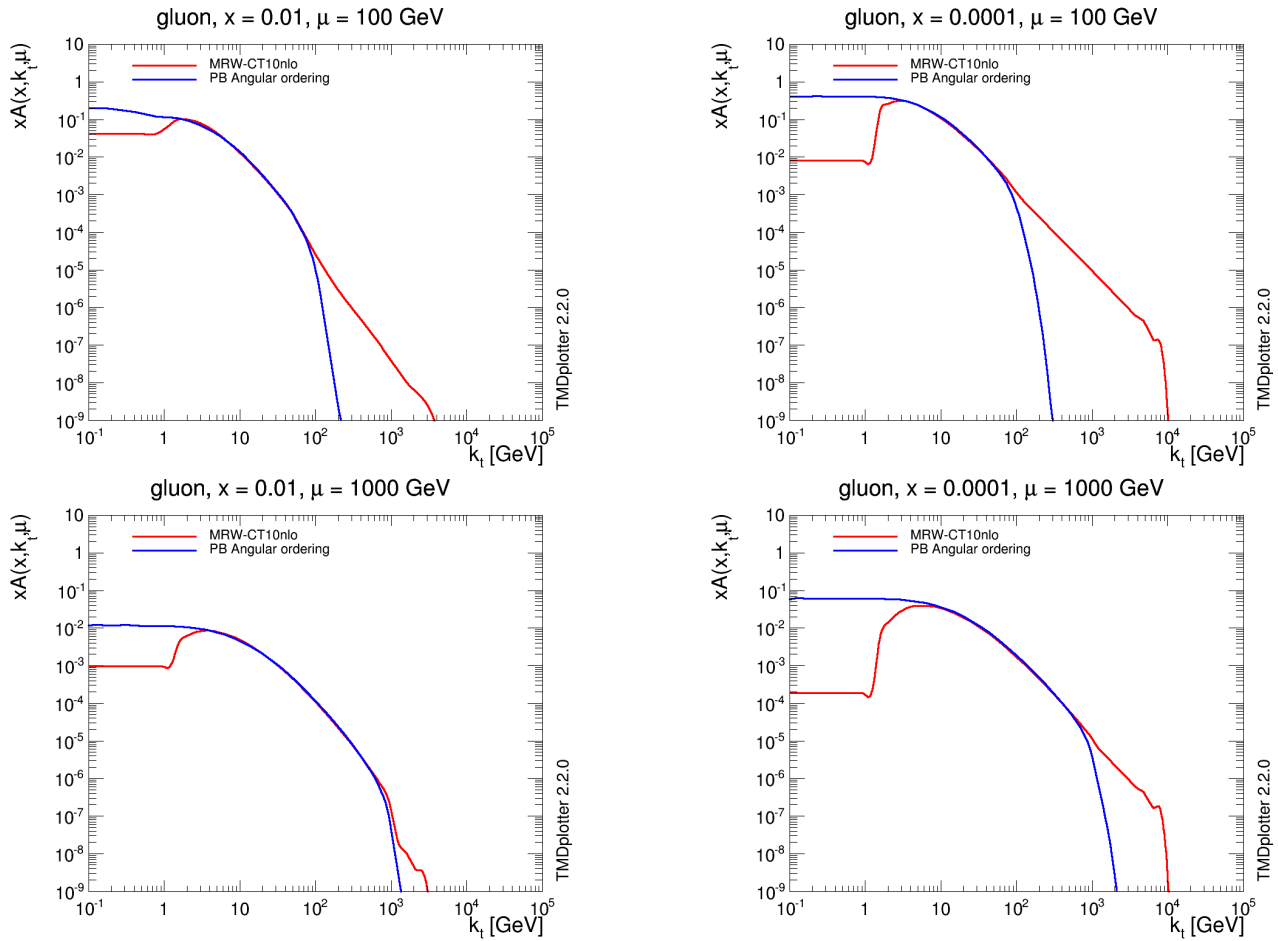


Figure 8.2: Momentum weighted gluon TMDs versus k_{\perp} for different values of the upper scale μ (upper plots: $\mu = 100$ GeV, lower plots: $\mu = 1000$ GeV) and longitudinal momentum fraction x (left plots: $x = 10^{-2}$, right plots: $x = 10^{-4}$). The red curves are results from KMRW with angular ordering using the differential formulation, the blue curves are results from PB with angular ordering. Note the logarithmic scales on both axes.

transverse momentum $q_{\perp} = (1 - z)\mu'$, the transverse momentum can become small for large z . In KMRW, for $k_{\perp} < 1$ GeV, the values of $x\mathcal{A}(k_{\perp}, \mu)$ are put to a constant.

Secondly, in the middle k_{\perp} region, KMRW and PB agree very well. Middle k_{\perp} means the region between the low scale (1 GeV) and the hard scale μ . This is remarkable since the analytical expressions show many differences. The third observation is that at large transverse momenta $k_{\perp} > \mu$, the PB TMD drops quickly while the one from KMRW has a longer tail that proceeds to much larger transverse momentum.

Considering the large k_{\perp} tail, this leads to the last observation which is a discontinuity at the beginning of the large k_{\perp} tail of KMRW. In each plot this effect is observed. It is due to the non-physical behaviour of the Sudakov for transverse momenta larger than the upper evolution scale. The Sudakov T_a for $k_{\perp} > \mu$ is put to one as in (6.11).

In figure 8.3, TMDs of the up quark are shown for $\mu = 100$ GeV and different x values. Similar observations as for the gluon TMDs can be made in the quark distributions.

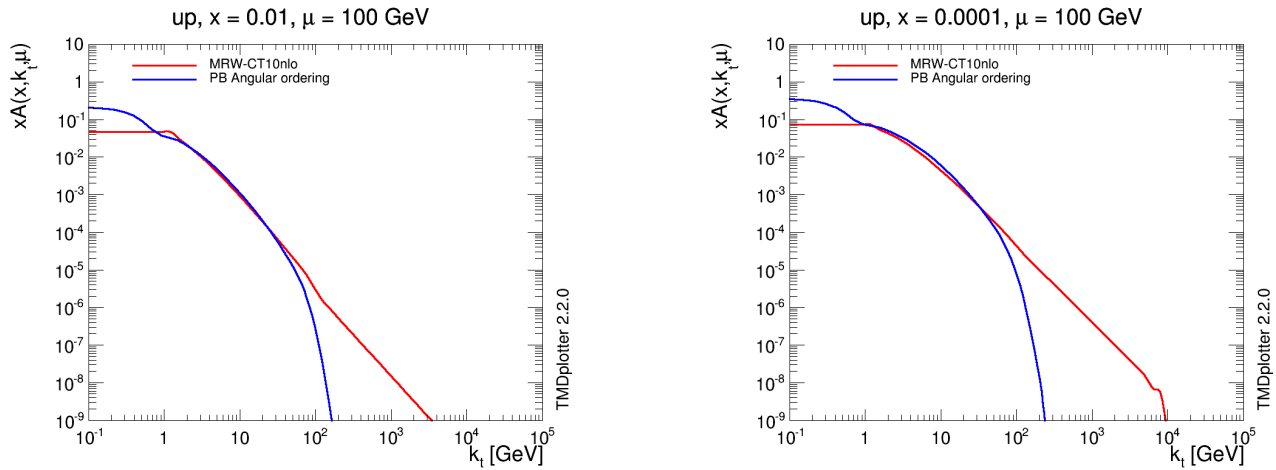


Figure 8.3: Momentum weighted up quark TMDs versus k_\perp for $\mu = 100$ GeV and $x = 10^{-2}$ (left) and $x = 10^{-4}$ (right). The red curves are results from KMRW with angular ordering using the differential formulation, the blue curves are results from PB with angular ordering.

8.4.2 TMDs versus x

It could be informative to compare the TMDs when plotted versus longitudinal momentum (for fixed k_\perp). Four gluon TMDs are shown in figure 8.4 for the same hard scale ($\mu = 1000$ GeV) but for different fixed values of transverse momentum. The MRW distribution has a strong fall at high x which is not related to the KMRW evolution, but to technical issues with binning.

These results fortify the observation from section 8.4.1 that KMRW and PB are similar in the middle k_\perp region. That is, for $k_\perp = 10$ GeV and $k_\perp = 100$ GeV both at $\mu = 1000$ GeV, the TMDs correspond very well. However, for low and high transverse momenta, they do not match that well.

8.4.3 iTMDs

By integration of the TMDs over the transverse momentum (as in equation (3.3)), collinear PDFs are formed. This can be checked for the TMDs that are evolved by PB and KMRW in previous sections. These TMDs are all constructed from the collinear starting distribution CT10nlo. It is not necessarily true that integration over the full k_\perp domain results in the original collinear PDF since with the construction of a TMD soft gluons are resummed and more information about the dynamics is included in the parton distribution function. KMRW extends the transverse momentum domain by their choice of the cut-off, so that the integration of transverse momentum up to the upper scale μ would not yield the same distribution as the integration up to infinity. The parton branching TMD would not change a lot by integration up to μ instead of taking into account all transverse momenta while it is expected that the KMRW distribution does differ for these integration boundaries.

In figure 8.5 the integrated TMDs (iTMDs) for both PB and KMRW are shown at $\mu = 100$ GeV. In the left plot there is integrated up to μ and the integration in the right plot is up to $q_\perp = 10^{10}$ GeV (which approaches the integration up to infinity). In both plots the collinear PDF CT10nlo

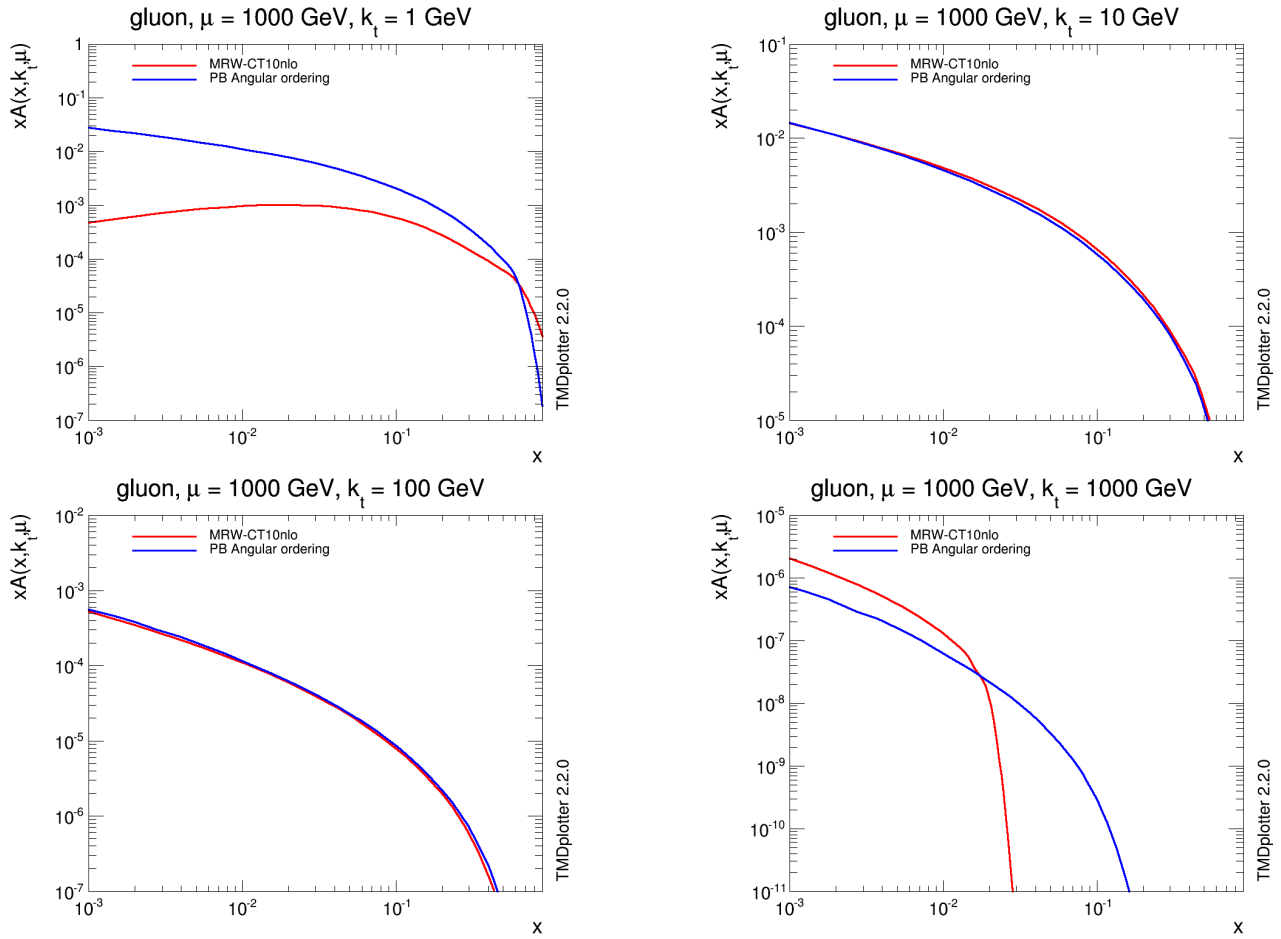


Figure 8.4: Momentum weighted gluon TMDs versus longitudinal momentum x for different values of transverse momentum $k_{\perp} = \{1, 10, 100, 1000\}$ GeV. Red curves are KMRW AO results and blue curves are from parton branching with angular ordering.

is also shown and the relative difference of both the KMRW and PB results with this distribution are shown on the bottom figure.

In figure 8.6, a single plot shows iTMDs that are calculated with one method. Each plot contains two curves, one of a TMD integrated up to the maximum evolution scale μ and the one of a TMD integrated up to infinity.

Since parton branching does not generate transverse momenta far above the upper evolution scale, the difference between integration up to μ and up to infinity is not large. The results for KMRW certify that the large k_{\perp} tail for $k_{\perp} > \mu$ influences the integrated TMDs strongly.

8.4.4 Z boson p_{\perp} spectrum

A final comparison is related to one of the arguments of constructing TMDs in the first place. In chapter 3 it was argued that with collinear factorization, the p_{\perp} spectrum of the Z boson cannot be described accurately in the very low p_{\perp} region. There the soft gluon emission effects are important

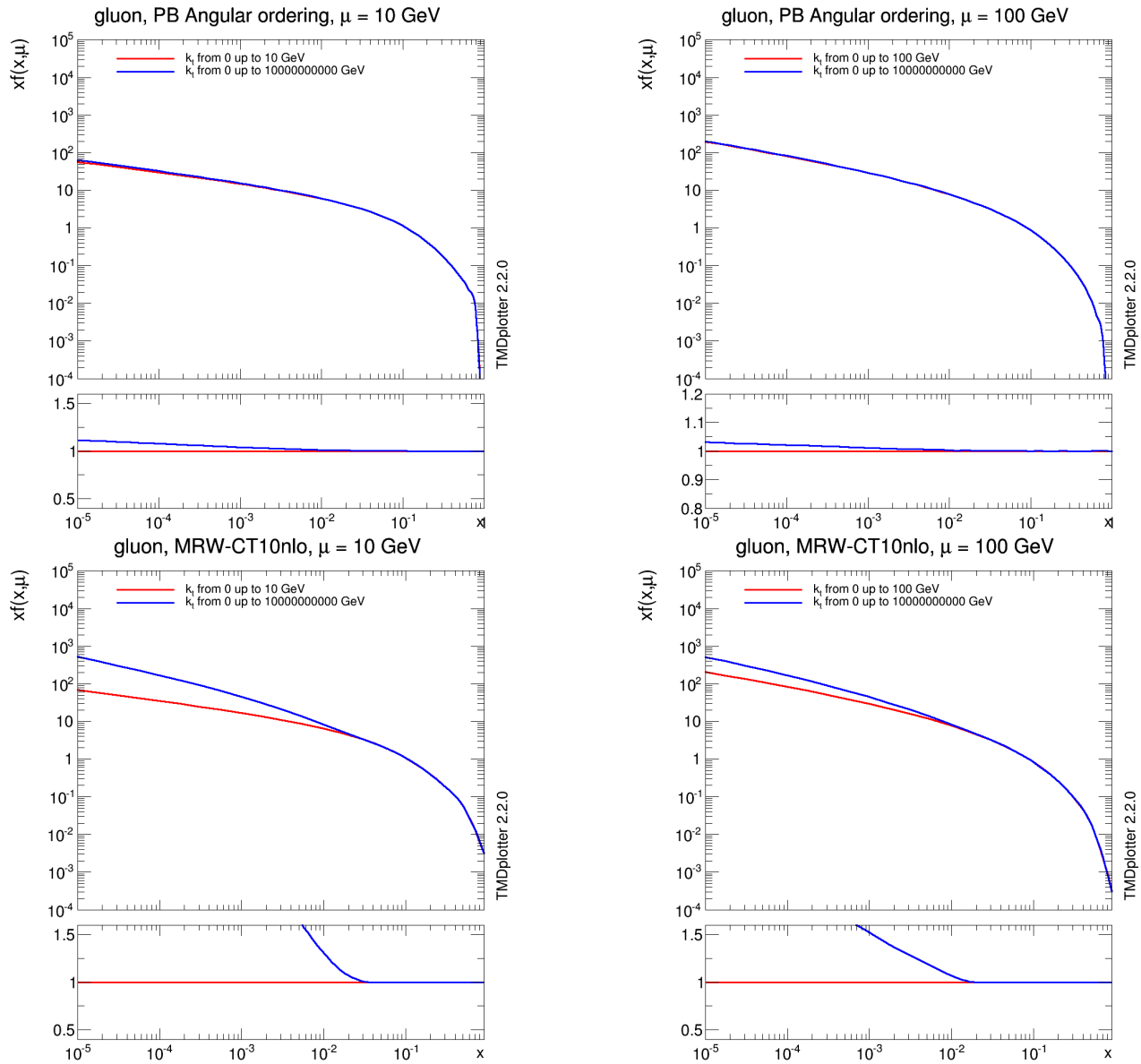


Figure 8.6: iTMDs from parton branching (upper two plots) and KMRW (bottom two plots) integrated up to μ (red curve) and integrated up to infinity (blue curve). The left plots show this for $\mu = 10$ GeV, the right plots for $\mu = 100$ GeV.

8.5 Summary

The PB method with the angular ordering condition and KMRW have been compared analytically and numerically. Conceptually they pursue the same goal: constructing transverse momentum dependent parton densities. This is accomplished by including soft gluon resummation within the DGLAP evolution equations. In order to compare the analytical structures of the methods, the PB formula has been written with the transverse momentum as evolution variable and a subdivision of two scenarios (in the low and high x region) is made.

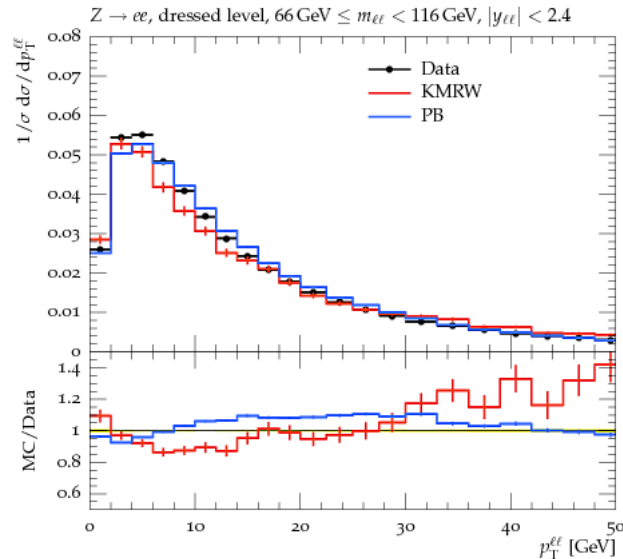


Figure 8.7: Z boson p_{\perp} spectrum described by experimental data (black points) and by calculations from KMRW (red curve) and PB (blue curve).

Analytical differences that were observed in the equations (5.26) and (8.15) are the lower scale of the Sudakov, the scale of the input PDFs \tilde{f}_b and the upper integration limits. These effects are not directly related to numerical observations, but they do influence the way in which the evolution is performed. Besides, KMRW carries out a single-step evolution where transverse momentum is generated in one branching while PB is characterized by a branching cascade where the transverse momentum is summed over all the branchings. KMRW has two definitions of the evolution equations, namely an integral (8.16) and a differential (6.5) form. Moreover, there are two ordering conditions for the cut-off: strong and angular ordering. With KMRW angular ordering, the cut-off does not correspond to the angular order PB cut-off. With both SO and AO, the k_{\perp} domain is extended because it takes values larger than the upper evolution scale μ . This implies that the Sudakov becomes unphysical which results in a discontinuity in the TMD observable in the numerical results.

The numerical results indicate that PB and KMRW work very similar in the middle k_{\perp} region. This can be concluded from both the plots versus k_{\perp} as the plots versus x . At small transverse momentum, KMRW does not agree with PB, it is flat because it is parameterized as intrinsic k_{\perp} . The evolution does not lead to the generation of transverse momentum under to lower evolution scale. This does happen in PB because of the step-by-step evolution. In the high k_{\perp} region the two methods do also not coincide. The KMRW angular ordering condition leads to a large k_{\perp} tail with a discontinuity because of the unphysical Sudakov form factor. Furthermore, by the investigation of integrated TMDs, it can be seen that with integration up to the evolved scale there is a large agreement of both the iTMDs with the original collinear PDF CT10nlo. However, when integrated over the full transverse momentum range, KMRW does not reproduce the collinear PDF anymore.

9 Conclusions

The description of the fundamental particles of nature and their interactions is very accurate within the standard model. Despite this, progress can still be made within the SM and beyond because both experimental and theoretical observations hint to unknown physics. With the LHC and future colliders, particle physicists try to find deviations from SM predictions. The collinear factorization theorem provides a good framework for the calculation of experimental quantities, but there are observables that cannot be described well with this. The TMD factorization framework is a tool to describe observables in a larger area of the phase space so that more accurate SM predictions can be made.

The recently developed parton branching method is a formalism that can be classified in high- k_{\perp} factorization. This method results in TMDs that match or even improve those from other methods [15, 28, 38]. At the end, the search for improvements of evolution formalisms of TMDs is still ongoing. Within the same framework of high- k_{\perp} factorization, there is the KMRW approach. Besides these formalisms that find their strong basis at the DGLAP evolution equations, there are other approaches to include transverse momentum dependencies in the description of high energetic particle collisions. CSS provides an expression for the Drell Yan cross section in \mathbf{b} -space. Despite the deviant line of the CSS approach compared to that of PB and KMRW, these formalisms have the same goal: describing processes of pp collisions with higher precision using the parton dynamics in the transverse plane. Communities that make use of TMDs mostly focus on one formalism that corresponds more to the application for which it is used. However, since parton distribution functions are universal objects, the formalisms that describes them should somehow have connections with each other. In this thesis, PB is compared with KMRW and CSS.

PB and CSS At first instance CSS and PB look very different, but with the detailed study and comparison of both approaches as performed here, one to one relations can be found. This correspondence concerns the Sudakov form factor which resums large logarithmic terms of the form $\alpha_s^n \ln^{2n-1}(Q^2/q_{\perp}^2)$ that come from soft gluon emissions. The coefficients from the perturbative series expansion of the functions of the Sudakov have been compared order by order. Concluding this comparison, the $A_a(\alpha_s)$ and $B_a(\alpha_s)$ from CSS respectively correspond to the $k_a(\alpha_s)$ and $d_a(\alpha_s)$ functions from PB up to NLL. At NNLL there is a difference in the expressions for $B^{(2)}$ and $d^{(1)}$ which can be explained by a renormalization group transformation of the hard scattering function in CSS. The hard scattering matrix element does not appear in PB because it only concerns about the TMDs, while these are only a part of the differential DY cross section.

The result that CSS and PB agree up to NNLL connects the different TMD communities. It could lead of more studies to the correspondences and analogies of the two methods. Further investigations on the perturbative coefficients of the Sudakov can be performed and one could search for relations between other factors of CSS and PB.

PB and KMRW The formulation of the PB method is closer to that of the KMRW model than to that of CSS because the former two provide evolution equations for transverse momentum dependent parton distribution functions. They do this by introducing an IR cut-off and using a Sudakov form factor. The evolution in transverse momentum is implemented differently since the PB method associates the evolution scale with rescaled transverse momentum according to an ordering condition that influences not only the evolution scale but also the cut-off and the way in which transverse momentum accumulates in the branching cascade. In KMRW however, only the cut-off changes for different ordering conditions. The transverse momentum arises just in the last step of the KMRW evolution.

The analytical differences result in differences in the numerical calculations. It has been investigated what these differences are. The main conclusion from the comparison of the TMDs is that they agree very well in the middle k_{\perp} region compared to the scale. The small k_{\perp} region is parameterized by a constant in KMRW; the evolution does not lead to final transverse momentum smaller than the starting scale. The PB solution using angular ordering does generate transverse momentum smaller than the starting scale because of the multiple step approach and the association of the evolution variable with rescaled transverse momentum $\mu' = \bar{q}_{\perp} = q_{\perp}/(1-z)$. TMDs produced with KMRW have a larger k_{\perp} , which is due to the influence of the choice of the cut-off to the k_{\perp} domain. This leads to discrepancy with the PB TMDs. With the study of iTMDs (TMDs integrated over the transverse momentum) it could be seen that the resulting collinear PDFs from PB and KMRW do not agree with each other. The iTMDs from KMRW reach higher values than these from PB. Finally, the TMDs have been subjected to a comparison with a measurement of the Z boson p_{\perp} spectrum. Both TMDs perform well and produce an accurate results at small p_{\perp} . KMRW does less well at large p_{\perp} than PB.

An overall consideration of the differences that were found seems to indicate that the PB method is capable to produce TMDs in a more consistent way than KMRW does. Reasons for this are that there are no discontinuities visible at large k_{\perp} and the small k_{\perp} region and the description of the Z boson p_{\perp} spectrum is better for large p_{\perp} .

Bibliography

- [1] F. Mandl and G. Shaw, *QUANTUM FIELD THEORY*. 1985.
- [2] M. Thomson, *Modern particle physics*. Cambridge University Press, 2013.
- [3] M. E. Peskin and D. V. Schroeder, "*An Introduction to quantum field theory*". Addison-Wesley Publishing Company, 1995.
- [4] L. D. Faddeev and V. N. Popov, Phys. Lett. **B25**, 29 (1967). [[325\(1967\)](#)].
- [5] J. M. Jauch and F. Rohrlich, *The theory of photons and electrons. The relativistic quantum field theory of charged particles with spin one-half*, in Texts and Monographs in Physics. Springer, Berlin, 1976.
- [6] R. Altmann, M. Lamont, and S. Myers, Nuclear Physics B - Proceedings Supplements **109**, 17 (2002). Proceedings of the 7th Topical Seminar.
- [7] R. D. Field, Front. Phys. **77**, 1 (1989).
- [8] B. W. R. Keith Ellis, W. James Stirling, *QCD and collider physics*. Cambridge University Press, 1996.
- [9] V. K. et al. [CMS Collaboration], Eur. Phys. J. C. no.5, 186 (2015).
- [10] M. Gell-Mann (1961).
- [11] R. P. Walker, Conf. Proc. **C9209071**, 437 (1992).
- [12] A. D. Martin, Acta Phys. Polon. **B39**, 2025 (2008). [0802.0161](#).
- [13] J. O. J. Bertrand, P. Bertrand, *The Mellin Transform*. CRC Press LLC, 2000.
- [14] A. Vogt, F. Herzog, S. Moch, B. Ruijl, T. Ueda, and J. A. M. Vermaseren, PoS **LL2018**, 050 (2018). [1808.08981](#).
- [15] A. Lelek, *Determination of TMD parton densities from HERA data and application to pp processes*. Ph.D. Thesis, DESY, Hamburg, 2018.
- [16] E. A. Kuraev, L. N. Lipatov, and V. S. Fadin, Sov. Phys. JETP **44**, 443 (1976). [[Zh. Eksp. Teor. Fiz.71,840\(1976\)](#)].
- [17] E. A. Kuraev, L. N. Lipatov, and V. S. Fadin, Sov. Phys. JETP **45**, 199 (1977). [[Zh. Eksp. Teor. Fiz.72,377\(1977\)](#)].
- [18] S. Catani, F. Fiorani, and G. Marchesini, Nucl. Phys. **B336**, 18 (1990).
- [19] R. Angeles-Martinez *et al.*, Acta Phys. Polon. **B46**, 2501 (2015). [1507.05267](#).

- [20] CDF Collaboration, F. Abe *et al.*, Phys. Rev. Lett. **66**, 2951 (1991).
- [21] J. C. Collins, D. E. Soper, and G. F. Sterman, Nucl. Phys. B (1985).
- [22] J. Collins, Camb. Monogr. Part. Phys. Nucl. Phys. Cosmol. **32**, 1 (2011).
- [23] J. C. Collins and D. E. Soper, Nucl. Phys. **B193**, 381 (1981). [Erratum: Nucl. Phys. B213,545(1983)].
- [24] C. T. H. Davies and W. J. Stirling, Nucl. Phys. **B244**, 337 (1984).
- [25] D. de Florian and M. Grazzini, Phys. Rev. Lett. **85**, 4678 (2000). hep-ph/0008152.
- [26] S. Catani, D. de Florian, and M. Grazzini, Nucl. Phys. **B596**, 299 (2001). hep-ph/0008184.
- [27] F. Hautmann, H. Jung, A. Lelek, V. Radescu, and R. Zlebcik, Phys. Lett. **B772**, 446 (2017). 1704.01757.
- [28] F. Hautmann, H. Jung, A. Lelek, V. Radescu, and R. Zlebcik, JHEP **01**, 070 (2018). 1708.03279.
- [29] G. Bohm and G. Zech, *Introduction to Statistics and Data Analysis for Physicists*. Deutsches Elektronen-Synchrotron, 2010.
- [30] A. E. Chudakov, Izvestiya Akademii Nauk SSSR, Seriya Fizicheskaya 19 650 (1955).
- [31] S. Catani, F. Fiorani, and G. Marchesini, Phys. Lett. **B234**, 339 (1990).
- [32] G. Marchesini, Nucl. Phys. **B445**, 49 (1995). hep-ph/9412327.
- [33] M. A. Kimber, A. D. Martin, and M. G. Ryskin, Eur. Phys. J. **C12**, 655 (2000). hep-ph/9911379.
- [34] M. A. Kimber, A. D. Martin, and M. G. Ryskin, Phys. Rev. **D63**, 114027 (2001). hep-ph/0101348.
- [35] G. Watt, A. D. Martin, and M. G. Ryskin, Eur. Phys. J. **C31**, 73 (2003). hep-ph/0306169.
- [36] S. P. Baranov, A. V. Lipatov, and M. A. Malyshev, Eur. Phys. J. **C78**, 820 (2018). 1808.06233.
- [37] K. Golec-Biernat and A. M. Stasto, Phys. Lett. **B781**, 633 (2018). 1803.06246.
- [38] A. Bermudez Martinez, P. Connor, H. Jung, A. Lelek, R. Žlebčík, F. Hautmann, and V. Radescu, Phys. Rev. **D99**, 074008 (2019). 1804.11152.
- [39] F. Hautmann, L. Keersmaekers, A. Lelek, and A. M. van Kampen, Paper in preparation (2019).
- [40] S. Catani and M. Grazzini, Eur. Phys. J. **C72**, 2013 (2012). [Erratum: Eur. Phys. J. C72,2132(2012)], 1106.4652.
- [41] S. Catani, L. Cieri, D. de Florian, G. Ferrera, and M. Grazzini, Eur. Phys. J. **C72**, 2195 (2012). 1209.0158.

-
- [42] F. Hautmann, L. Keersmaekers, A. Lelek, and A. M. van Kampen, Paper in preparation (2019).
- [43] F. Hautmann, H. Jung, M. Krämer, P. J. Mulders, E. R. Nocera, T. C. Rogers, and A. Signori, *Eur. Phys. J.* **C74**, 3220 (2014). 1408.3015.
- [44] P. L. S. Connor, H. Jung, F. Hautmann, and J. Scheller, *PoS DIS2016*, 039 (2016).
- [45] M. Bury, A. van Hameren, H. Jung, K. Kutak, S. Sapeta, and M. Serino, *Eur. Phys. J.* **C78**, 137 (2018). 1712.05932.
- [46] H.-L. Lai, M. Guzzi, J. Huston, Z. Li, P. M. Nadolsky, J. Pumplin, and C. P. Yuan, *Phys. Rev.* **D82**, 074024 (2010). 1007.2241.
- [47] F. Hautmann, H. Jung, and S. T. Monfared, *Eur. Phys. J.* **C74**, 3082 (2014). 1407.5935.
- [48] ATLAS Collaboration, G. Aad *et al.*, *JHEP* **09**, 145 (2014). 1406.3660.
- [49] H. Jung *et al.*, *Eur. Phys. J.* **C70**, 1237 (2010). 1008.0152.